CHARACTERISTICS OF THUNDER AND RELATIONSHIPS TO LIGHTNING SOURCES IN THE MAGDALENA MOUNTAINS, CENTRAL NEW MEXICO

by

Rebecca Lyn Johnson

Submitted in Partial Fulfillment

of the Requirements for the Degree of

Master of Science in Geophysics (Solid Earth)

New Mexico Institute of Mining and Technology

Socorro, New Mexico

May, 2013

It’s shocking how little we know about lightning.

Harald Edens

ABSTRACT

I catalog signals and characterize attributes, energy, and spectral content of thunder from storms in the Magdalena Mountains near Socorro, New Mexico during the 2011 summer monsoon season. Our group deployed a network of between eight and twenty continuously recording, broadband (0.01 to 500 Hz) acoustic sensors in multiple 4-sensor array configurations. I utilize coincident Lightning Mapping Array (LMA) data to identify lightning flash timing and source locations and develop a method for cataloging high-quality thunder signals. Because thunder is generated primarily by rapid heating and shocking of the atmosphere around tortuous and extensive lightning channels, the recorded acoustic signals are widely variable across a network of stations. I use National Lightning Detection Network (NLDN) data to differentiate between lightning events that strike the ground (CG) and lightning that remains in the cloud (IC). I study 191 events from thirty-four stormy periods occurring between July and September of 2011. I observe overall higher peak pressures and total acoustic energies for CG thunder, compared to IC thunder. CG thunder also contains more energy in the audible band. These differences are due to both sensor locations relative to lightning sources and inherent source properties. My analysis contributes to understanding characteristics of acoustic radiation for various storms and types of lightning events.

Keywords: THUNDER; ACOUSTIC ENERGY; POWER SPECTRUM; LIGHTNING

ACKNOWLEDGMENTS

I acknowledge Ronald Thomas and Harald Edens for the hours they dedicated to teaching me about the Lightning Mapping Array and helping me to utilize the data. I greatly appreciate their willingness to share their wealth of knowledge on lightning behavior. I would also like to thank Elias Badillo and Jake Anderson for their work to produce and maintain equipment, their assistance in the field, and their insightful discussions. I acknowledge Paul Krehbiel, Bill Rison, Omar Marcillo, Ken Minschwaner, and Jeffrey Kramer for their insight and helpful questions and comments. I acknowledge Mark Murray for providing highly accurate GPS coordinates for our network elements. Finally, I would like to acknowledge my adviser, Jeffrey Johnson; and my committee members, Rene Arechiga, Richard Aster, and Mark Murray for their invaluable instruction, assistance, and constructive criticism throughout my studies and the development and defense of my thesis.

Lightning photography ©Harald Edens, reproduced with permission, from www.weather-photography.com. Lightning Mapping Array data were provided by Harald Edens. National Lightning Detection Network data were provided by Vaisala (2011), Ref. B210412EN-F. This project was funded by NSF grant AGS-0934472.

This thesis was typeset with LaTeX[1] by the author.

[1]The LaTeX document preparation system was developed by Leslie Lamport as a special version of Donald Knuth's TeX program for computer typesetting. TeX is a trademark of the American Mathematical Society. The LaTeX macro package for the New Mexico Institute of Mining and Technology thesis format was written for the Tech Computer Center by John W. Shipman.

TABLE OF CONTENTS

LIST OF TABLES

LIST OF FIGURES

This thesis is accepted on behalf of the faculty of the Institute by the following committee:

_____

Jeffrey Johnson, Advisor

_____

_____

_____

I release this document to the New Mexico Institute of Mining and Technology.

_____

Rebecca Lyn Johnson Date

CHAPTER 1

INTRODUCTION

A recorded thunder signal is influenced by a combination of source characteristics, detection location relative to thunder sources, and background noise. In this study I utilize thunder data recorded with a network of arrays of acoustic sensors in 2011 in the Magdalena Mountains, central New Mexico to characterize and quantify thunder signal attributes at both recording and thunder source locations. There are two widely accepted mechanisms of thunder production: rapid heating and expansion of the atmosphere around a current-conveying channel and charge redistribution and relaxation in a cloud region following lightning processes [*Few et al.*, 1967; *Dessler*, 1973]. Additionally, there are two distinct types of lightning - flashes that remain in the cloud region, and those that strike the ground - and it is believed that these produce distinct thunder signals.

Previous thunder studies have focused largely on detecting and developing analytic descriptions for the two thunder mechanisms, and, more recently, locating thunder sources. The primary descriptive studies of thunder signals were completed 30 or more years ago and were limited, mostly by equipment and computational ability. I provide an updated overview of thunder behavior. I discuss challenges in studying thunder due to complex, unpredictable source geometries and atmospheric effects. I present a method for developing a catalog of isolated thunder signals using Lightning Mapping Array (LMA) data and note that storm

behavior can be described in terms of the number of concurrent thunder events. I describe metrics of thunder signals and see that the complex signals are not well-correlated between stations and may not be indicative of overall signal behavior. My study therefore demonstrates the need for multi-station observations of thunder. I examine total acoustic energy and ratios of energy contained in different frequency bands and see relationships between thunder and lightning source type.

The network of acoustic sensors used in my study was located in an area that is ideal for lightning and thunder studies. Langmuir Laboratory for Atmospheric Research was built in its present location in the Magdalena Mountains because multiple isolated storms occur there during the summer season. The entire acoustic network was located within within 3 km of Langmuir Laboratory. The high altitude of the network increases proximity to nearby thunder sources. My study is unique in that available LMA and National Lightning Detection Network (NLDN) data provide valuable information about lightning flash timing, location, structure, and type. This information is important for finding isolated thunder signals and relating thunder characteristics to lightning flash type. Thunder signals result from lightning process that differ from those detected by the LMA and NLDN. The acoustic data set I use is therefore complementary to other lightning studies.

My data set incorporates a large number of quality thunder events recorded at spatially distributed sensors. In this thesis I describe thunder signal metrics and their relationships to lightning sources. The information I provide may be of interest for future studies of thunder, charge behavior during a storm, or atmospheric acoustics.

CHAPTER 2

BACKGROUND

2.1 LIGHTNING INITIATION

Rakov and Uman [2003] compiled summaries of various areas of lightning research in a comprehensive volume. In this section I summarize information from *Rakov and Uman* [2003] on storm and lightning formation.

The Earth and near atmosphere can be viewed simplistically as a leaky, spherical, parallel plate capacitor with an electric field of about 100 V/m directed toward the Earth (using the physics sign convention wherein Earth is negatively charged). This theoretical capacitor should be discharged in about 10 minutes because the atmosphere is not a perfect insulator. However, the field is maintained, in large part by lightning, which tends to replenish the Earth's negative charge.

A thundercloud, a cumulonimbus, forms via the rising of parcels of warm, moist air that remain buoyant and fuel convection. In the prevalent model for cloud electrification, the cloud contains graupel and ice particles. These hydrometeors collide and become charged; this effect is enhanced by the presence of liquid water. The heavier, negatively charged graupel tends to settle in the base of the cloud while positively charged particles are buoyantly lifted. A very general model for thundercloud charge structure involves a positive charge region at the top, a negative charge region below it, and a small positive charge region at the cloud base. The electric field beneath a thundercloud is reversed relative to the

fair-weather field and is on the order of 1-10 kV/m. Figure 2.1 shows a schematic of the electric field during a storm.

Figure 2.1: Photograph showing a thundercloud with overlain charge centers and electric field direction that occur during a thunderstorm. Photograph ©Harald Edens, reproduced with permission.

When the electric field is sufficiently high and the necessary conditions are met, ionization and breakdown of the air occur between cloud regions or between a cloud region and the ground. Current is then able to propagate in what is observed as a lightning flash. Flashes that strike the ground are known as cloud-to-ground (CG) and those that remain within a cloud, or occur between clouds, are known as intra- or inter-could (IC). IC events are generally 2+ times more common than CG events. A significant portion of each CG flash is contained within the cloud. CG flashes involve multiple ground strokes: a leader lowering toward ground followed by one or more upward propagating return strokes. The

initial return stroke in a CG flash can carry on the order of 30 kA of current and channel temperatures can exceed 20,000 K. There are a number of current conveying processes that can occur during a flash (M-components, J-components, continuing current, etc.) that are beyond the scope of this discussion.

The intense, abrupt interactions between a lightning flash and the surrounding atmosphere result in thunder (see Section 2.3). The initial return stroke in a CG flash produces louder thunder than other lightning processes (see also [*Few*, 1969] and [*Colgate and McKee*, 1969]). Recorded thunder signal characteristics depend on source channel distance, flash geometry, atmospheric properties, and channel electric properties. Lightning studies applying a variety of methods have detected, characterized, and located lightning events. However, these methods do not provide a complete picture of charge movement and its effects on the atmosphere. Acoustic studies of thunder therefore complement and enhance these techniques.

2.2 THE LIGHTNING MAPPING ARRAY (LMA) AND NATIONAL LIGHTNING DETECTION NETWORK (NLDN)

The Lightning Mapping Array (LMA) in New Mexico provides accurate lightning channel locations that can be assumed to correspond to thunder sources. The 2011 LMA consists of twelve stations spanning about 60 km in central New Mexico. Stations detect very high frequency (VHF) electromagnetic pulses in the 60-66 MHz band with measurement windows of 80 or 100 μs and timing accuracy of 35 ns made possible by GPS receivers. The VHF energy is produced by atmospheric breakdown processes in a lightning flash. The LMA determines three-dimensional locations and timing of radiation point sources along lightning

channels using time-of-arrival differences at multiple stations for high-amplitude events [*Rison et al.*, 1999]. Because each LMA station detects on the order of hundreds to thousands of breakdown events per flash, spatial distribution and complexity of flashes can be resolved [*Thomas et al.*, 2004]. An example of LMA data for an individual flash is shown in Figure 2.2.

LMA detections are biased toward positively charged cloud regions [*Rison et al.*, 1999]. Location uncertainty is influenced by factors including inherent timing errors, the number of stations used for locating sources, and source distance and position relative to the network. Uncertainties for individual points located within the network are 6-12 m rms (horizontal) and 20-30 m rms (vertical) [*Thomas et al.*, 2004]. The LMA's geometry results in decreased resolution and detection for points nearing the horizontal plane of the array as obstacles block necessary line-of-sight to air breakdown locations. This inherent array property is a limiting factor for fully characterizing some CG events [*R.Thomas*, personal communication, 2012].

The National Lightning Detection Network (NLDN), operated by Vaisala, Inc., spans the continental United States and is the largest lightning detection network in the world [*Orville*, 2008]. The NLDN is a very low frequency (VLF) magnetic direction finder system that uses time-of-arrival differences between stations to detect and locate (primarily) CG return strokes. The NLDN can detect IC flashes with adequately high amplitude VLF/LF pulses. NLDN data include a point location, stroke type (IC or CG), and current value for all detectable strokes for a flash: a single CG flash, for example, may include multiple IC and CG strokes [*Cummins and Murphy*, 2009]. The current values provided in NLDN data are not necessarily representative of the total current for a flash, as not all lightning processes, such as continuing current in CG strokes, are detected.

Figure 2.2: An example of a CG flash that occurred on 22 July 2011 is shown from multiple perspectives. Point color indicates time (advancing blue to red). The top plot shows altitude versus time. The flash lasted about 1.2 s and struck the ground at about 1 s. The lower left plot is a map view of the flash - Langmuir Laboratory is the origin and green boxes indicate LMA station locations. The adjacent plots show altitude versus East-West distance from Langmuir and North-South distance versus altitude. The histogram shows the total number of LMA points at all altitudes for the flash. Langmuir is located at about 3 km altitude and most detections were between 8 and 9 km altitude.

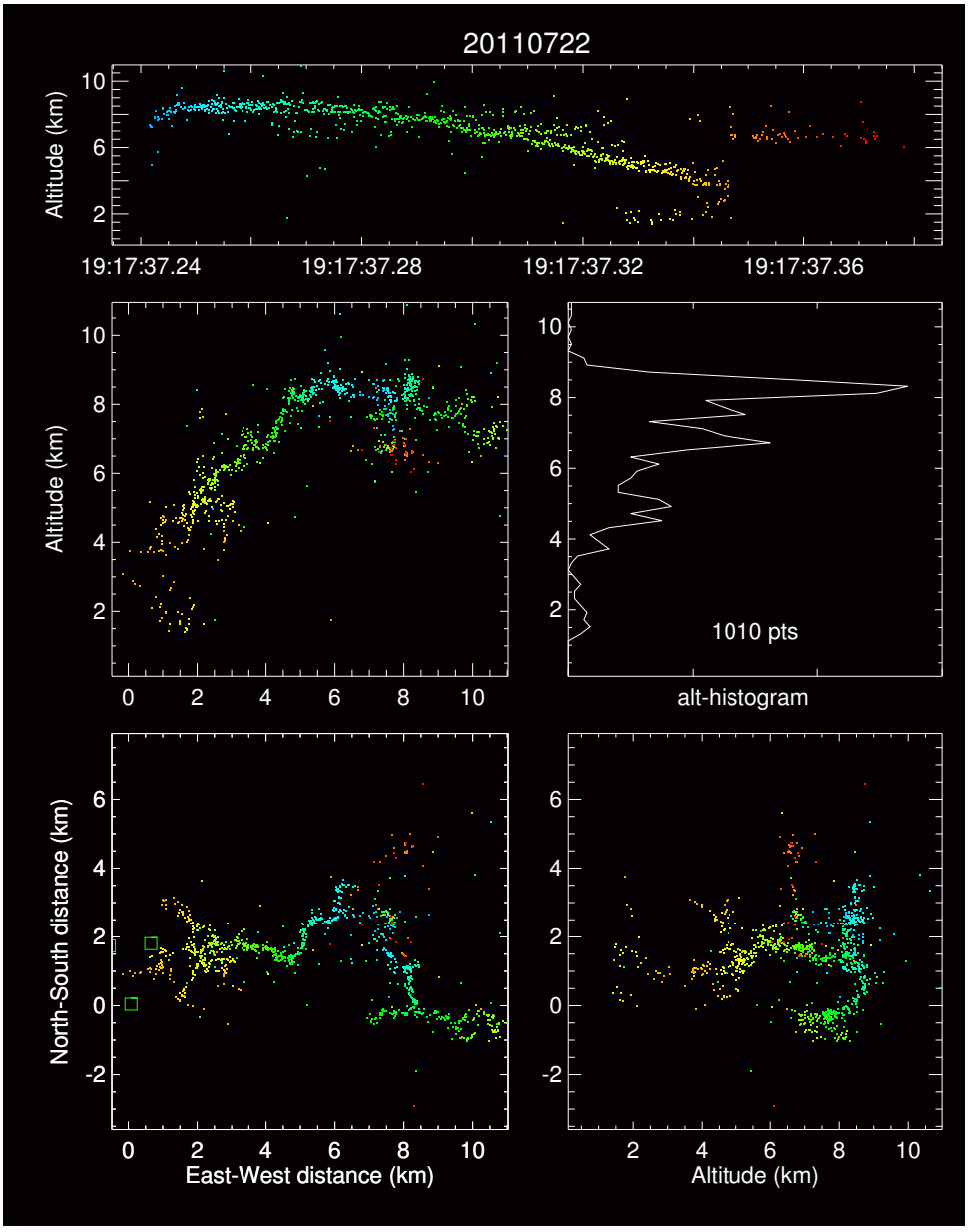

The availability of LMA and NLDN data allows determination of source type and detailed location for thunder produced by lightning channels. It also makes feasible the comparison of thunder signal characteristics to other lightning parameters.

2.3 AUDIBLE AND INFRASONIC THUNDER

There are two generally accepted sources of thunder. The first, which produces broadband thunder, is a direct result of current conveyance in lightning channels. Current traveling in a flash results in superheating and expansion of the surrounding atmosphere, creating an outward propagating shock wave. At some distance between a few centimeters and a few meters beyond the channel, the shock wave transitions to an acoustic wave that has broadband energy [*Few*, 1969; *Depasse*, 1994; *Holmes et al.*, 1971]. The resulting thunder signal is inherently complex due to lightning channel tortuosity - the signal represents a superposition of sound from multiple, relatively short channel segments [*Few et al.*, 1967]. *Few* [1969] developed a simplifying model for audible thunder that treats channel segments as long cylinders generating pressure waves that expand cylindrically in the region of shock formation, then transition to diverge spherically as acoustic waves beyond a characteristic radius close to the channel. Laboratory measurements have shown that most acoustic energy from each part of a cylindrical channel remains within a narrow angle as it travels outward. Because rays travel approximately perpendicular to the channel axis, acoustic signal will be dependent on the relative observation angle [*Depasse*, 1994]. An observer perpendicular to a channel axis should hear louder thunder than an observer at the tip of a channel and an observer close to a long channel will only hear thunder produced from a portion of the channel's length.

A second mechanism for thunder generation, specifically thunder below 2 Hz, is electrostatic relaxation of a cloud volume after a lightning discharge. When lightning occurs, the electrostatic field in the cloud source region is significantly reduced via removal of charges from individual hydrometeor droplets. The cloud volume contracts to restore equilibrium in response to this sudden change in charge distribution [*Wilson*, 1920; *Dessler*, 1973]. This produces an acoustic signal estimated to be infrasonic, at a frequency between 0.2–2 Hz. Additionally, due to the volume's non-spherical geometry, the signal is highly directed, limiting detection to a narrow angle relative to the source [*Dessler*, 1973].

Balachandran [1979] rarely observed thunder from the electrostatic mechanism over a five-year study, a fact attributed to the directed nature of the source and the prevalence of wind during storms. Wind peaks in the infrasonic band, often masking the signal [*Bohannon et al.*, 1977]. An additional constraint is discussed by *Pasko* [2009]: high charge densities in the cloud region are necessary for strong pulses to be generated. Observed peak-to-peak pulse amplitudes were on the order of tenths of pascals at distances between 1.8 and 2.7 km from the source [*Bohannon et al.*, 1977] up to 1 Pa at an unknown recording distance directly below a thunder cloud [*Balachandran*, 1979]. Though thunder signals due to cloud charge relaxation are challenging to detect, studies of this thunder are a step toward understanding charge distribution in the cloud [*Few*, 1985; *Balachandran*, 1979].

Both the expanding channel and electrostatic mechanisms can produce infrasonic thunder. *Assink et al.* [2008] used infrasound arrays and an EM detection network to study infrasonic thunder from CG flashes, noting signals peaking between 1-5 Hz associated with blast waves from lightning channels at distances

between a few kilometers and 50 km. The observed infrasound signals were corroborated with electromagnetic detections from lightning discharges. The infrasound originated from incidence angles not in agreement with the electrostatic mechanism (the electrostatic source should be located directly above recording locations) [*Assink et al.*, 2008; *Balachandran*, 1979]. It is important to consider both thunder production mechanisms when studying infrasonic thunder. In this study I focus on broadband thunder and acknowledge that infrasonic energy in some signals may originate from an electrostatic source.

2.4 THUNDER SPECTRAL CONTENT AND ENERGY

Previous studies have developed theory for and made observations of the spectral content of thunder. The spectrum of thunder is the parameter least affected by small-scale source complexity and relative observation position [*Few*, 1969]. The power spectrum should be a superposition of thunder spectra from all strokes in a lightning flash [*Few*, 1969; *Holmes et al.*, 1971]. Most of the energy in thunder signals is contained below 500 Hz [*Few*, 1969; *Holmes et al.*, 1971], though *Depasse* [1994] studied signals close to flash sources with spectral content in the thousands of hertz. *Few* [1969] measured and predicted a thunder spectrum peaking below 100 Hz with some subsidiary peaks. *Holmes et al.* [1971] observed 40 thunder events in the Magdalena Mountains in 1967 and 1968 with peak frequencies between $<$4 and 125 Hz. Wind noise can dominate lower frequencies and significantly lower peak frequency for thunder signals, biasing spectral estimates [*Holmes et al.*, 1971; *Bohannon et al.*, 1977].

Thunder sources are spatially distributed and contain many channel segments propagating different amounts of current. Signals are therefore non-stationary,

as reflected in temporally varying spectra. High frequencies would be expected to decay monotonically for a simple acoustic source. *Holmes et al.* [1971] observed thunder spectrograms showing high-frequency peaks throughout the recorded signal, reflecting electric processes in different parts of the complex lightning channel.

The energy contained in an acoustic signal is related to source strength [*Kinsler et al.*, 1999]. *Few* [1969] relates thunder peak frequency, f_{max}, to the energy per unit length of a lightning flash. The specific energy of a lightning flash, $\int I^2 \mathrm{d}t$, where I is current, can be used to estimate the energy per unit length if the time-current signature for the flash is known [*Depasse*, 1994]. *Assink et al.* [2008] notes a relationship between specific energy for a flash and thunder signal volumetric energy density at the recording location, E_{vol}. *Depasse* [1994] quantifies relationships between E_{vol}, f_{max}, and $\int I^2 \mathrm{d}t$ for short, narrow-band thunder signals recorded 70 m from a triggered lightning source.

Because E_{vol} is calculated at the receiver location, estimates are less meaningful when studying broadband signals recorded at variable distances from the source. Total acoustic energy, W, for thunder signals propagating beyond the shock region (in the zone of spherical divergence) can be estimated within an order of magnitude using the recorded pressures, $p(t)$, and assuming constant atmospheric density (ρ_0) and sound speed (c) [*Holmes et al.*, 1971; *Johnson et al.*, 2011]:

$$W = \frac{4\pi}{\rho_0 c} \int_{t_0}^{t_0+T} p(t)^2 r^2 \, \mathrm{d}t \tag{2.1}$$

The distance from the source location, r, is estimated:

$$r = c\,(t - t_0) \tag{2.2}$$

where time-of-arrival relative to the time of the lightning flash $(t - t_0)$ is known. Validity of this estimate depends on external factors influencing the signal as discussed in Section 2.5 and in *Holmes et al.* [1971]. *Holmes et al.* [1971] observed low acoustic energies (W) and peak frequencies (f_{max}) for IC flashes, compared to CG flashes.

2.5 PROPAGATION EFFECTS

Sound pressure decays inversely with distance [*Kinsler et al.*, 1999] such that pressure p_2 at distance r_2 from a source can be determined knowing pressure p_1 at distance r_1:

$$p_2 = p_1 \frac{r_1}{r_2} \tag{2.3}$$

In addition to this decrease in pressure amplitude, propagating thunder signals are influenced by numerous factors, including temperature, wind shear, turbulence, local topography, and molecular interactions. Thunder waveforms undergo refraction due to dynamic temperature and wind gradients, attenuation (an exponential falloff that is frequency dependent), non-linear finite amplitude propagation, dispersion, and reflection off of topographic features [*Few*, 1995; *Depasse*, 1994].

Thunder is rarely detected from beyond 25 km due to amplitude decay (Equation 2.3) and refraction of the acoustic waves by the atmosphere. *Fleagle* [1949] demonstrated the nearly parabolic nature of the refraction using Snell's Law and assuming a linear lapse rate. Both the atmospheric temperature gradient and horizontal wind shear contribute to a reduced range of audibility for thunder.

The audible range of thunder is hindered further by attenuation [*Fleagle*, 1949; *Bass and Losey*, 1975]. Attenuation of thunder results in a frequency-dependent falloff in pressure amplitude with distance [*Few*, 1995]. Attenuation is caused by viscosity (motions within the medium during transmission of sound waves), thermal conduction losses that occur between condensations and rarefactions in the waveform, and molecular attenuation (kinetic energy is converted to other forms due to molecular interactions) [*Few*, 1995; *Kinsler et al.*, 1999]. Attenuation effects are generally considered insignificant at frequencies below 100 Hz [*Bass and Losey*, 1975; *Few*, 1995].

Few [1995] discusses the probability that clouds act to enhance attenuation and scattering, especially for IC lightning. For example, increased humidity may increase scattering at high frequencies [*Rakov and Uman*, 2003] while turbulence may reduce low-frequency energy [*Few*, 1995]. These effects cannot, in general, be modeled or quantified.

CHAPTER 3

METHODS

3.1 EXPERIMENT

During the 2011 summer monsoon season, which extended from the end of July to late September, a network of between two and four arrays of continuously recording acoustic sensors was deployed near Langmuir Laboratories and the summit of South Baldy Peak in the Magdalena Mountains in west-central New Mexico (Figure 3.1). Each array consisted of four broadband microphones (AllSensors^{TM} 0.5–1 in MEMS transducers) with a linear dynamic range of +/- 125 Pa, low noise (5.62 mPa rms at 0.05-20 Hz), and flat response above 0.01 Hz [*Marcillo et al.*, 2012]. The sensors were developed and built in-house at New Mexico Tech.

The network consisted of arrays spaced between 0.5 and 3 km apart, located in forested environments (vegetation acts as a filter for some wind noise). Arrays GTM and LAN were placed in relatively flat areas. Array WKN was placed near the top of a ridge to achieve proximity to storms and KVH was located on a hillside near the location where Langmuir Laboratories triggers lightning flashes using wired rockets. While GTM and KVH were operable for the season's duration, stations KVH and WKN were removed for much of the month of August. Array configurations at each station consisted of one sensor and the recording device placed at the center node, with the other three microphones

placed as vertices of an approximately equilateral triangle (Figure 3.2). Each vertex was approximately thirty meters from the central node. Data were continuously acquired at 1000 Hz by GPS time-synced Reftek RT-130 data loggers with a resolution of 24 bits.

Figure 3.1: Map showing the 2011 network configuration; the Magdalena Mountains are a short distance west of Socorro, New Mexico. The small rectangle on the inset map of New Mexico corresponds to the large map. The large map shows local topography, the location of Langmuir Laboratory, and the locations of the four stations: KVH, GTM, WKN, and LAN.

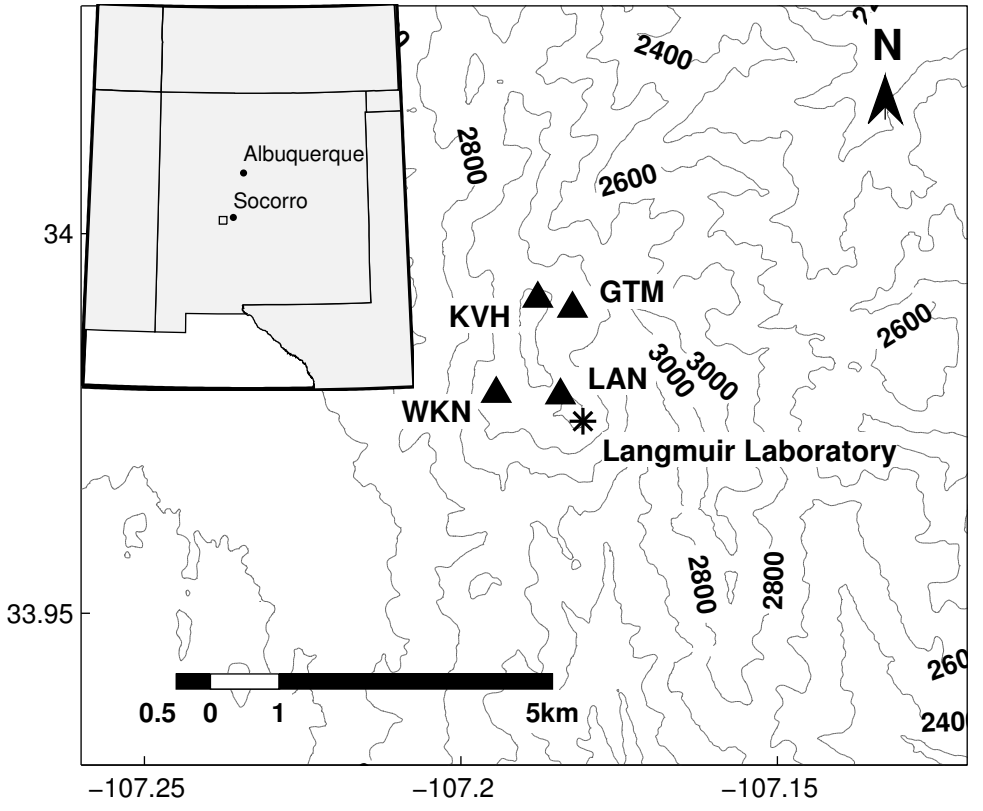

Figure 3.2: A close-up view of each array showing individual array configurations. Each array consisted of four broadband acoustic sensors: one at the central node, co-located with the recording device, and three additional sensors branching outward. Each sensor location is shown relative to the central node, in meters, and north is up in all cases.

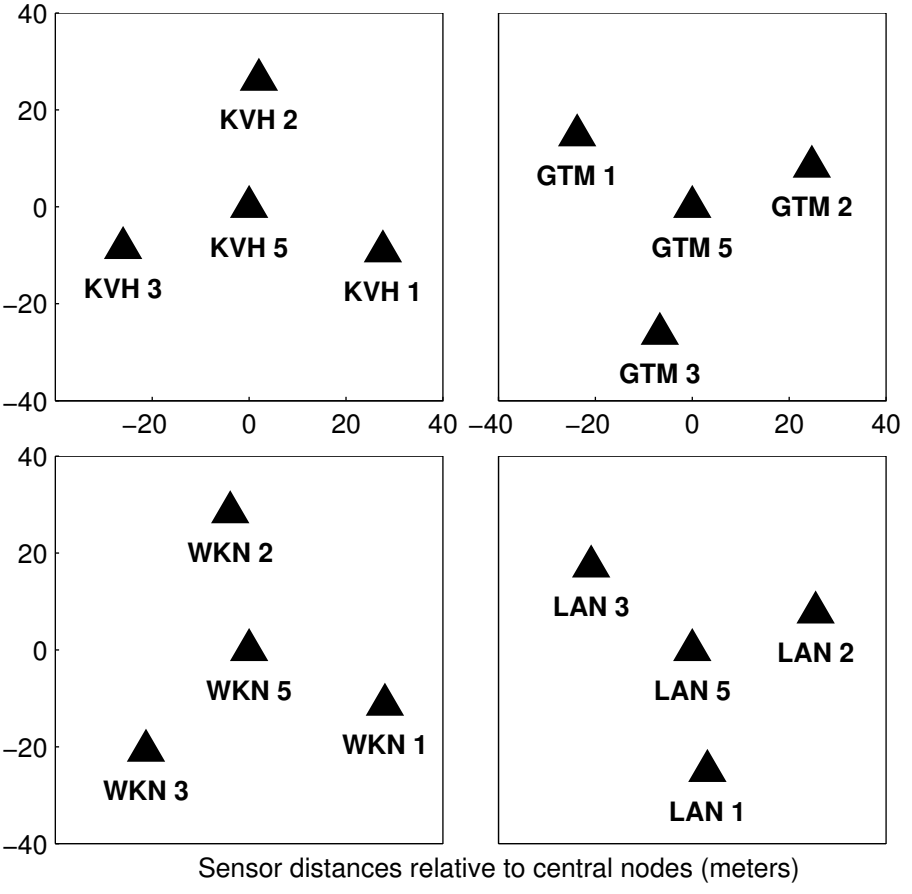

A differential GPS survey was performed to estimate WGS84 locations for the network. The survey used Topcon GB-1000 receivers to find station positions relative to reference SC01 located on Socorro Peak. Because antennae were offset from sensors in some instances, primarily due to overhead vegetation or terrain difficulty, the locations are believed to be accurate to the decimeter level.

3.2 USING LMA DATA TO ESTIMATE THUNDER SIGNAL ARRIVAL AND DURATION

While thousands of individual lightning events occur during a storm season, I carefully select a small percentage for analysis. I note the importance of evaluating thunder signals with high signal-to-noise ratio (SNR) that are not influenced by significant wind or rain noise, nor overlapping signal from other nearby lightning/thunder events. The last of these goals, while difficult to achieve in previous studies, is feasible with this data set due to available LMA data. LMA data provide highly accurate (Section 2.2) lightning channel locations, making it possible to estimate arrival times and durations for thunder signals recorded across the network during the 2011 season.

Using visual inspection of thunder data, 34 stormy periods were selected ranging in duration from a few minutes to three hours during which thunder signals were recorded. I apply a flash sorting algorithm (developed by Ronald Thomas of the New Mexico Tech Electrical Engineering department) to organize the LMA data for each selected storm period into individual flashes [*Wiens et al.*, 2005]. The algorithm uses relative position and timing of located breakdown points and groups them; it then characterizes each group as a flash. The algorithm provides location and timing information for all points affiliated with a

flash, incorporates NLDN information (flash type and current) when available, and uses LMA point distributions to determine flash type if NLDN data are not available.

Individual LMA flash detections contain tens to thousands of individual breakdown point sources. The flash sorting algorithm considers a flash to be "big" if it contains more than 75 LMA points. To reduce LMA location uncertainties mentioned in Section 2.2, I use only breakdown points detected by at least eight LMA stations with a chi^2 value of 3 or less. I eliminate noisy LMA point locations that manifest below the ground surface using interpolated Shuttle Radar Topography Mission (SRTM) elevation data. For comprehensive analysis of thunder, I obtain individual point timing and location information for all big flashes centered within 20 km of Langmuir Laboratory. Though I limit the number of flashes analyzed in these steps, I see no indications in the data that I fail to detect significant thunder events. For the 34 periods of interest, the flash sorting algorithm identifies 4911 flashes.

I use LMA locations to estimate thunder arrival times for all flashes at each of the stations using a constant sound speed. I first calculate flash-to-sensor distances:

$$D_{ij} = \sqrt{(x_i - x_j)^2 + (y_i - y_j)^2 + (z_i - z_j)^2} \tag{3.1}$$

where D_{ij} is the distance between the i^{th} LMA point and the j^{th} station. Assuming that all points located by the LMA produce detectable thunder, and using a constant sound speed c=340 m/s (15°C at 1.2 kg/m^3), I estimate the time of arrival (t) of sound from each LMA point occurring at time t_0 [*Arechiga et al.*, 2011]

$$t = t_0 + \frac{D_{ij}}{c} \tag{3.2}$$

To reduce the contribution of any remaining noise, I consider only the 98^{th} percentile of arrival times. I calculate the first and last arrival of each thunder signal at each station using the minimum and maximum t values, respectively.

For some events, the first estimated thunder arrival is later than the observed arrival, sometimes by an order of seconds. This is the case for CG events that are close to the stations and is related to the limited ability of the LMA to detect low-altitude breakdown events that are close to the plane of the array. Additionally, the LMA requires six stations with direct line-of-sight to qualify a flash detection. Thunder signal, however, is related primarily to channel electric properties and proximity [*Few*, 1969; *Rakov and Uman*, 2003]. Only one sensor near a flash is required to identify an event. Using multiple acoustic sensors, it is possible to detect and locate nearby lightning channels, even with the LMA is unable to do so [*Arechiga et al.*, 2011; *Johnson et al.*, 2011].

3.3 DEVELOPMENT OF A ROBUST THUNDER CATALOG

From my work with LMA data, I develop a listing of all thunder events I expect to have recorded in 2011. Appendix A shows continuously recorded signal for the 34 time periods used for analysis. These time periods were selected using visual inspection of the thunder data, as discussed in Section 3.2.

Though many lightning flashes span tens of kilometers, thunder in most conditions is not detectable from beyond 25 km due to attenuation and refraction of sound waves caused by the atmospheric thermal gradient [*Fleagle*, 1949] (see Section 2.5). I truncate any arrival times estimated using Equation 3.2 that exceed 80 s after the LMA flash time. An arrival at 80 s corresponds to a travel distance of about 27 km. Though some infrasonic thunder may be detectable in low noise

conditions from tens of kilometers away [*Assink et al.*, 2008], almost all signals at this distance should either be refracted or have amplitudes too low to interfere with other thunder signals.

For my analysis I focus only on isolated thunder signals. During most storms multiple lightning flashes occur over a large distance within a short period of time. Grouping acoustic signals with the correct flashes is extremely challenging without available lightning detection and location data. I find all isolated thunder events with buffers of 8 s prior to and 2 s after estimated signal arrivals. This buffer accounts for arrival time estimate errors and provides a "quiet" period prior to thunder signals that can used for signal-to-noise analyses. Figure 3.3 shows histograms of counts of concurrent thunder signals during all storm time periods analyzed. There are times when up to 20 thunder signals may be superimposed in the recordings. Signals arriving at the same time may be from spatially distant sources and therefore have very different amplitudes and characteristics. In Section 4.1 I further describe the characteristics of storms observed in Figure 3.3.

The quality of signals is highly dependent on source position and location, source electric properties, and varying atmospheric influences (e.g., wind noise and direction). I calculate signal-to-noise ratio (SNR) for the isolated thunder signals at channels 3 at stations GTM and KVH. I focus much of my analysis on these two channels, as they exhibit the highest quality data and were continuously recording for the entire season. Signal corresponds to the acoustic data in the time window of expected thunder arrivals estimated by using LMA data. Noise is assumed to be the background recorded prior to the estimated thunder arrivals. I first calculate the RMS amplitude, S_{rms}, for each thunder signal using

Figure 3.3: Plots indicating total number of thunder signals arriving at MGTM during the time periods analyzed. Maximum numbers of superimposed thunder signals are indicated on the left, next to the date and start time of the time period. Total number of thunder signals for each time period are recorded on the right side of the axes. Time axis is in hours. There were up to 20 synchronous thunder signals recorded (July 31).

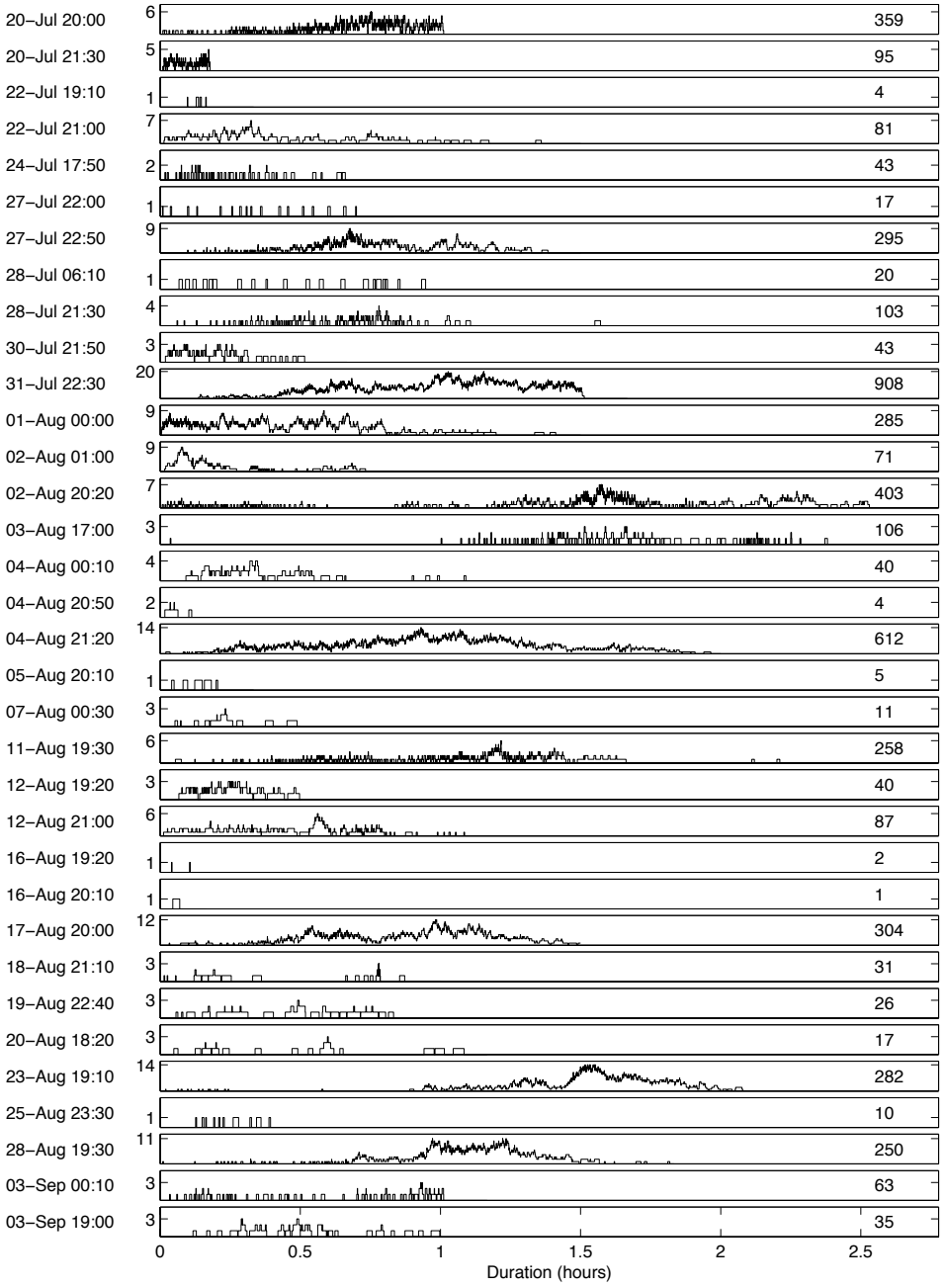

the acoustic record for the estimated arrival time and duration (maximum 80 s after the flash):

$$S_{rms} = \sqrt{\frac{\sum_{i=1}^{n} signal_i^2}{n}} \tag{3.3}$$

where n is the duration of the signal in samples. I similarly calculate the RMS amplitude, N_{rms}, for a noise window beginning 8 s prior to the initial thunder arrival and lasting 4 s:

$$N_{rms} = \sqrt{\frac{\sum_{i=1}^{n} noise_i^2}{n}} \tag{3.4}$$

where n is the duration of noise, in samples ($n = 4000$ in this case). I retain those signals that, on channel 3 at both GTM and KVH, have SNR$\geq$3:

$$SNR = 20\log_{10}\left(\frac{S_{rms}}{N_{rms}}\right) \tag{3.5}$$

As a final step in developing a thunder catalog, I visually inspect all isolated, high-SNR signals and their spectrograms to eliminate signals tainted by unusual noise sources (e.g., from nearby machinery or vehicles). The result is a catalog of 191 high-quality thunder signals occurring during 29 of the 34 predetermined storm periods that are detected across the network. This represents thunder from only about 4% of the 4911 regional flashes identified in the LMA data. Each event includes thunder arrival time estimates for all network stations, LMA flash times, and flash type and current information, if available. Timing information for GTM and KVH is included as metadata in Appendix B.

3.4 FILTERING

Because of my interest in thunder spectra, I require a finite impulse, zero-phase filter with a flat response in the passband. I therefore use an acausal Butter-

worth filter on all signals. For most observations, unless otherwise noted, I filter signals above 4 s (0.25 Hz). Recall that Nyquist frequency for these recordings is 500 Hz. I select 4 s as my cutoff to eliminate very low frequency noise while preserving infrasonic thunder that may originate from the blast wave [*Assink et al.*, 2008] or the electrostatic mechanism [*Balachandran*, 1979].

3.5 REDUCED PRESSURE, TOTAL ACOUSTIC ENERGY, AND SPECTRAL ESTIMATES

Due to wide variations in source-receiver distances, recorded pressure amplitudes for multiple events cannot be directly compared. Other influences neglected, sound pressure decays as $1/r$ (Equation 2.3). I can calculate source-receiver distances, r, using Equation 2.2 and estimate signal amplitudes at some distance r_2. To study thunder signal amplitudes, I reduce all signals to r_2 =1 km, which is in the region of spherical acoustic wave expansion [*Few*, 1969]. An example of a resultant normalized signal is shown in Figure 3.4. Observations of peak pressures, comparison of estimates between stations, and pressure estimate differences for IC and CG flashes are discussed in Section 4.1.

Thunder energy is a useful metric for characterizing signals. I discuss the differences between volumetric energy density, E_{vol}, and total acoustic energy, W, in Section 2.4. The data set contains long-duration broadband signals at widely varying source-receiver distances. I therefore seek to normalize energy estimates and utilize W (Equation 2.1) in all of my calculations. I assume a sound velocity, c, of 340 m/s and atmospheric density, ρ_0, of 0.82, which is appropriate for the high altitude of my study.

Thunder signals are short-duration, non-stationary, and have variable spectra [*Few*, 1969]. Finding the power spectral density (PSD) of a signal using the fast

Figure 3.4: Recorded and reduced thunder signals are shown. Recorded thunder (left panel overlay, blue) is for to the third CG event in Figure 4.3 at GTM. Recorded thunder multiplied by calculated distance (right panel) provides a reduced signal (left panel, black). I assume a constant c of 340 m/s.

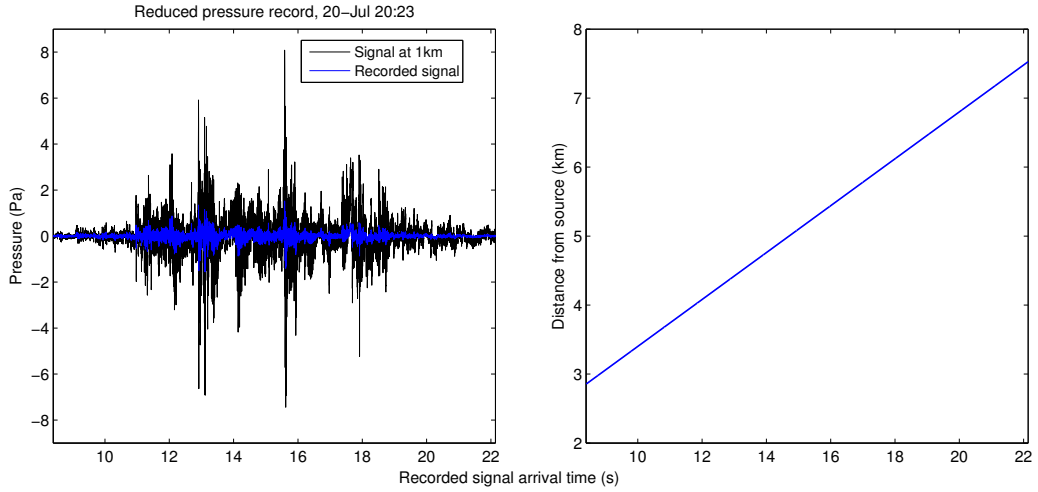

Fourier transform is not robust as it results in spectral leakage and non-trivial variance [*Thomson*, 1982]. A common approach to minimizing PSD noise is to window and taper the signal prior to producing the PSD. Such approaches, including Welch's method, discard portions of the signal, sacrificing energy resolution. The multitaper method of spectral estimation applies multiple, orthogonal tapers to a signal and finds a weighted average of the results. Though more computationally intensive, the method was developed as an approach to balance the problems of spectral leakage with energy resolution. The method is useful specifically for short series with varied spectra, though non-stationary signals may still present problems [*Thomson*, 1982]. In the interest of retaining energy information, and acknowledging the loss of accurate power amplitudes, I produce PSDs using the multitaper method (time-bandwidth product = 4).

Because time of arrival estimates using Equation 3.2 may not be accurate, I manually pick first and last arrivals of thunder signals at all stations. I window

signals to minimize contributions from background noise, especially in spectral estimates. I verify my observations of pressure, total acoustic energy, peak frequency, and high- and low-frequency spectral content by estimating mean values for these parameters across the entire network.

CHAPTER 4

RESULTS

4.1 GENERAL SIGNAL OBSERVATIONS

Thunder signals are inherently complex due source variability. Each lightning flash can span a different source region with dimensions on the order of tens of kilometers, can have numerous channels that convey varying amounts of current, and may or may not strike the ground. Additionally, storm systems exhibit dramatic anisotropy in humidity, temperature, pressure, and wind. Because multiple lightning flashes occur within a short time period, multiple thunder signals frequently overlap, as discussed in Section 3.3. All of these factors contribute to the traits (pressure amplitudes, energies, spectra, etc.) of the signals recorded.

Thunder signal occurence and overlap varies between storms. Figure 4.1 shows enlarged examples of thunder signal count for two storms shown in Figure 3.3. The storm on 27 July lasts less than one hour and has discreet lightning-thunder sequences. There is no clear increase in storm intensity. I classify time periods displaying this behavior as ”isolated sequences.” The second storm, on 28 August, exhibits a brief isolated sequence at the beginning of the storm, a rapid increase in event frequency, and a decline in events toward the end of the storm, culminating with discreet events. The storm lasts nearly 2 hours. Time periods with multiple events occuring simultaneously I classify as ”overlapping thunder.” Periods exhibiting both types of thunder overlap I describe as ”hybrid.”

Figure 4.1: Estimated total number of thunder signals detected during storms on 27 July and 28 August are shown. The y-axis denotes total number of thunder events and the x-axis denotes time since the beginning of the window analyzed. Note differences in the x-axis and y-axis scales for the two storms.

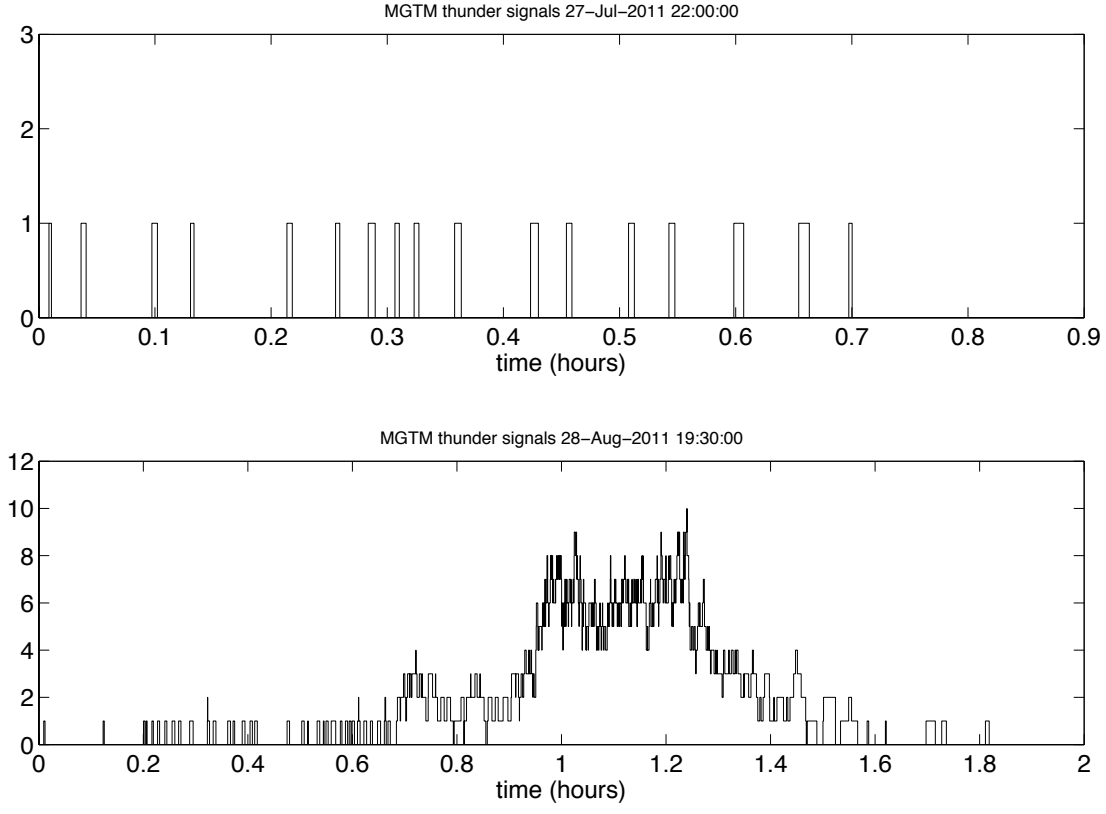

In Figure 4.2 I show a helicorder of thunder signal at station KVH for a storm on 20 July 2011. The time period analyzed lasts one hour during which there are 359 LMA-detected flashes near the network. I see isolated flashes followed by overlapping thunder, similar to the storm on 28 August. High amplitude thunder events coincide with esitmated arrivals, though as overlap increases, it becomes challenging to differentiate individual signals. Signal amplitudes and envelopes are widely variable. Refer to Appendix A to see similar records at station GTM for all analyzed time periods. The frequency of lightning (and hence the number of detected thunder signals in the data set) is related to storm size and duration, though the relatioship to other physical processes is poorly understood [*Rakov and Uman*, 2003].

My catalog of 191 events includes thunder from 82 flashes identified as IC, 106 CG, and 3 unclassified. IC events are far more common than CG events [*Rakov and Uman*, 2003] but CG events are detected more easily due to the nature of their signals, as described below and discussed in Section 5. While NLDN current values are available for all CG events in my catalog, only 11 IC events have stroke currents high enough to be detected by the NLDN. Individual stroke currents do not reflect total current for a flash. The majority of the events included in my catalog occur at the beginning or end of storms or during isolated thunder sequences. I note that, as can be seen in Appendix A, there are many high-quality thunder signals that I do not analyze because the signals may have interference from concurrent events. As a storm system moves and progresses, and as the charge distributions change, the detected thunder should also change. I am often unable to characterize the thunder during the most intense storm periods because of potential signal overlap. These factors may introduce some bias as most of the

Figure 4.2: Helicorder showing thunder data recorded at station KVH for 70 minutes during a storm on 20 July (times shown are GMT). Vertical lines delineate LMA event times. Line height is scaled relative to mean radial distance between Langmuir Laboratory and flash LMA point locations with longer lines indicating closer flashes. Each vertical line has a corresponding horizontal line (of the same height and color) that shows the predicted duration of the thunder signal. See data for this storm at station GTM in Figure A.1.

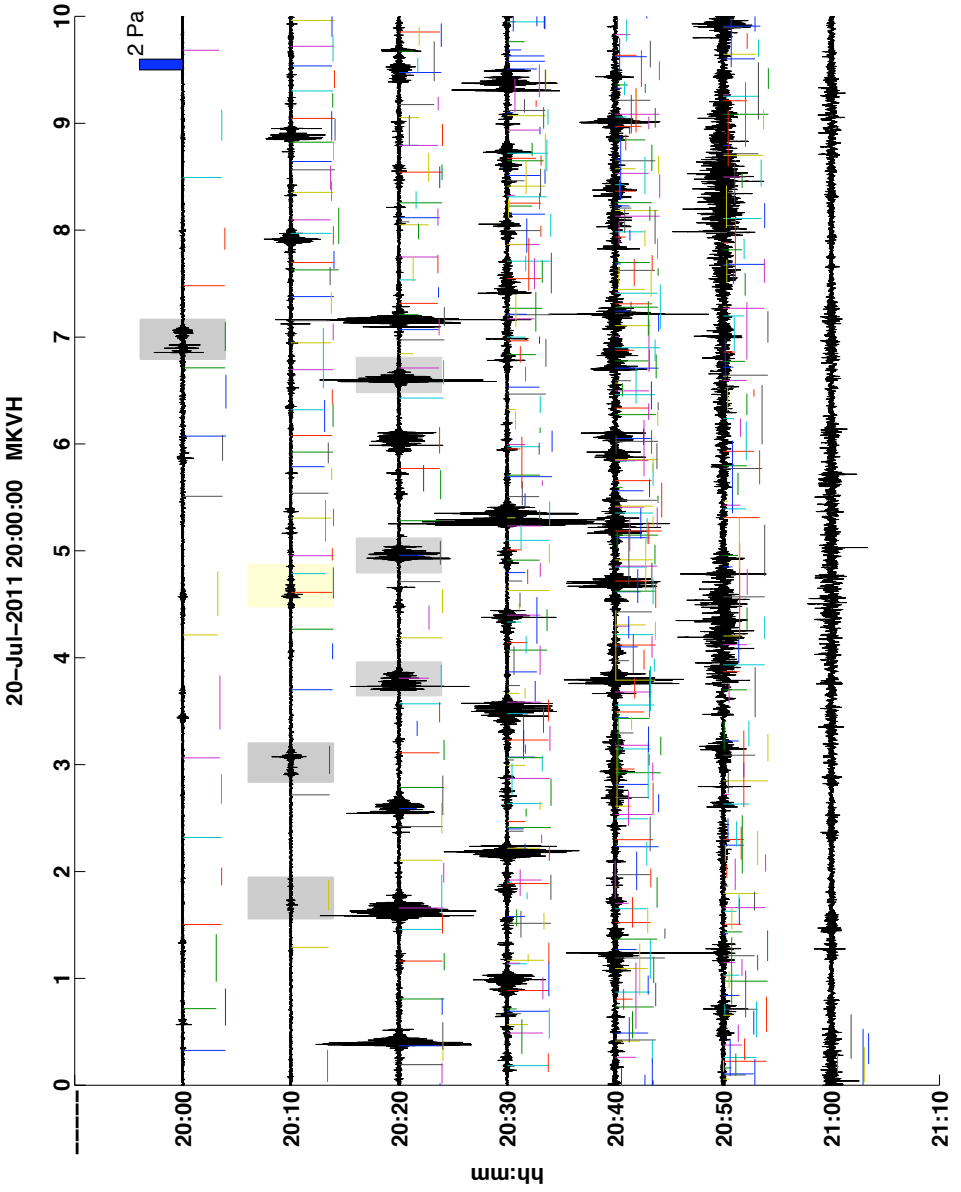

signals in my catalog are from CG flashes during a limited portion of the thunder storms.

In Figures 4.3 and 4.4 I show a selection CG and IC events, respectively, at channels 3 at KVH and GTM. Thunder signals often exhibit multiple pressure peaks, as opposed to a peak followed by signal decay that would be expected from a single expanding monopole point source. I record peak amplitudes that are widely varied (ranging from tenths of Pa to 140 Pa for my entire catalog), but tend to be higher for CG events. This is related both to source-receiver distance and source strength for CG events. The duration of primary energy is shorter for CG thunder, while IC thunder energy tends to be more distributed and sustained. Signal duration is frequently on the order of tens of seconds for both CG and IC events. This primarily reflects the intracloud portion of the lightning, which spans much greater distances than individual ground strokes. Of note is that thunder signals tend to be poorly correlated between stations. I filter the signals at both stations between 4 s and 5 Hz and perform cross-correlation (correlation window: 19 s). Correlation coefficients rarely exceed 0.5, even for quality signals filtered in a low-frequency band. This makes some signal detection and processing techniques difficult to use for thunder data analysis.

In Figures 4.5 and 4.6 I show a CG and an IC thunder signal, respectively, recorded all all network stations. There is clear variability in signal character between arrays. All sensors at an array should record similar signals. In Figure 4.5 I see signal amplitudes up to nearly 5 Pa. Amplitude variations at different arrays are due to relative source distances. Linear frequency scale PSDs show broadband behavior while logarithmic scales emphasize low-frequency characteristics. Most operable sensors have a frequency peak in the 0.5 – 2.2 Hz range. However,

Figure 4.3: Examples of CG events (20) from various storms are shown for two stations. LMA flash times are on the far left. The time axis is in seconds since the flash occurred. Station GTM is shown in the left panel; station KVH in the right. Each signal is normalized to its peak recorded pressure (peak pressure amplitude, in pascals, displayed for each signal). The GTM/KVH cross-correlation coefficients for the signals filtered between 4 s and 5 Hz (not shown) are on the far right (correlation window = 19 s).

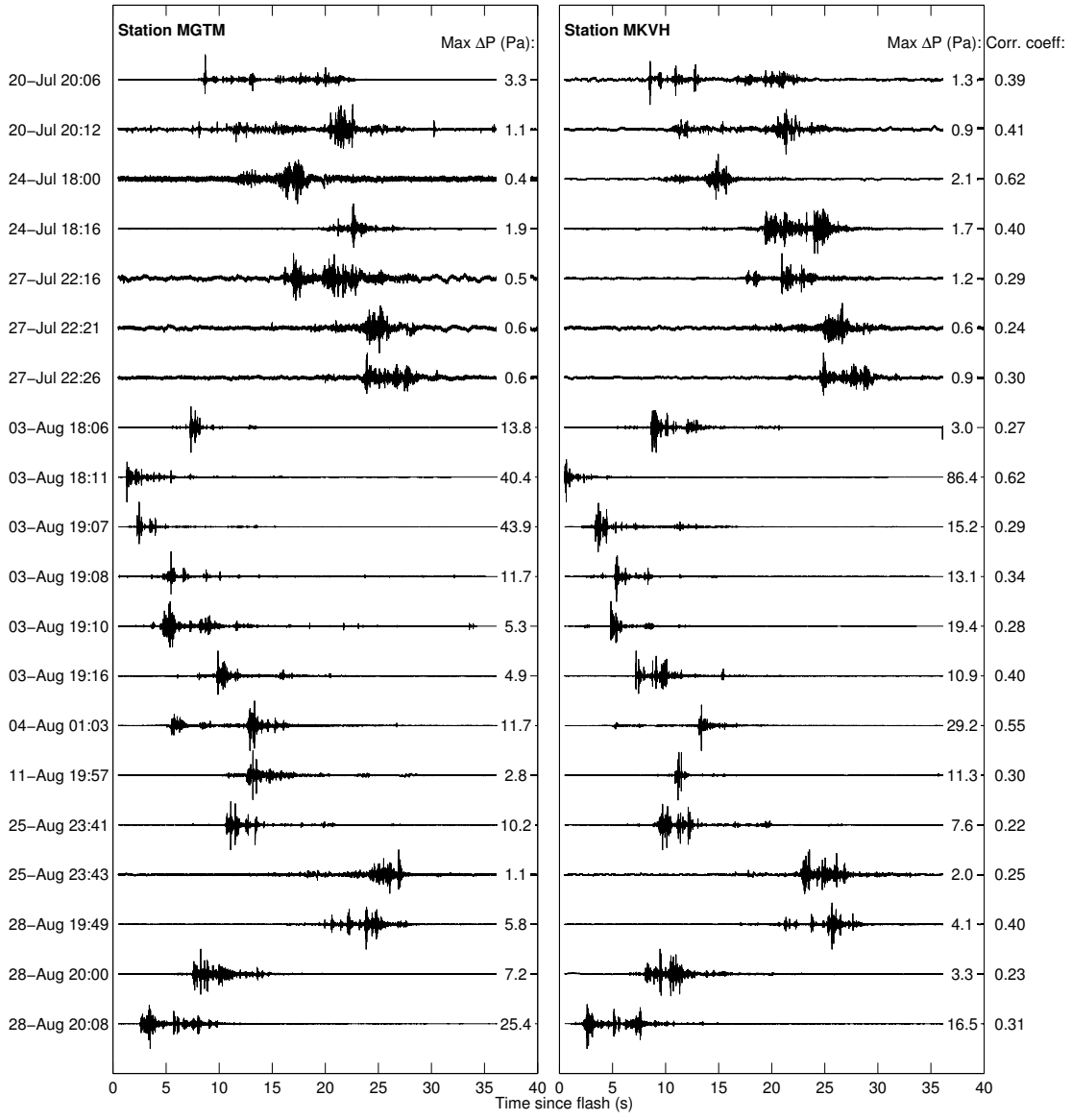

Figure 4.4: Selected IC events (17) are displayed similarly to CG events. See Figure 4.3.

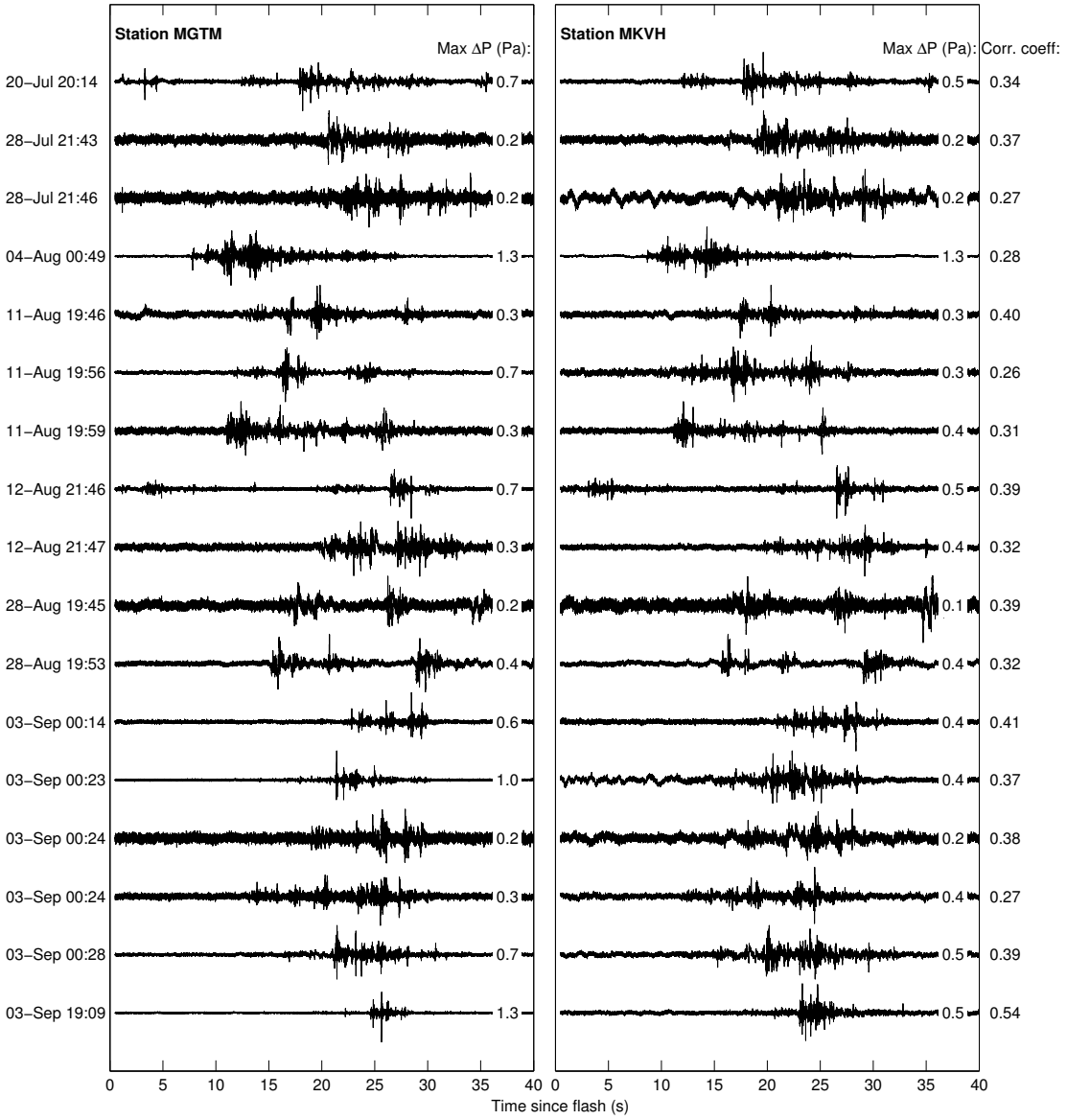

there is notable high-frequency content. Some sensors are not included in further analyses due to malfunctioning or excessive background noise. For example, the high-frequency spikes at LAN 2 are not real and are present for the month of July. Noise including highly directed wind gusts can occasionally mask signal at individual sensors or arrays.

I show similar plots for thunder originating from an IC flash in Figure 4.6. Amplitudes do not exceed approximately 1 Pa in this case. Low-frequency peaks are again prevalent and most energy at higher frequencies is contained below 100 Hz. Signal behavior is again unique to array locations. I show further examples of signals recorded across the network in Appendix C. These examples demonstrate the complexity of thunder signals and their dependence on relative observation position. This emphasizes the necessity of recording thunder data at multiple sensor locations.

In the Sections 4.2 and 4.3 I investigate the following parameters for signals of interest, primarily at GTM and KVH: peak reduced pressure, total acoustic energy, peak frequency, and energy ratio (see Section 4.3). I first consider whether arrays may exhibit location-specific biases. I calculate mean values for maximum reduced pressure, total acoustic energy, peak frequency, and energy ratio at individual arrays for my catalog. These values are plotted for the first 100 events in Figure 4.7 and for the last 91 events in Figure 4.8. Scales are logarithmic to show variation, especially for lower values. I sometimes see series of events with consistently high or low parameter estimates and some of these may be from the same storm - indicating storm location or properties. Variance between arrays is larger for higher values. However, none of the arrays show preferentially high or low average values for the season. Though some sites may be more or less subject

Figure 4.5: Signals and PSDs (both linear and logarithmic frequency axes) are shown for all stations for a CG event occurring on 20 July. Station name and channel number are to the left of the time series. Peak frequencies, in hertz, are noted on the logarithmic PSD plots. Vertical lines indicate the filter cutoff at 4 s. Y-axis limits vary.

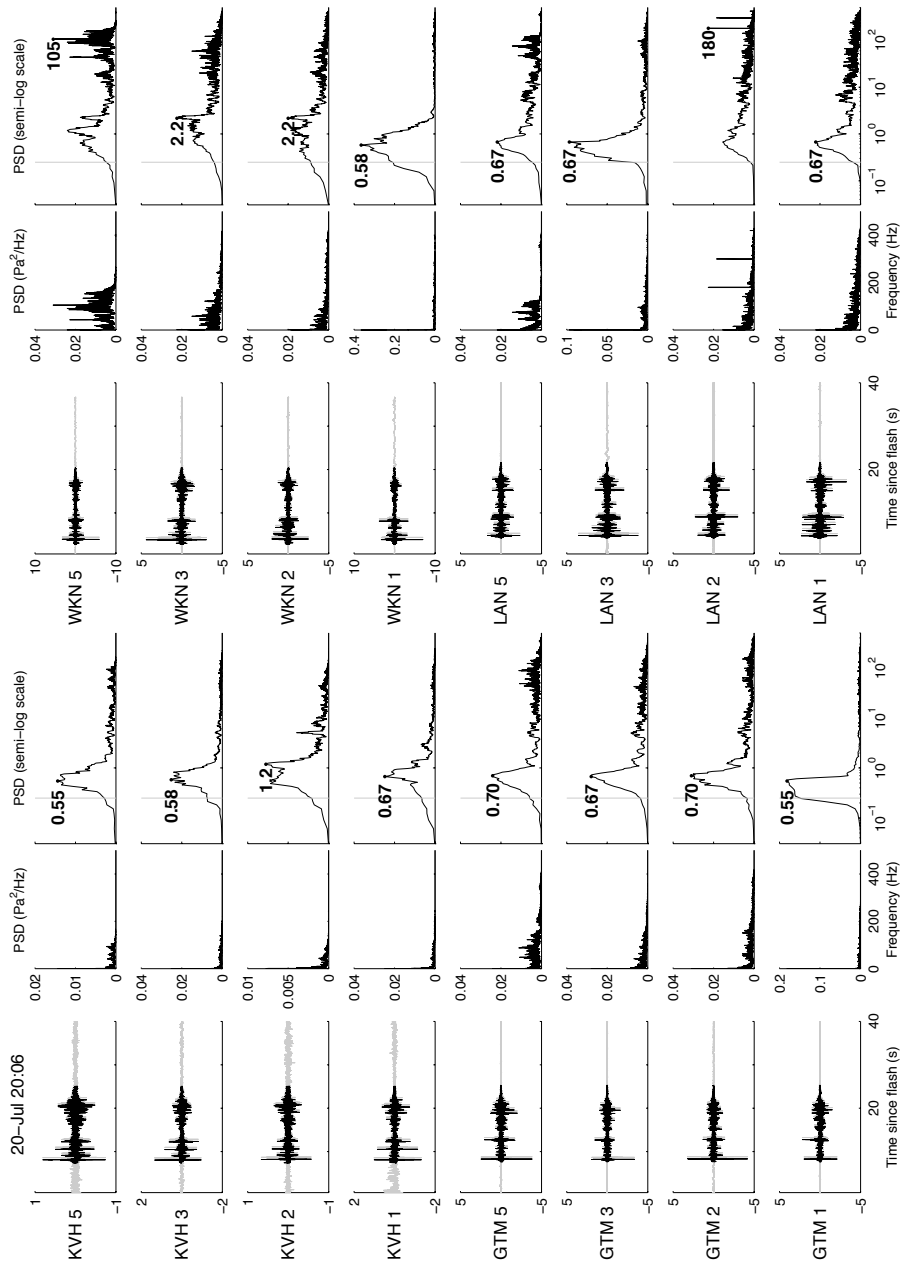

Figure 4.6: Signals and PSDs are shown for all stations for an IC event on 20 July. See Figure 4.5 for a detailed description of plot layout.

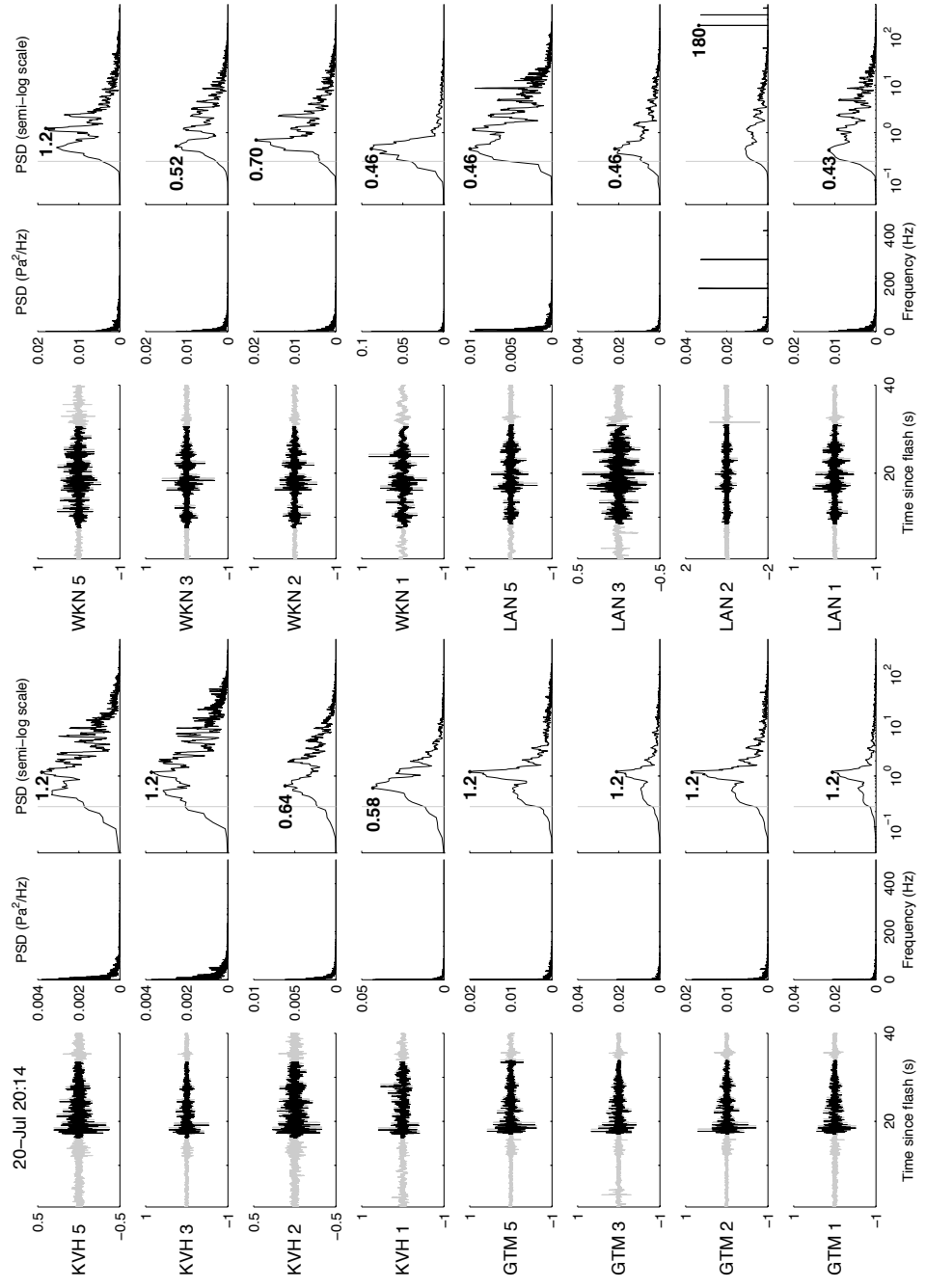

to noise sources, signal recorded at all arrays is useful for application to thunder studies.

Figure 4.7: Mean estimates of reduced peak pressure, total energy, peak frequency, and energy ratio are calculated for each event at each array. Events 1–100 are shown in this figure. CG and IC events are indicated by dots and triangles, respectively. Vertical axes are logarithmic. The number of channels contributing to the estimates at each array are shown in the bottom plot. Stations LAN and WKN were removed for a portion of the season.

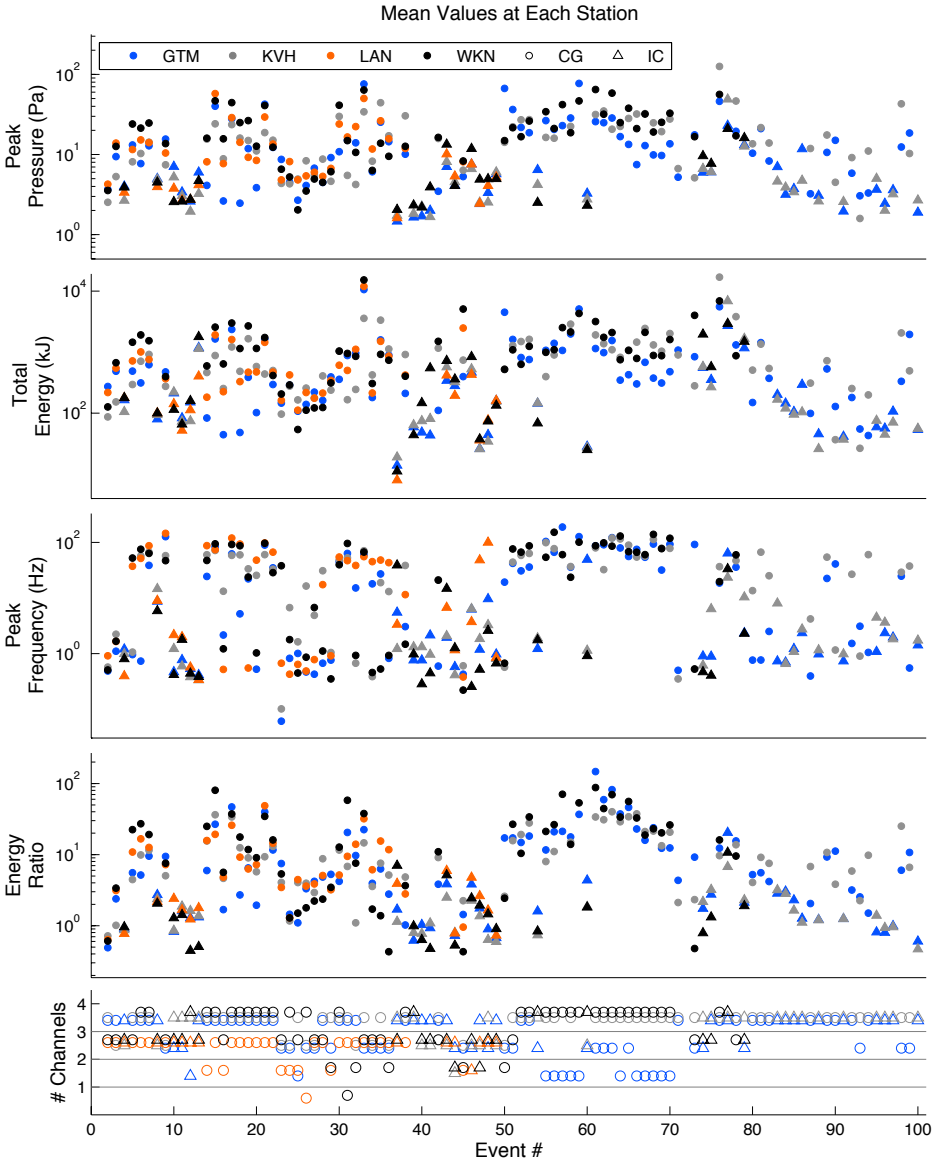

Figure 4.8: Array mean estimates of peak pressure, total energy, f_{max}, and R_E for events 101–191 in my catalog are shown. See Figure 4.7 for a figure description.

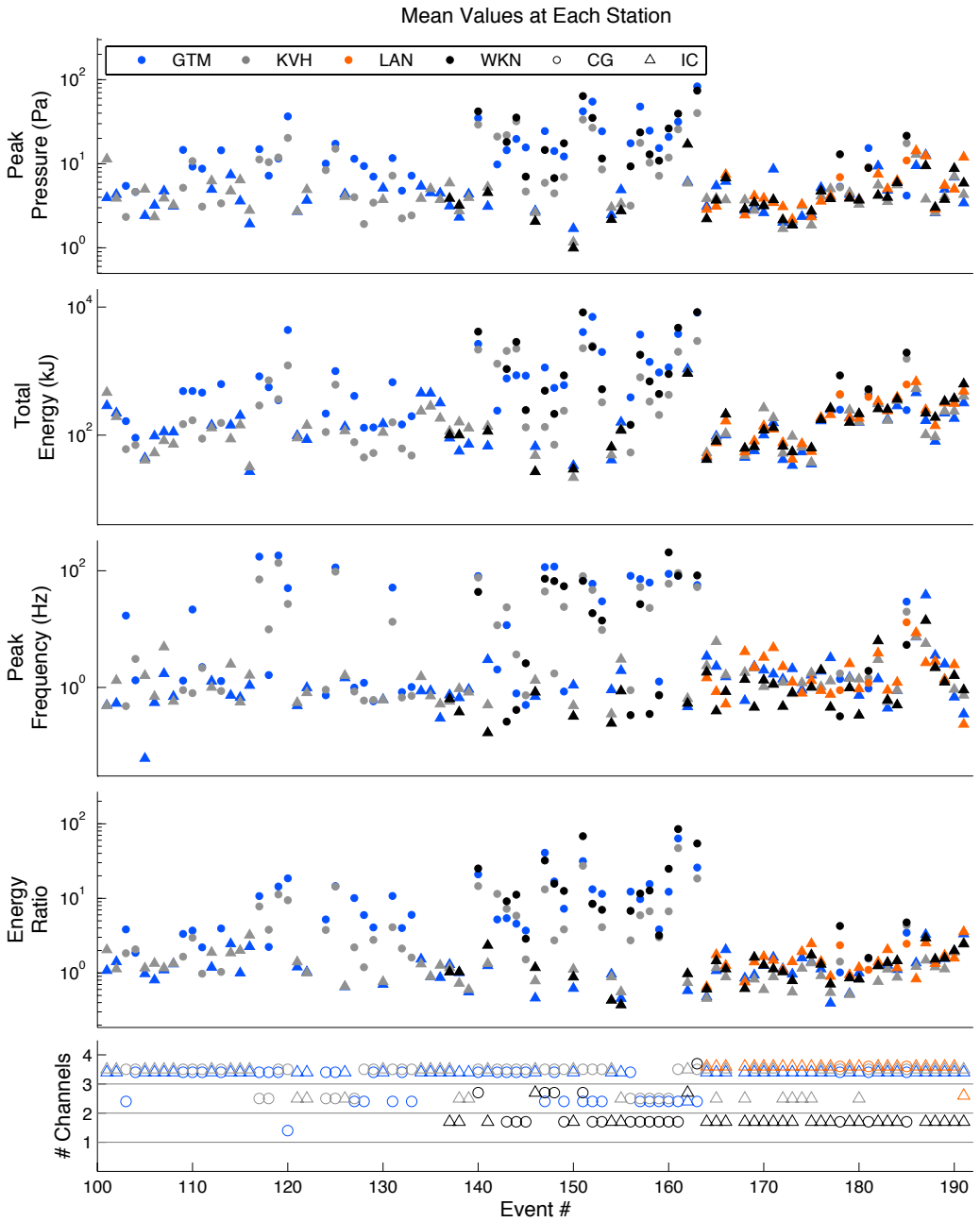

4.2 PEAK PRESSURES AND TOTAL ACOUSTIC ENERGY

In order to further quantify the similarities and differences between individual thunder signals, I focus on channels 3 at stations GTM and KVH. I first reduce all signal amplitudes to 1 km, as described in Section 3.5. Peak pressures for the reduced signals are sorted by flash type and are shown in Figure 4.9. I identify that thunder pressures at 1 km for IC lightning (median 4 Pa) are weaker than pressures for CG lightning (median 13 Pa). I compare the peak reduced pressures for all events at station KVH to station GTM in Figure 4.10. If signal amplitudes are not influenced by relative flash geometry, atmospheric variation, or array site effects, peak reduced pressures should be comparable at both stations. However, CG events ($R^2 = 0.31$) show poor correlation. Some pressure estimates vary by an order of magnitude between KVH and GTM. IC events show better agreement ($R^2 = 0.69$). Though reduced peak pressures are inconsistent between stations, high pressure values for CG thunder, compared to IC thunder, are indicative of intrinsic source properties.

Thunder acoustic energy is related to lightning source strength [*Depasse*, 1994; *Kinsler et al.*, 1999]. Because energy is calculated using entire signals, I expect energy estimates to be less influenced than peak pressures by atmospheric and recording site irregularities. I estimate total acoustic energy (W) for all signals in my catalog using Equation 2.1. Histograms of energies, differentiated by lightning flash type, are shown in Figure 4.11. Median energy for CG flashes is around 500 kJ, which is higher than the median energy of around 100 kJ for IC flashes. Mean energy estimates for CG and IC flashes are around 1000 kJ and 240 kJ, respectively. These are lower than mean values of 6400 kJ and 1900 kJ cited

Figure 4.9: Histograms showing peak pressures for all signals at 1 km. Estimates from KVH and GTM for 106 CG events are shown on the left and for 82 IC events on the right. Note logarithmic x-scale (this was necessary to demonstrate variation).

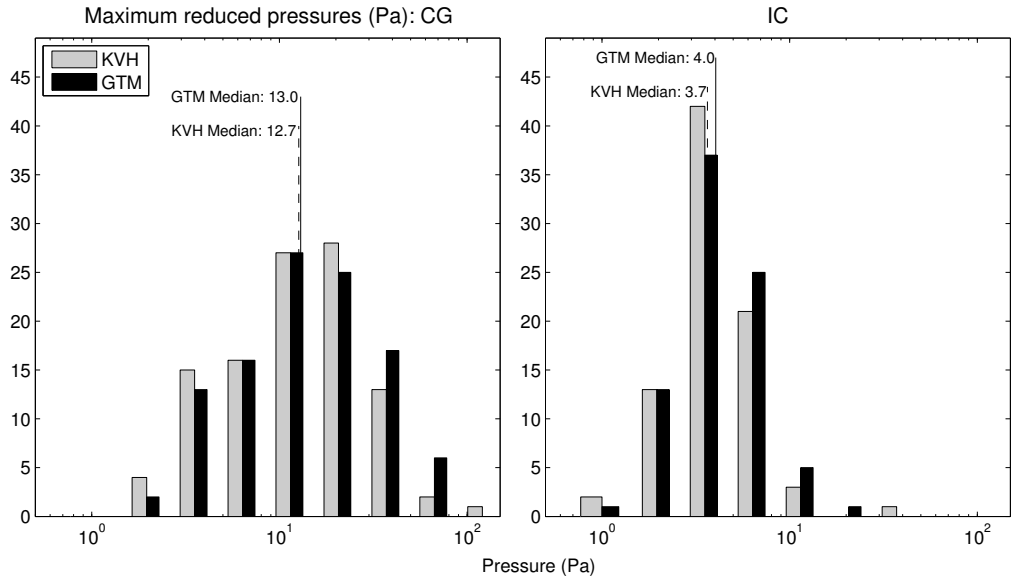

by *Holmes et al.* [1971], likely due to a larger available data set and lower detection threshold. Figures 4.9 and 4.11 show that CG thunder is "louder" and more energetic than IC thunder.

A comparison between estimated energies at stations KVH and GTM is shown in Figure 4.12. I see improved agreement for energy estimates compared to reduced pressures (Figure 4.10), though correlation for IC events ($R^2 = 0.87$) is again much higher than for CG events ($R^2 = 0.37$). I quantify scatter using a ratio of energies for all events at each station (E_{KVH}/E_{GTM}). I expect this ratio to be close to 1 if stations are well-correlated. The mean energy ratio for IC events is 0.96 with a standard deviation of 0.37. For CG events the mean ratio is 1.6 with a standard deviation of 2.3. Differences for these two flash types may be due to relative source-receiver distances, as described in Section 5.1.

Figure 4.10: Reduced peak pressures, in pascals, are plotted at KVH versus GTM. Log-log scale is used for display purposes; R^2 value for linear relationship is given. IC events (triangles) and CG events (dots) are differentiated.

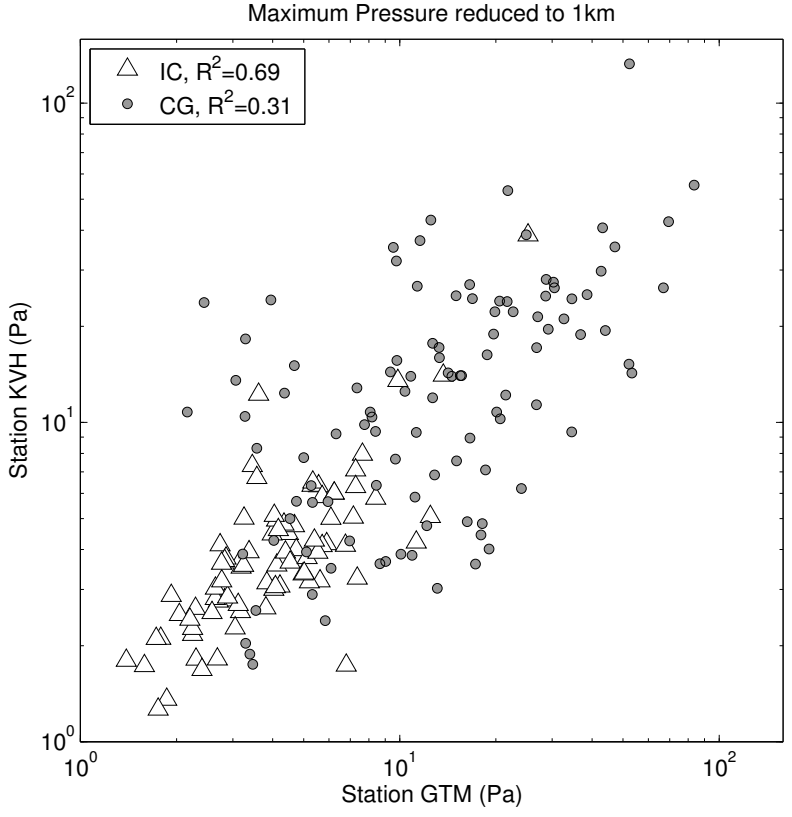

Figure 4.11: Histograms showing total acoustic energy (kJ) estimated for KVH and GTM for all signals. Note that x-axis is logarithmic.

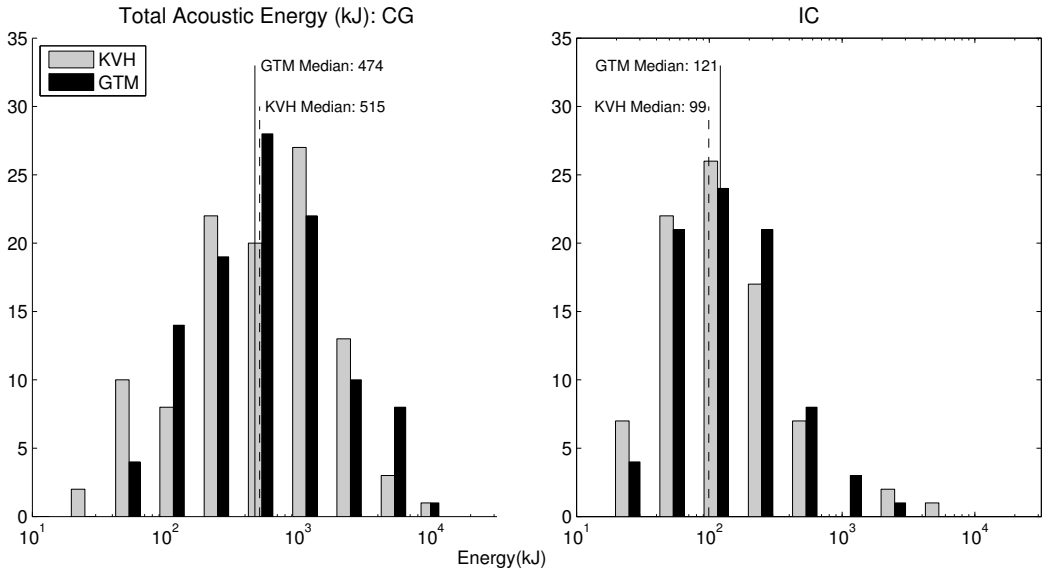

In order to test the robustness of my observations I find the mean and standard deviation of peak reduced pressure and total acoustic energy for each event at all functioning sensors. These values are shown for the first 100 cataloged events in Figure 4.13 and for the last 91 events in Figure 4.14. I see higher means and deviations for both metrics for thunder originating from CG flashes, as compared with IC. My detailed analysis at sensors at GTM and KVH indicate that energy values are more representative of overall signal behavior than reduced presures. Energies can be robustly estimated for IC thunder; however, caution must be used when assuming a series of point source locations to quantify thunder energies.

Figure 4.12: Total energy is plotted for all events comparing estimates at KVH and GTM. R^2 values are given for a linear relationship.

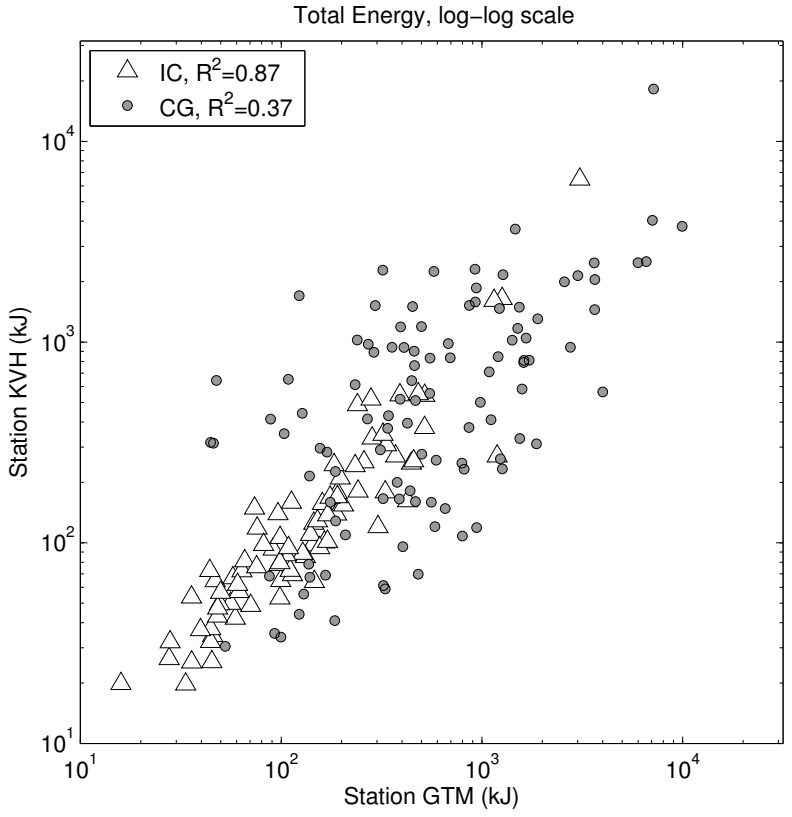

Figure 4.13: Mean reduced peak pressure (top) and mean total acoustic energy (middle) are shown for the first 100 catalog events utilizing all stations. Horizontal axis is event number, and while chronological, does not indicate actual elapsed time. CG and IC events are differentiated by dots and triangles, respectively. The bottom plot indicates how many channels contributed to each estimate.

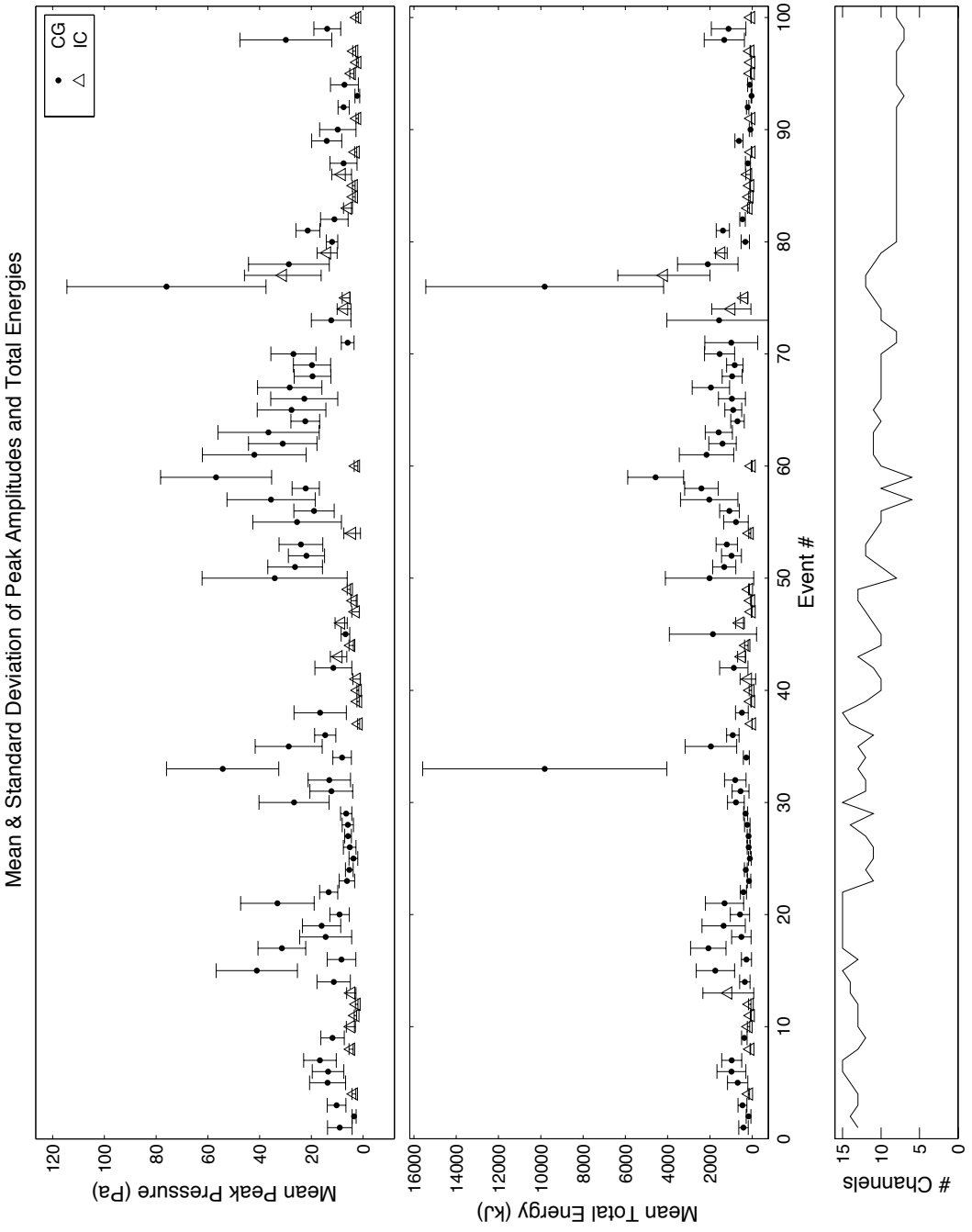

Figure 4.14: Mean and standard deviation of peak pressures and total energies are shown for events 101–191 in my catalog. The bottom plot indicates the number of channels contributing to the mean.

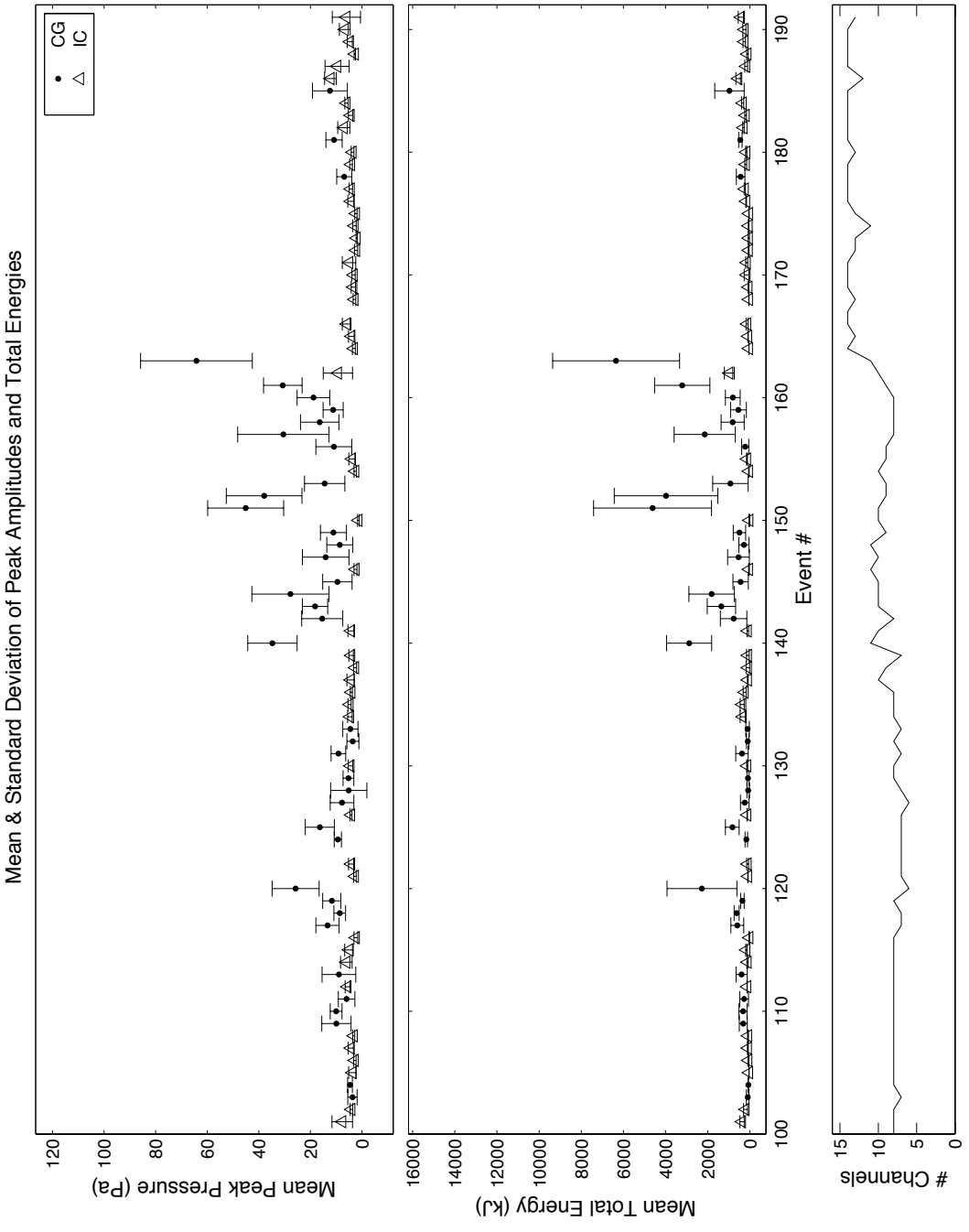

4.3 SPECTRAL CONTENT OF THUNDER

The spectrum of a thunder signal from one lightning flash is a superposition of spectra from multiple channel segments and strokes [*Few*, 1969]. Details in the power spectrum of thunder are dependent on recording position. The distance dependence of the spectrum can be qualitatively observed - consider how the sound of thunder differs for a nearby flash, compared to a distant one. Atmospheric effects, such as directed winds, also influence spectral content [*Bohannon et al.*, 1977]. For signals recorded at varying distances, the majority of the spectrum is contained in the first couple hundreds of Hz [*Few*, 1969; *Holmes et al.*, 1971] though *Depasse* [1994] investigated energy up to 10 kHz.

In Figure 4.15 I show a selection of nine CG signals (and their corresponding PSDs) from Figure 4.3. PSDs are very jagged with peak frequencies between tenths of hertz and just over 100 Hz. Recorded peak frequencies (f_{max}) at the two stations are not always similar. Many PSDs have a low f_{max} value but significant structure at high frequencies (e.g. 24 July 18:00). Figure 4.16 shows 9 IC signals from Figure 4.4. Peak frequencies are below 5 Hz in all cases but are still variable between stations. There appears to be less energy at higher frequencies, compared to the CG records.

I inspect general thunder spectral behavior at KVH and GTM. Figure 4.17 shows the percentage of total power recorded at channel 3 at each station for all events, in 20 Hz bands between 0 and 500 Hz. The stations show similar trends. For IC events, most power is contained below 100 Hz and the power falls off rapidly above this point, due to both source characteristics and atmospheric attenuation. For CG events, power covers a broader spectral range, though most energy is contained below 200 Hz.

Figure 4.15: Plots showing signals and PSDs for 9 CG events (GTM plots left, KVH plots right). PSDs are shown with both linear and logarithmic frequency axis. Peak frequencies (in hertz) are indicated for each signal on logarithmic PSD.

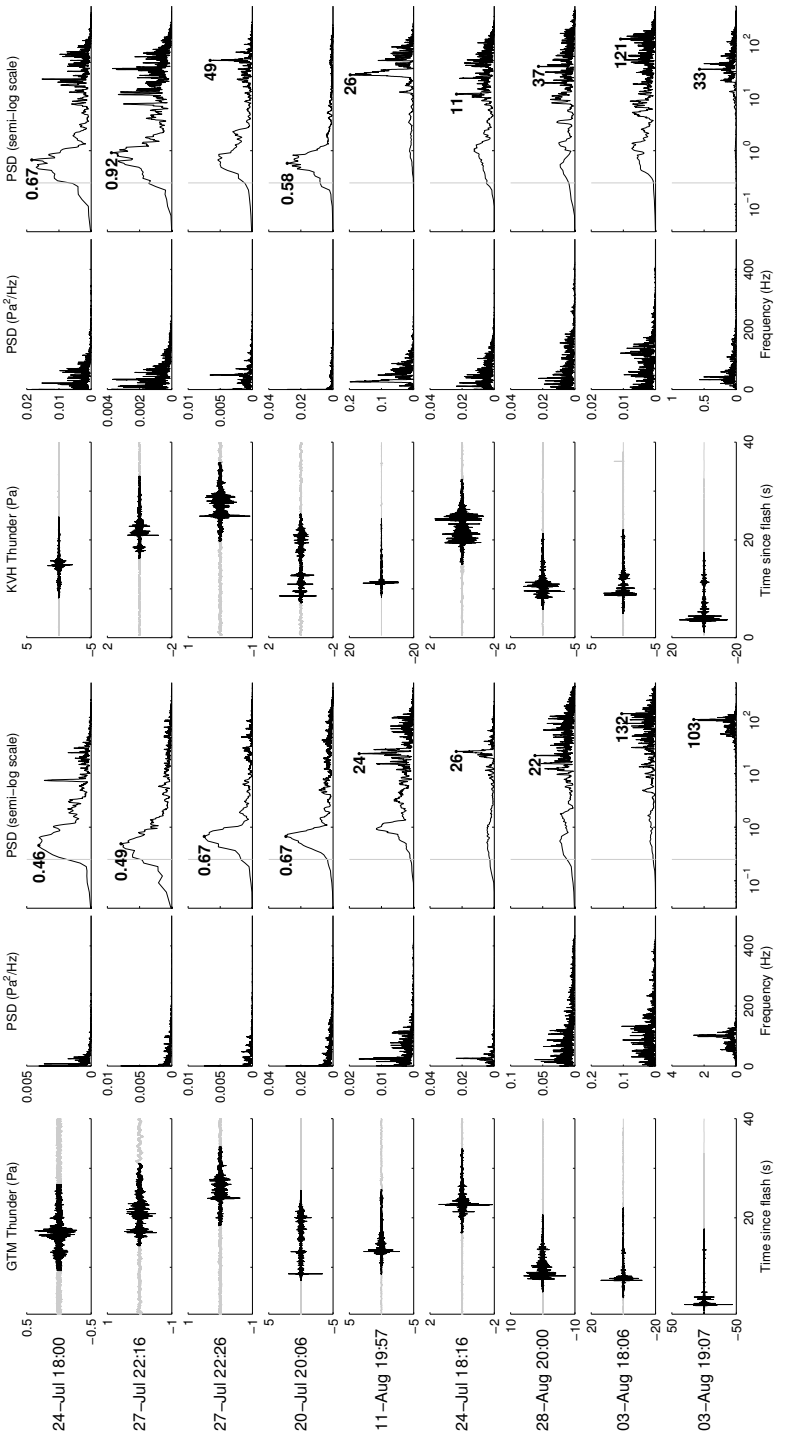

Figure 4.16: Plots showing signals and PSDs for 9 IC events at GTM and KVH.

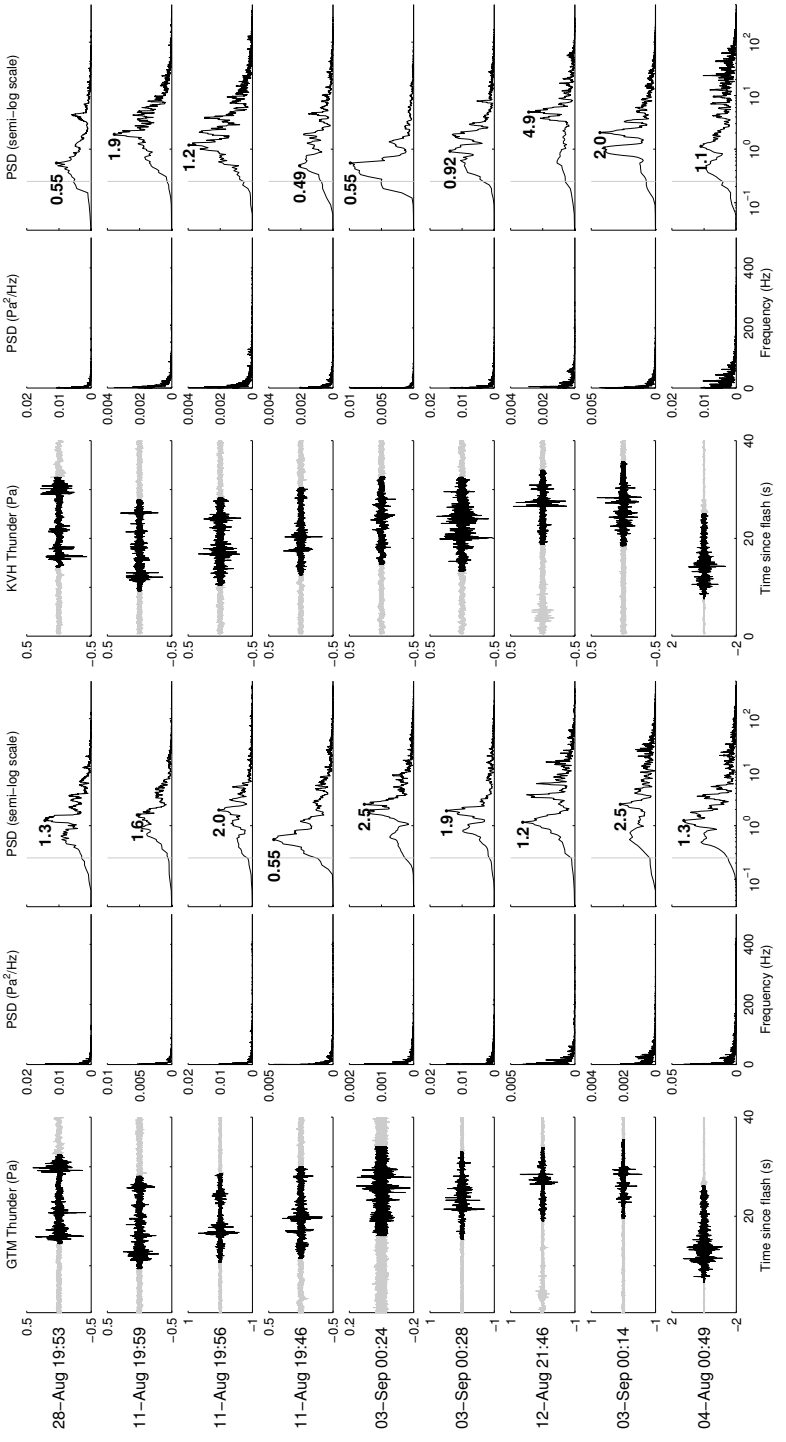

Figure 4.17: Percentage of total power recorded for all events at KVH and GTM shown in consecutive 20 Hz bands (0–20, 20–40...480–500 Hz). Values are shown on the left for CG events and on the right for IC events. Point locations are at the midpoint of each band (10, 30...490 Hz).

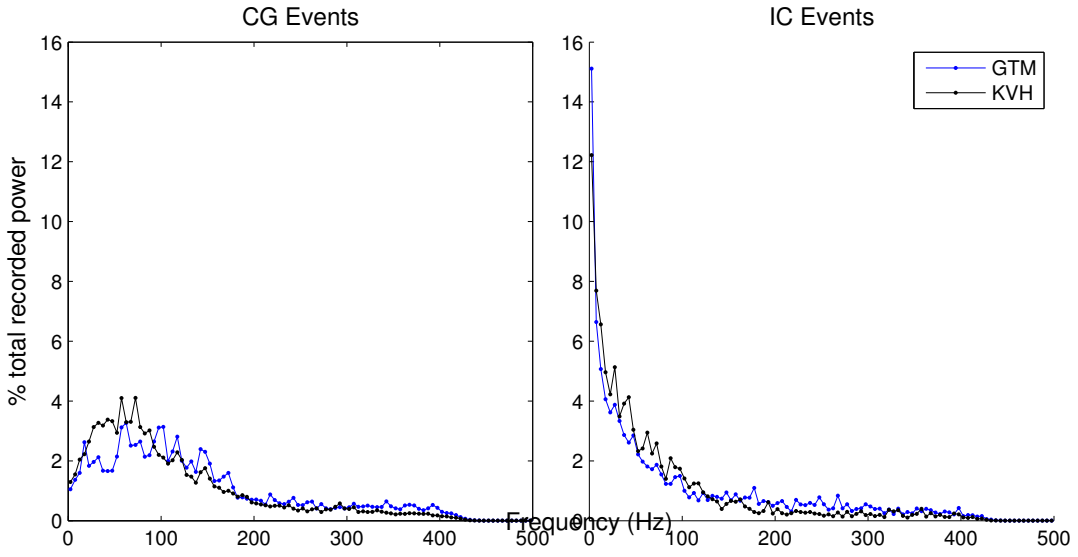

I estimate median PSDs for the 106 CG events and 82 IC events in my catalog (Figure 4.18). The median is a more robust estimate than the mean in this case due to the jaggedness of PSDs. Median PSDs at KVH and GTM show similar behavior, though small-scale variations may be due to local site effects such as topography. The interquartile range is also shown and significant variability is evident. The estimated median PSD for IC thunder peaks at or below 1 Hz and falls off monotonically at higher frequencies. The estimated PSD for CG events has a significant peak around 1 Hz similar to that for IC events but also has a peak near 100 Hz. The rapid falloff above 100 Hz is due largely to attenuation, though thunder usually peaks at or below 100 Hz [*Few*, 1969; *Holmes et al.*, 1971]. Peak power amplitudes are much higher for the CG median PSD than for the IC median PSD.

Figure 4.18: Median PSDs for CG (106 events) and IC (82 events) thunder and corresponding median PSDs for noise intervals spanning 5 s to 1 s prior to event onsets are calculated. Plots show event medians in black with the interquartile range shaded gray. Noise medians are in red with the interquartile range shaded in red. Median PSDs for station GTM are on top and for KVH are on the bottom. CG thunder contains more power overall and more structure at high frequencies.

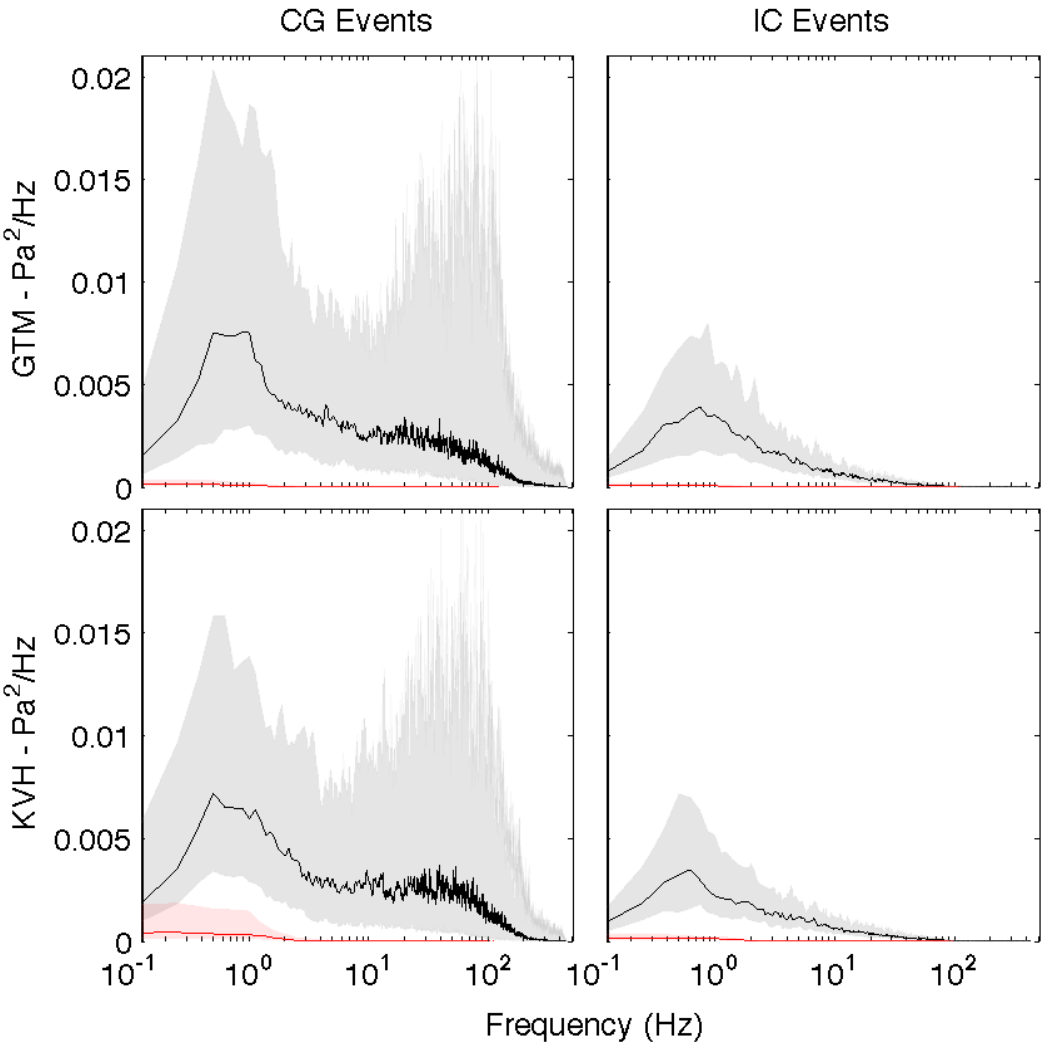

I compare and show a histogram of peak frequencies recorded at KVH and GTM in Figure 4.19. Peak frequencies span a wide range of the spectrum between tenths of hertz and hundreds of hertz. The highest peak frequency observed at GTM is 240 Hz and at KVH is 134 Hz. There is an apparent bimodal distribution in f_{max} with a low point at around approximately 10–15 Hz. Of the recorded IC events, 97% peak at less than 15 Hz at both stations. KVH records a number of events with high peak frequencies not seen at GTM. KVH may be preferentially closer to storm systems (reducing high-frequency attenuation). Alternatively, GTM may have regular sources of noise, such as local winds. In Section 4.1, I investigate mean estimates at each array to ensure there is no location-specific systematic bias.

The wide range of peak frequencies, the jaggedness of the PSDs shown in Figures 4.15 and 4.16, and the lack of correlation in f_{max} between stations (see the left plot in Figure 4.19) indicate that peak frequency is not necessarily an ideal metric for quantifying broadband thunder spectra. For example, local winds or the presence of the electrostatic mechanism explained in Section 2.3 can create a low frequency peak in a thunder signal that is dominated by high frequency content. Quantifying the energy in a passband averages the effects of a noisy spectrum.

Though peak frequencies may be biased or vary depending on recording location, the distribution in Figure 4.19 suggests two classes of thunder signals: those with most energy in the infrasonic band and those with most energy in the audible band. I calculate and compare total acoustic energy (W, calculated using Equation 2.1) in multiple bandwidths for all signals. I filter signals in two bands and investigate the ratio in energy, R_E:

$$R_E = \frac{W_{band1}}{W_{band2}} \tag{4.1}$$

Figure 4.19: I compare peak frequencies between stations KVH and GTM (channel 3) and show peak frequencies differentiated by flash type (left panel). Left plot is on a log-log scale. Histogram of peak frequencies for all events at both KVH and GTM is shown on the right. Note logarithmic x-scale. Low point in the distribution is between 10 and 15 Hz.

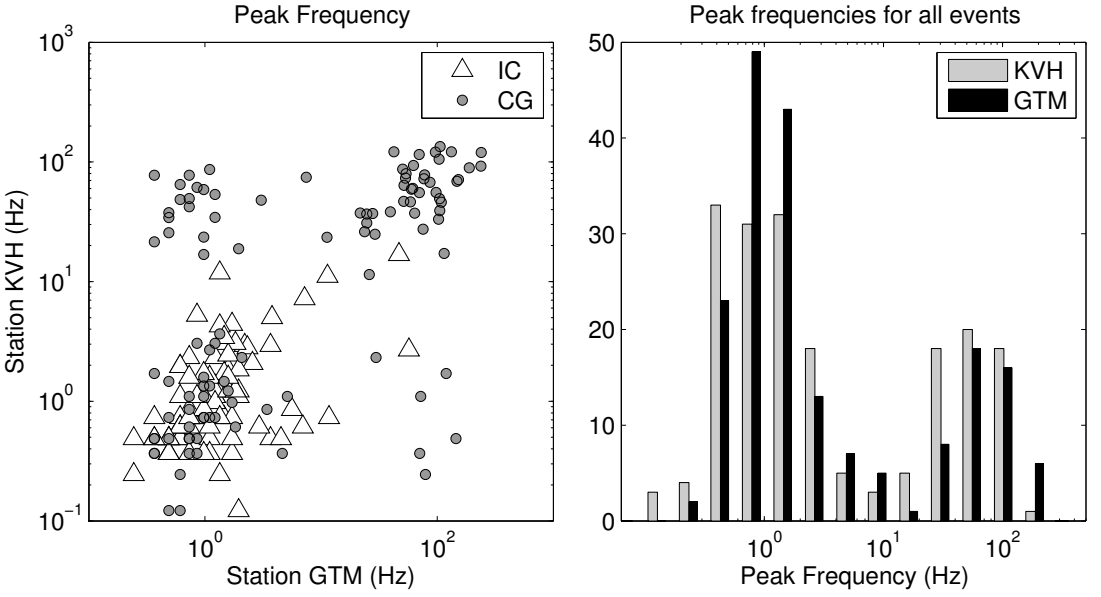

I find that, by comparing the total energy contained above 15 Hz to the energy between 1–15 Hz I see distinct distributions for IC and CG signals. A signal with $R_E = 1$ contains equal amounts of estimated energy in both bands. I note that the calculation of total acoustic energy will tend to favor low frequencies for signals recorded at greater distances. Because high-frequency energy is attenuated, especially above 100 Hz, the estimate of W will be low. I compare R_E at both channels and show a histogram of R_E values for all events in Figure 4.20. R_E values are better correlated between stations than f_{max} values. The R_E distribution is non-normal with a median value of approximately 2.5 (corresponding to signals containing $\approx 70\%$ of their total energy above 15 Hz).

Figure 4.20: R_E for channels 3 at stations KVH and GTM (>15 Hz compared to 1–15 Hz) is shown on the left with IC and CG lightning sources indicated. Histogram of R_E for all signals at KVH and GTM is on the right. Note logarithmic x-scale. Median R_E is noted for each station on the histogram.

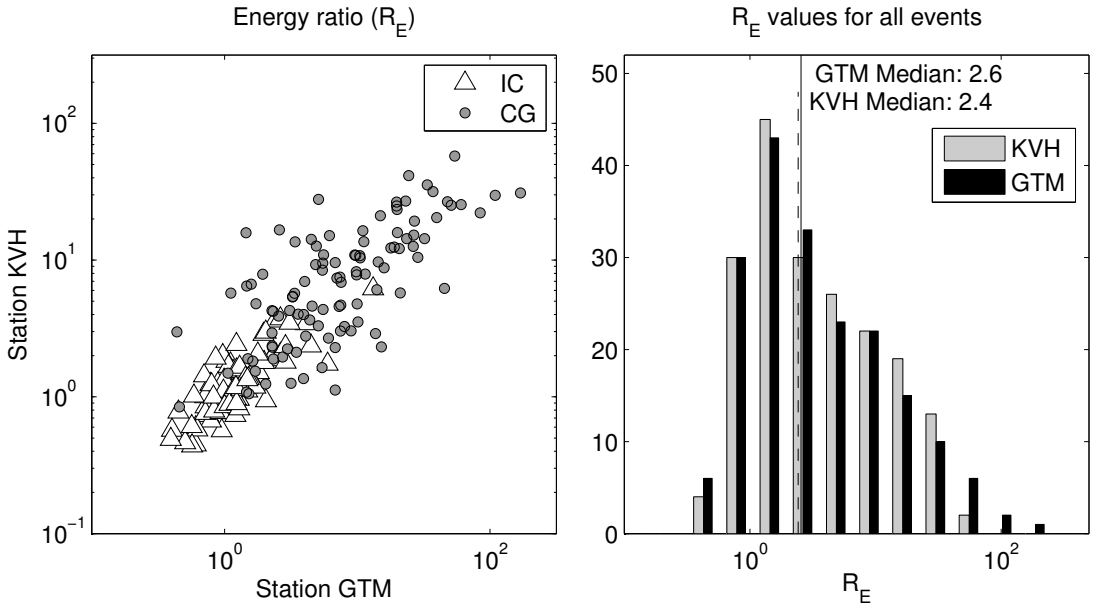

I demonstrate in Section 4.2 that CG and IC thunder signals tend to have different pressure amplitudes and energies. In Figure 4.21 I compare R_E distributions for CG and IC events at both GTM and KVH. The two flash types show

noticeably different distributions. The median of the IC distribution at both stations is 1.1, indicating nearly equal amounts of energy in both bands. CG events show a broader distribution but tend to have more high-frequency energy.

Figure 4.21: Energy ratio histograms separated by flash type (CG and IC) shown at KVH and GTM. R_E=4 is indicated. Median R_E is ≈ 7 for CG events and ≈ 1.1 for IC events at both stations.

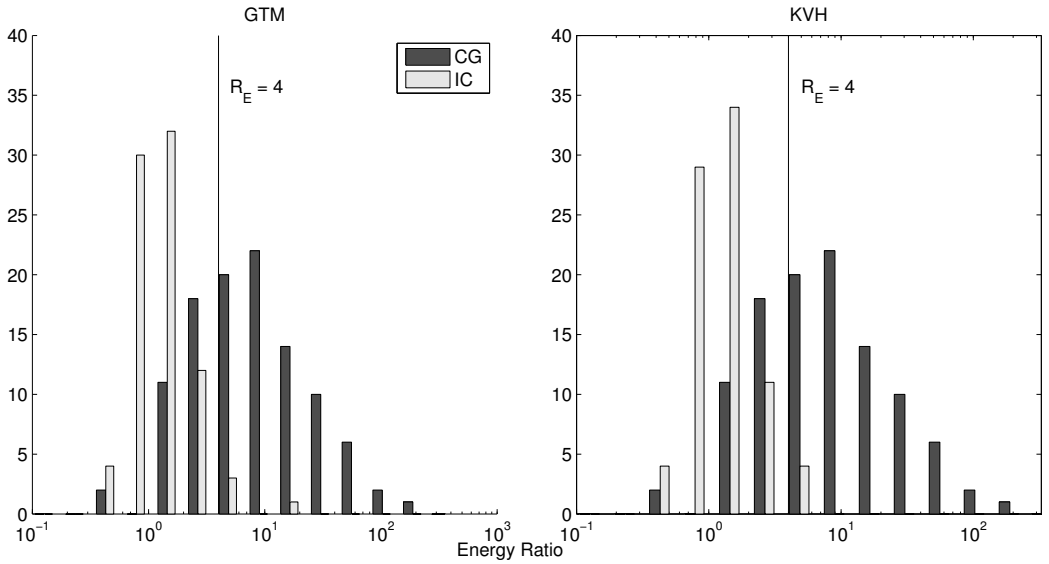

I consider the influence of distance on the frequency content of thunder. I can estimate the minimum distance to the lightning flash from each station using Equation 2.2. In Figure 4.22 I compare f_{max} and R_E for all events at GTM and KVH (channel 3) to their corresponding minimum distances. The nearest flash location may not correspond to the most energetic part of the flash but Figure 4.22 provides a general idea of distance dependence of f_{max} and R_E. High peak frequency events correspond to lightning that has at least one channel extending to within 5 km of the arrays. IC thunder events, even with nearby lightning channels, rarely exhibit high peak frequencies. Energy ratio shows a falloff with distance to the nearest channel. This is expected, as low frequency energy is

Figure 4.22: Peak frequency (top panel) and energy ratio (bottom panel) are compared to minimum distance to lightning source for each event. The minimum distance is estimated using the earliest thunder arrival for each station.

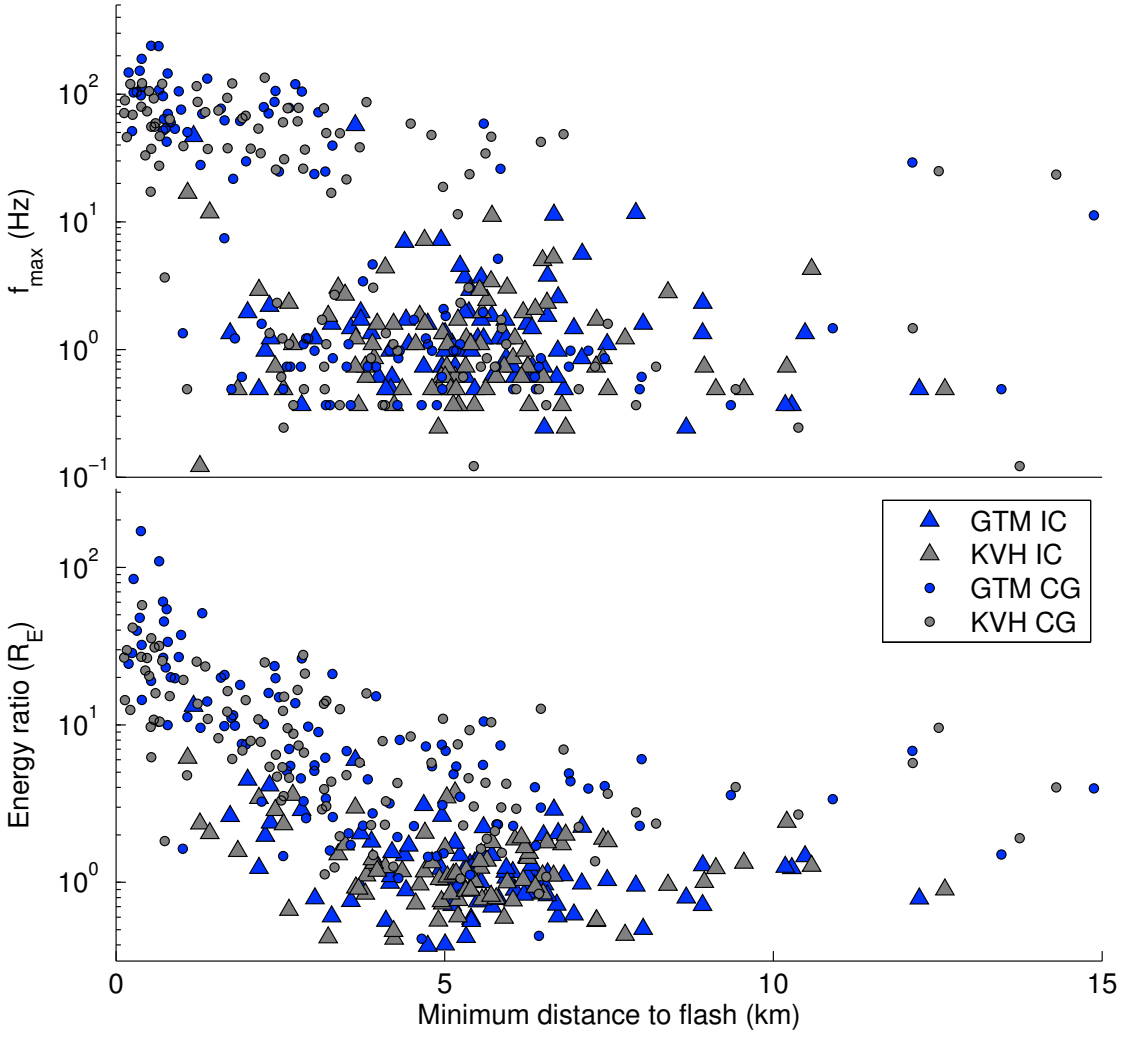

enhanced in the calculation of R_E for distant sources. However, R_E is consistently lower for IC thunder for all minimum channel-array distances.

An important consideration is the consistency in frequency content recorded across the network. Low frequencies may be due to site-specific noise. I show in Figures 4.23 and 4.24 the mean and standard deviation for f_{max} and R_E for each event. The mean for each event incorporates values from all sensors that are functioning properly. Low frequency content is often consistently recorded across the network, indicating that these low frequencies are indeed real. I verified in Section 4.1 that individual arrays do not show location-specific bias for peak frequency or energy ratio (see Figures 4.7 and 4.8).

To further relate flash type to the frequency content of thunder I compare f_{max} and R_E values in Figure 4.25. The previously mentioned bimodal distribution in peak frequency is apparent. Lines at $R_E = 1$ and the median R_E of ≈ 2.5 from Figure 4.20 are shown. I find that there is a distribution in event type around a value of $R_E = 4$ (also shown). Events to the right of this line have at least 80% of their estimated total energy in the >15 Hz band. Events to the left of this line contain 20% or more of their total energy between 1–15 Hz. I classify events as "low-frequency" if they have an R_E less than 4 and "high-frequency" if R_E is greater than 4.

All CG events with $f_{max} > 15$ at either channel also have $R_E > 4$ at one or both stations. While only 63% of all CG events have $f_{max} > 15$ at either station, an additional 19% of CG events have an $R_E > 4$. These events have notable spectral character at high frequencies that is not reflected by their low peak frequencies. However, low peak frequencies may be important, as they may indicate a contribution from the electrostatic mechanism, as discussed in Section 5.2. Of

Figure 4.23: Mean peak frequency and mean energy ratio (middle) are estimated for events 1-100 in my catalog. Means are calculated using all functioning channels. Horizontal axis is event number, and while chronological, does not indicate actual elapsed time. CG and IC events are differentiated by dots and triangles, respectively. The bottom plot indicates how many channels contributed to each estimate.

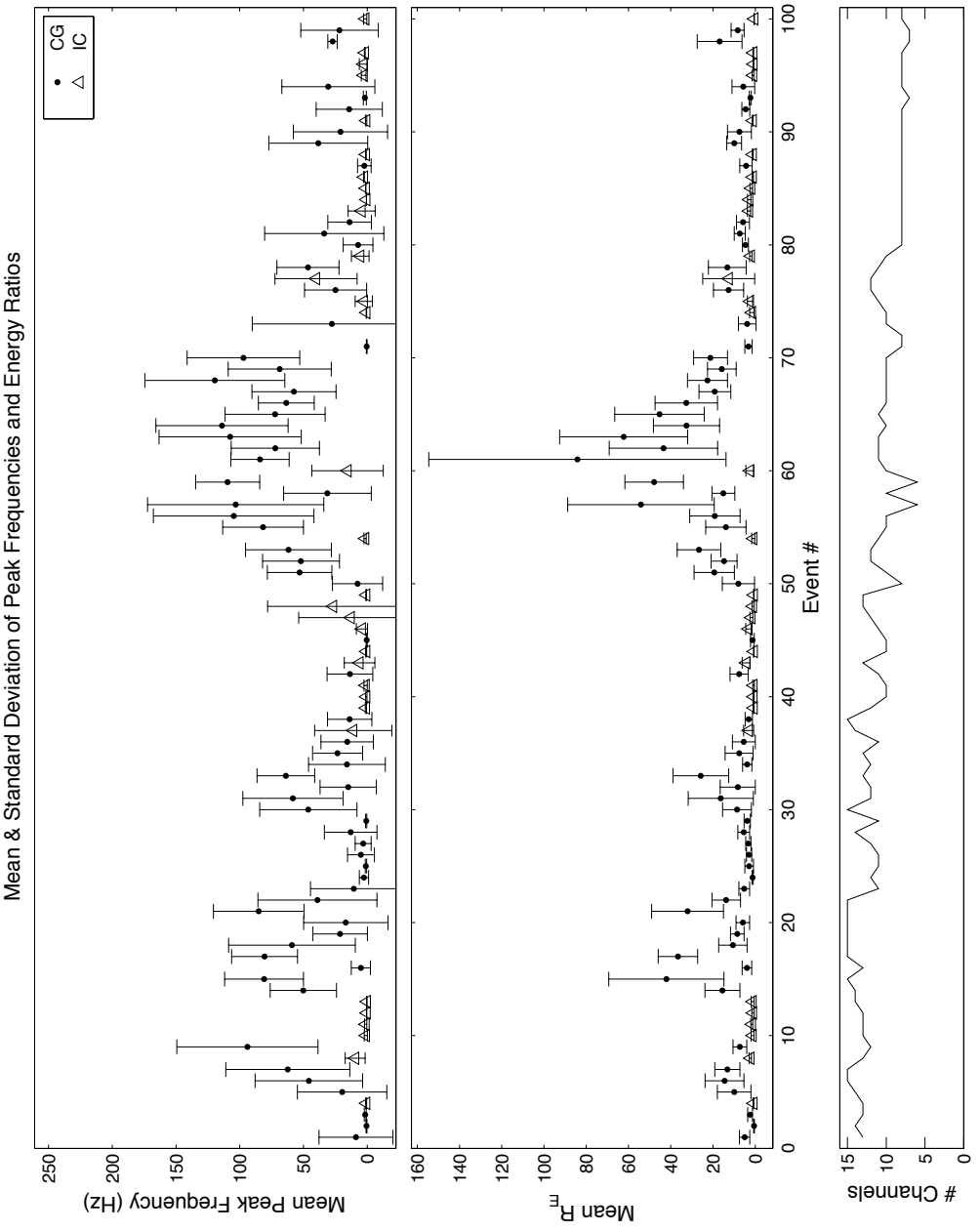

Figure 4.24: Means and standard deviations of peak frequency and energy ratio are estimated using all functioning sensors. Plots span events 101-191 in my catalog.

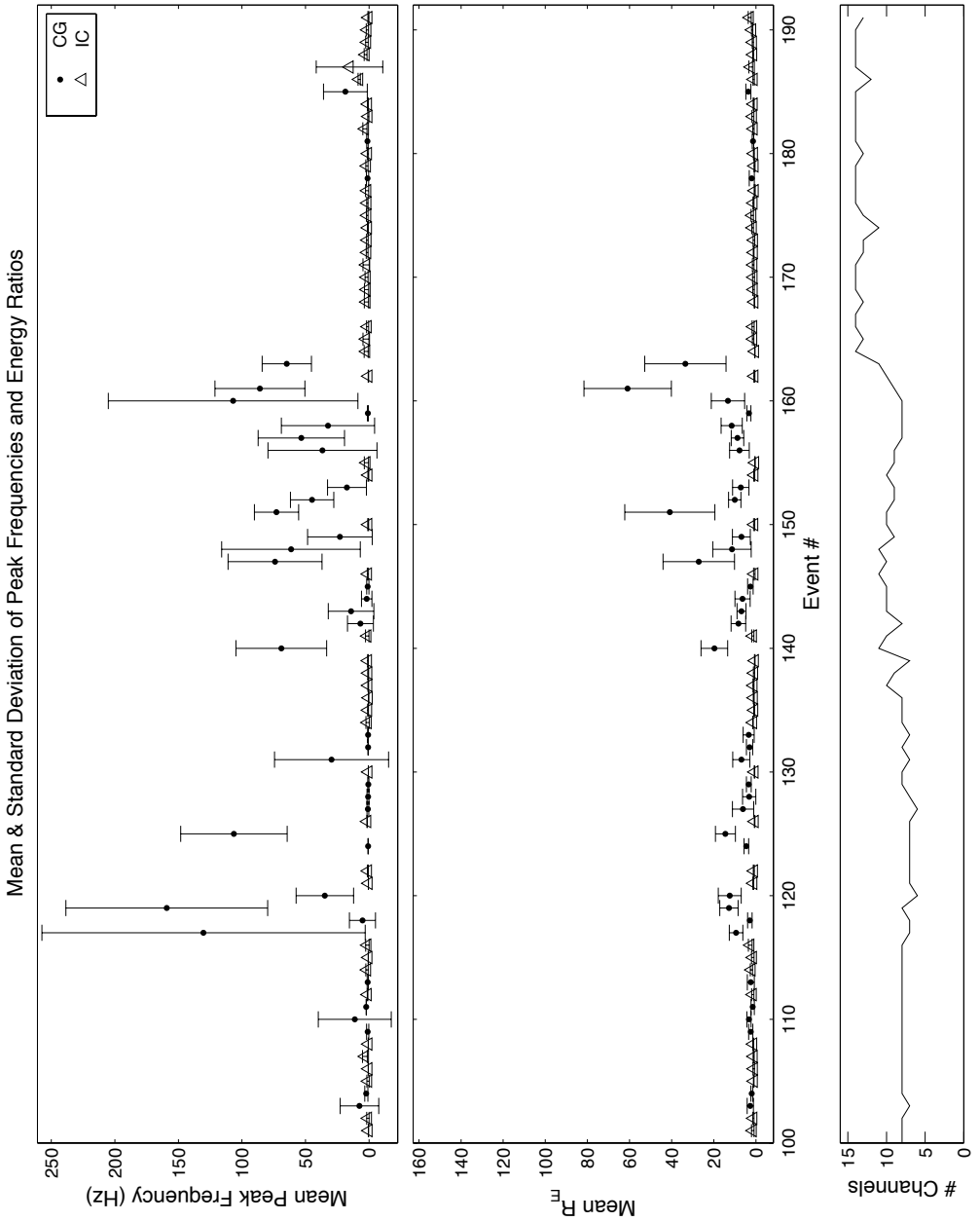

cataloged events, 95% with an R_E value greater than 4 at either KVH or GTM are from CG flashes while 80% of events with R_E less than 4 at both stations originate from IC flashes. Peak frequency, in conjunction with a ratio of high- and low-frequency energy at multiple stations, may indicate source lightning properties. Using multi-station observations of the spectral content of thunder, it may be possible to determine whether a lightning source includes a CG component.

I further emphasize the relationship between frequency content and source type in Figure 4.26. There are 131 events in my catalog for which the standard deviation is less than the mean for all metrics that I calculate (reduced peak pressure, total energy, peak frequency, and energy ratio). I show mean f_{max} versus mean R_E for these events using all functioning sensors across the network in each case. Nearly 80% of events with $R_E < 4$ and $f_{max} < 15$ originate from IC flashes. 98% events with high R_E and f_{max} are from CG lightning. The observations in Figure 4.25 are therefore consistent.

Figure 4.25: Peak frequency versus energy ratio plotted on a log-log scale. IC and CG events are differentiated and shown for both KVH and GTM. Horizontal line at 15 Hz indicates cutoff for R_E calculations. Vertical lines are shown for $R_E = 1$; the median of the R_E distribution, $R_E = 2.5$; and $R_E = 4$, the cutoff for identifying high- and low-frequency events.

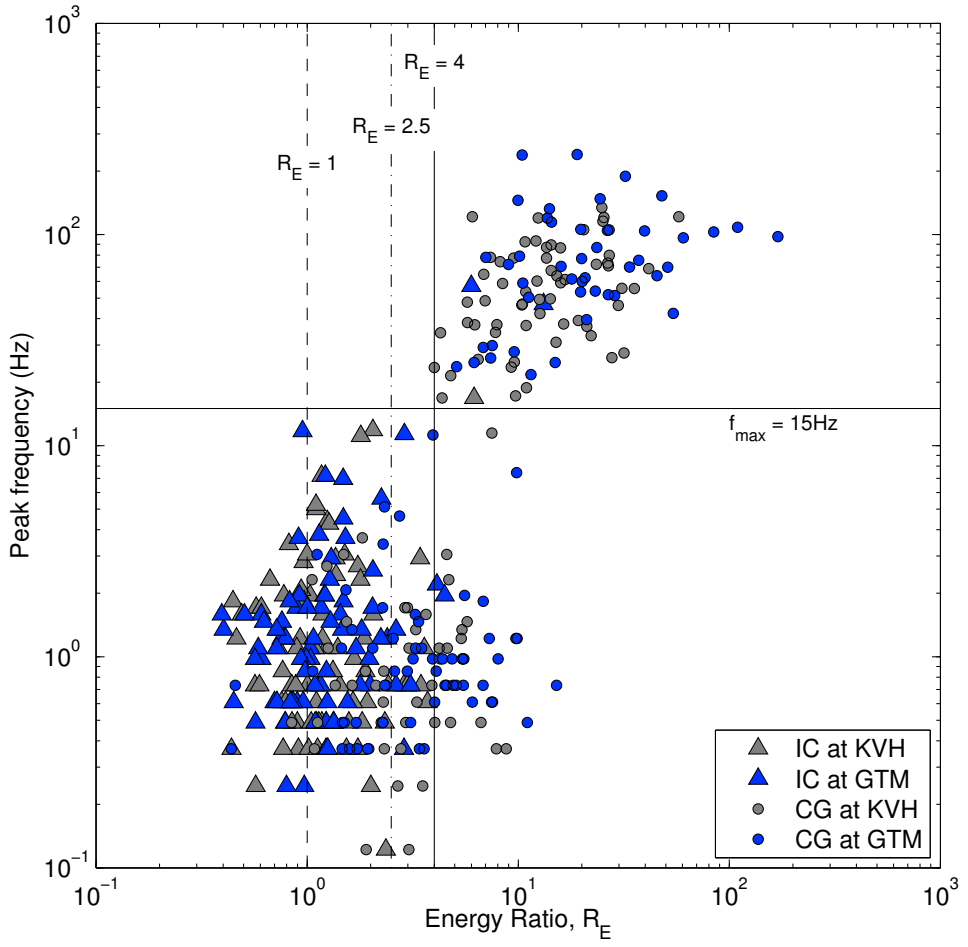

Figure 4.26: A log-log plot showing mean f_{max} and mean R_E for 131 events. The mean is calculated using all function channels. The events used had standard deviations less than means for all metrics of interest. Lines indicate $f_{max} = 15$ Hz and $R_E = 1$, 2.5, and 4, as in Figure 4.25. CG and IC sources are differentiated.

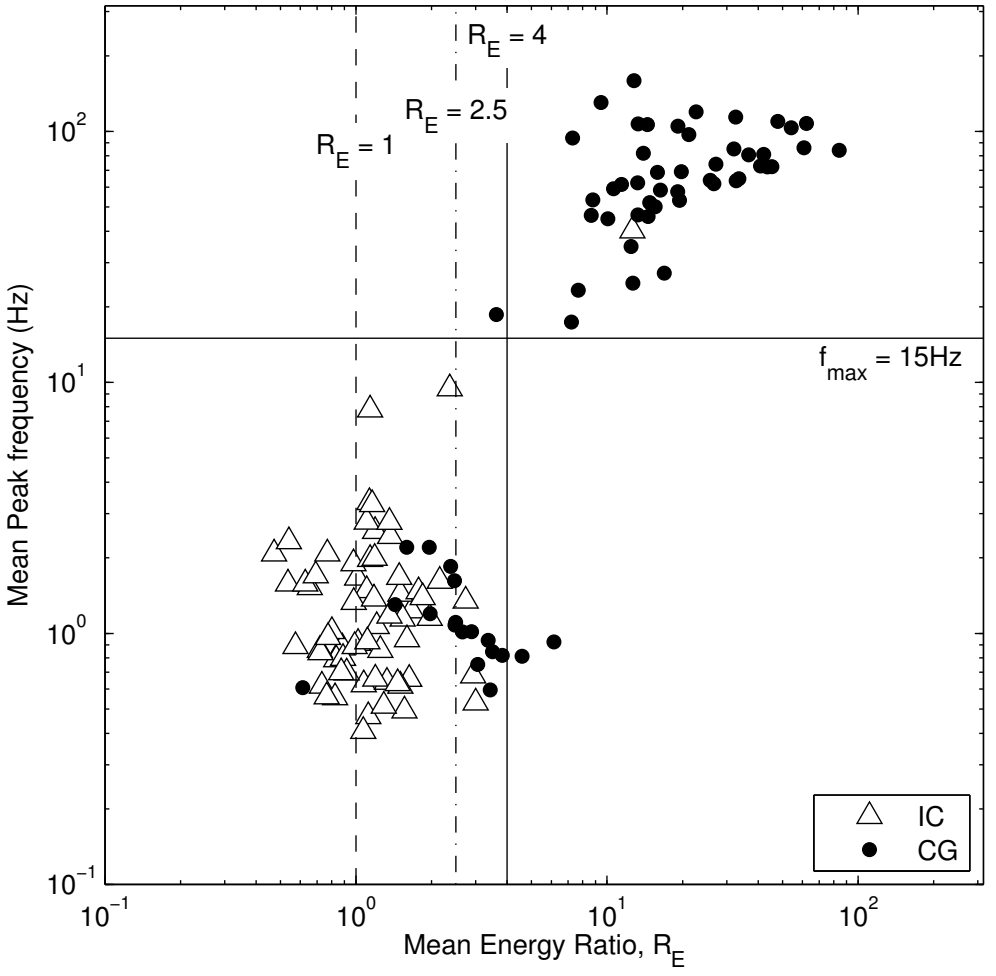

CHAPTER 5

DISCUSSION

My examination of thunder at multiple recording stations during many storms throughout a season provides a comprehensive description of signal characteristics. Previous studies were limited in this aspect by equipment, computational capabilities, or study duration. The incorporation of LMA and NLDN data is a unique and important aspect of my study as I am able to relate thunder signals to source location and type. I observe distinct trends in thunder signal concurrence that I believe are related to storm electrical properties. I utilize this information to find isolated signals for further analysis.

I do note that many distinct, high-energy signals, mainly occurring during the most intense portions of storms, are eliminated by my procedure. My catalog of events only covers about 4% of the total flashes detected by the LMA for the times I am interested in and preferentially includes CG events. While I suspect that thunder during more energetic portions of storms may exhibit some distinct characteristics, and that I lack information about IC events because they are lower-energy and more difficult to detect, my primary concern is analysis of thunder that is not contaminated by excessive noise or overlapping thunder from multiple flashes. I achieve this goal through my comprehensive study.

5.1 PRESSURE AMPLITUDE AND ENERGY OF IC AND CG THUNDER

I examine trends in peak pressures and total acoustic energies for the events in my catalog and their relationship to to source flash type. Peak pressures for thunder signals reduced to 1 km from the source range in amplitude from tenths of Pa to over 100 Pa. CG thunder pressure estimates span a wide range of values and have a much higher median than thunder from IC sources. IC thunder peak pressures are almost always below 10 Pa. These reduced pressure estimates are not consistent between stations GTM and KVH.

Because reduced pressure amplitudes are variable and highly subject to local and atmospheric effects, I estimate total acoustic energies to better characterize thunder signals. Energies range from tens to thousands of kJ. Total acoustic energy is a more useful metric than volumetric energy density in my study because I am examining long-duration, broadband signals. I observe overall higher energies for CG thunder than IC thunder. Robust energy estimates should be similar for multiple stations since they account for source-receiver distances. I observe two populations of events: IC thunder energies are well correlated between stations and tend to have low values compared to CG thunder. CG thunder has energies spanning a wider range, with overall higher energies, and significant scatter when compared between stations. I also see these trends with an overview of mean peak pressures and energies recorded across the network. I consider explanations for higher overall observed pressures and energies for CG events.

First, lightning source geometry and the relative positions of the stations may influence estimates. I account for geometric decay in signal amplitudes in both my pressure and energy estimates [*Kinsler et al.*, 1999; *Johnson et al.*, 2011;

Holmes et al., 1971]. Observation angle relative to the channel axis also influences recorded thunder signal (see Section 2.3 and *Depasse* [1994]). Thunder travels radially outward from lightning channels and most of the acoustic energy is focused approximately perpendicular to the channel axis [*Depasse*, 1994]. CG ground strokes therefore produce acoustic waves propagating approximately parallel to the ground surface - this is ideal for recording thunder at sensors in the horizontal plane. The relative locations and directions of IC channels (and their propagated thunder signals) are less predictable. However, the complexity and spatial distribution of IC lightning (up to tens of kilometers in any horizontal direction) mean that, in most cases, there should be channels producing thunder directed toward the stations. I further mitigate the potential effects of relative observation angle by studying multiple events for many storms that occur within a restricted region around the network. I ensure that there is no persistent bias at any of the arrays. If all other parameters are similar for IC and CG lightning, I would expect to observe similar thunder energy and pressure amplitude distributions for both event types in my study.

Atmospheric effects may act to attenuate or scatter IC thunder signals more than CG signals. IC lightning is contained within the cloud region and is generally farther from the stations than CG ground strokes. Increased humidity in the cloud may enhance scattering, especially at higher frequencies [*Rakov and Uman*, 2003]. Small-scale turbulent eddies act to scatter low-frequency energy [*Few*, 1995]. Cloud particle interactions with acoustic waves can increase overall viscous attenuation and cloud boundaries may act as partial reflectors. These effects are extremely variable within individual storms and between multiple storms. A general description of the influences of cloud particle/thunder

signal interactions cannot be estimated for all cases. I note that atmospheric effects increase error in my energy and pressure calculations but would not expect the effects to be consistent for all events.

Another possible explanation for high pressure amplitudes and energies in CG thunder is that inherent differences in source properties result in different thunder signals. *Holmes et al.* [1971] notes a high mean total acoustic energy value for CG thunder, compared with IC thunder, for a limited number of events recorded at one station. *Depasse* [1994], *Few* [1969], and others suggest relationships between acoustic and electric parameters. For example, thunder source strength is related to specific energy of the lightning channel, $\int I^2 dt$ where I is total current [*Kinsler et al.*, 1999; *Assink et al.*, 2008]. See also Section 2.4. Return strokes in CG lightning propagate more current, in general, than other lightning processes and are believed to be the primary source of audible thunder [*Rakov and Uman*, 2003]. Though stroke currents recorded by the NLDN are not necessarily indicative of total current for a lightning flash, I note that of the events contained in my catalog, only 11 IC events produced peak currents sufficient to be detected by the NLDN. For 10 of those IC events, stroke currents fall below 96% of CG stroke current values.

I favor lightning source electric parameters as the primary explanation for low reduced pressures and total acoustic energies in IC thunder. This reflects observations made in previous studies and is in agreement with understanding of the physical processes that produce thunder (for the expanding channel mechanism). Though flash location and geometry may result in variability in pressure estimates (see Section 5.3), and may act to reduce pressure and energy values for IC thunder, I do not expect these effects to be consistent, especially for energy calculations.

5.2 SPECTRAL DIFFERENCES FOR IC AND CG THUNDER

I investigate thunder spectral content and emphasize the variability in observed thunder PSDs. Thunder has energy in a broad spectral band, but most energy is contained below 500 Hz, which is the upper limit of my investigation. The power spectrum of thunder is the parameter least affected by channel tortuosity [*Few*, 1969]. Thunder signal peak frequencies show distinct distributions above and below about 10–15 Hz, though nearly all IC thunder has peak frequencies below 15 Hz. Peak frequency is not always consistent between stations and does not fully characterize the spectral content of thunder.

Due to these limitations, I quantify energy above 15 Hz compared to energy between 1–15 Hz and calculate an energy ratio, R_E, as a method to characterize noisy spectra. Though this estimate is dependent on distance at close ranges, there are distinct populations for IC and CG events. Most events with an $R_E > 4$ are CG. Events with a low R_E and peak frequency tend to be IC. I see these results across the network. Both IC and CG thunder can contain significant infrasonic energy. A median PSD of all CG events shows significant spectral content up to 100 Hz. IC events are nearly always low-frequency dominated, with a median spectral peak at or below 1 Hz. I consider the explanations for these differences.

Low frequency noise is unavoidable in thunder recordings and may result in low spectral peaks. Wind noise peaks at infrasonic frequencies and is prevalent during storms. I attempt to mitigate the effects of background noise by only utilizing events with a signal-to-noise ratio greater than 3. I filter signals above 4 s to further reduce infrasonic noise. I use median estimates of PSDs (as the means would be biased by outlying values in noisy spectra). In my calculation of R_E I

filter the lower band above 1 Hz to further eliminate wind noise in some events (though CG events with energy below 1 Hz may be of interest for investigating the electrostatic mechanism). Because wind magnitude and direction is highly variable and often localized, wind noise is not correlated across a network. I therefore study the consistency in low frequencies at multiple sensors and arrays. I see that low frequencies are often consistent across the network. I use the benefit of multiple recording stations to reduce the influence of ambient noise in my investigation of thunder spectral content.

One possible explanation for the deficiency of high-frequency IC thunder signals is that greater source-receiver distances result in enhanced high-frequency attenuation. I see the effect of attenuation for high-frequency CG thunder in Figure 4.18: the median PSD falls off rapidly above 100 Hz. I also see variation in peak frequencies recorded at different arrays. Attenuation effects are not generally significant at frequencies below 100 Hz [*Bass and Losey*, 1975; *Few*, 1995]. Peak frequency and R_E are shown relative to minimum lightning channel-array distances in Figure 4.22. Peak frequencies higher than 15 Hz are rarely seen for minimum distances greater than 5 km. CG thunder shows preferentially higher peak frequencies than IC events when recorded at similar minimum distances. As I anticipate, R_E also shows distance dependence. Even at comparable minimum distances, however, CG and IC events have notably different relative amounts of high- and low-frequency energy. Though total energy in IC events may be reduced by attenuation within the cloud (Section 5.1), R_E values should be similar for lightning flashes with comparable source characteristics.

Though I primarily discuss the expanding channel mechanism for thunder production, many studies have investigated infrasonic thunder due to electrostatic relaxation in the cloud [*Wilson*, 1920; *Dessler*, 1973; *Bohannon et al.*, 1977;

Balachandran, 1979; *Few*, 1985]. This thunder should exhibit peak frequencies between tenths of Hz and approximately 2 Hz [*Dessler*, 1973; *Bohannon et al.*, 1977; *Balachandran*, 1979]. These signals are low-amplitude and can only be detected in ideal conditions: the directivity of the source means that it can only be observed directly beneath the cloud volume [*Dessler*, 1973; *Balachandran*, 1979]. Wind noise tends to dwarf these low-amplitude signals. The blast wave from the expanding channel also contains low-frequency thunder [*Assink et al.*, 2008]. It is likely that I detect thunder produced by charge relaxation in my study. A number of CG events have a probable electratostic source contribution evident in their significant low-frequency content. I believe that LMA data can be used to determine times when lightning activity is located directly above the network. Isolated thunder signals that are recorded during these time periods and that contain significant infrasonic energy, as determined using R_E and f_{max}, can then be identified. If the low-frequency signals are correlated across stations within an array, or between multiple arrays, they may indicate the presence of the electrostatic source. Because of the challenges inherent in detecting these signals, and because of their low amplitudes, I do not believe that they contribute significantly to the f_{max} and R_E values estimated for my catalog.

Peak frequency recorded at varying source-receiver distances does not reflect the overall thunder spectra, or the peak frequency near the lightning source. *Depasse* [1994] studied thunder at a consistent distance from ground strokes by investigating triggered lightning events. The study related peak frequency to lightning parameters. In most practical cases, however, this is not feasible and relative recording location is inconsistent [*Holmes et al.*, 1971]. I achieve a robust quantification of the frequency content of thunder by making observations throughout

an entire storm season at multiple stations and investigating ratios of energy contained in selected bandwidths. I therefore mitigate influences from noise, relative source positions and distances, and secondary sources of thunder production. I believe that the unique spectral contents of IC and CG thunder reflect lightning flash source properties. Though CG thunder has more high-frequency content, the presence of significant low-frequency energy in CG thunder could represent a combination of the IC portion of CG events, as well as low-frequency energy radiated from the ground stroke. CG events with low R_E values across the network (or across stations at an array) may be candidates for further investigation of the electrostatic source mechanism.

5.3 SCATTER IN INTER-STATION OBSERVATIONS

I attempt to explain the observed scatter in parameters calculated at KVH and GTM. Thunder peak pressure and peak frequency values are not perfectly correlated between stations. Source complexity, receiver distance, and local atmosphere variations will greatly alter pressures and spectral peaks for complex, non-stationary signals. These parameters do not reflect the overall character of thunder signals.

Quantified energy for IC thunder is correlated between KVH and GTM. CG events show less good correlation across the network (Figures 4.12, 4.13, and 4.14). Because energy calculations take source-receiver distances into account, discrepancies between stations suggest influences from either relative source geometry or atmospheric structure. Local wind turbulence and atmospheric effects would create scatter for both types of events (and perhaps be enhanced for IC

events). I show that there is not a consistent bias at any of the arrays, demonstrating that local site influences (such as topography) are not the cause of variations.

I believe that relative source geometry explains observed correlations in IC event metrics. IC lightning is contained in a large volume such that most of the flash is relatively distant from both stations, when compared with CG ground strokes. The overall source-observer angle for IC flashes is similar across a ground-based network. The stations can therefore be assumed to have similar vantage points for these flashes. A ground stroke, however, will almost always be located preferentially close to one station (unless centered between stations). The closer station will observe thunder from lower portions of the channel, as energy from each point on the channel is radiated within a narrow angle relative to the axis direction, as described in Section 5.1. Farther arrays will therefore "hear" influences from a greater proportion of the ground stroke.

Observed scatter between stations, especially for CG events, demonstrates the problems inherent in observing thunder at a single station. Individual thunder signals differ greatly depending on sensor location. Signals are not well correlated between stations at different locations. Single-station quantifications of thunder spectral content and energy are subject to considerable errors. In my study I am able to utilize signals from multiple recording locations to better understand thunder signal behavior.

CHAPTER 6

CONCLUSIONS

Studies of thunder provide information complementary to other lightning detection techniques. The presented data set is distinct in the availability of concurrent LMA and NLDN data. The data set is also unique in the number of channels of acoustic data and quantity of thunder recordings. I develop a thunder catalog using LMA data to limit analyzed thunder signals to those unadultered by overlapping events. This is an important step in my study that is not feasible by visual inspection of acoustic data alone. My methods can be used in the future to identify high-quality thunder signals for analysis in the Magdalenas and in other regions with lightning detection and location systems. Using LMA flash locations to estimate expected thunder signal arrivals at the stations, I classify different storm behaviors - those with isolated lightning-thunder sequences and those with overlapping thunder signals. I see time periods exhibiting either or both of these behaviors throughout the season.

I narrow my focus to 191 isolated thunder events with high signal-to-noise ratio. Using LMA and NLDN data, I determine the most likely type of lightning source, IC or CG, for 188 of these events. I investigate the events at two stations. I calculate reduced peak pressure, total acoustic energy, peak frequency, and a ratio of high-to-low frequency energy for all events. I verify my observations by estimating averages for these metrics across the entire network. I see that, due

to inherent signal complexity, peak pressure and peak frequency are not well-correlated between stations. Total acoustic energy can be estimated to within an order of magnitude, but values may not be consistent at different recording locations, especially for CG events. Despite scatter, many CG events show higher peak pressures, acoustic energies, and peak frequencies than most observed IC events. My study highlights the importance of using multiple stations to study non-stationary processes such as thunder.

When considering thunder spectra, the recorded power often falls off above 100 Hz due to attenuation. Thunder recorded close to the source contains significant broadband energy. At all recording distances, CG thunder has more energy above 15 Hz than IC thunder. The ratio of high- to low-frequency energy, in conjunction with peak frequency recorded at multiple sensors, may be useful for determining whether a recorded thunder signal results from an IC or CG flash.

Thunder signals reflect charge behavior, source energy, flash type, atmospheric influences, noise, and flash geometry. I have access to a thunder data set from multiple, continuously recording stations in 2011 with complementary LMA and NLDN data. I provide a comprehensive description of recorded signal characteristics. This information may be of interest for future studies of lightning, thunder, or atmospheric acoustics. I can isolate thunder signals and observe overall storm behavior. I am able to quantify the properties of thunder for nearly two-hundred high quality signals. I observe higher peak pressures, energies, and frequency content for CG events, compared to IC events, indicating inherent differences for the two flash types. I emphasize the importance of multi-station observations of thunder. I believe that the recorded thunder is related to storm electric properties and charge movement and that the relationships be-

tween lightning and thunder signals can be further understood and developed in focused studies of complementary acoustic and electric data.

APPENDIX A

GTM DATA FOR 34 STORMY TIME PERIODS

Data from 34 time periods recorded at channel 3 at station GTM are shown. Vertical lines delineate LMA event times. Line height is scaled relative to mean radial distance between Langmuir Laboratory and mean LMA point locations with longer lines indicating closer flashes. Each vertical line has a corresponding horizontal line (of the same height and color) that shows the predicted duration of the thunder signal. Different line lengths could indicate more than one storm center. Good agreement can be seen in most cases between the estimated arrival times and actual observed thunder. Times on figures are GMT (local times are 6 hours earlier). Events included in the catalog are highlighted from 5 s before to 2 s after the arrival times estimated using LMA data. CG events are highlighted in gray, IC events in yellow, and unclassified events in blue.

Figure A.1: The first recorded storm took place around 20:00 (14:00 local time) on 20 July 2011. Sixty minutes of signal are considered. The storm begins with about 15 minutes of isolated thunder. This is followed by a long period of overlapping thunder. The stations were being installed or serviced during this storm, so there is a break in data recorded at MGTM. From this storm, 7 signals are included in my catalog.

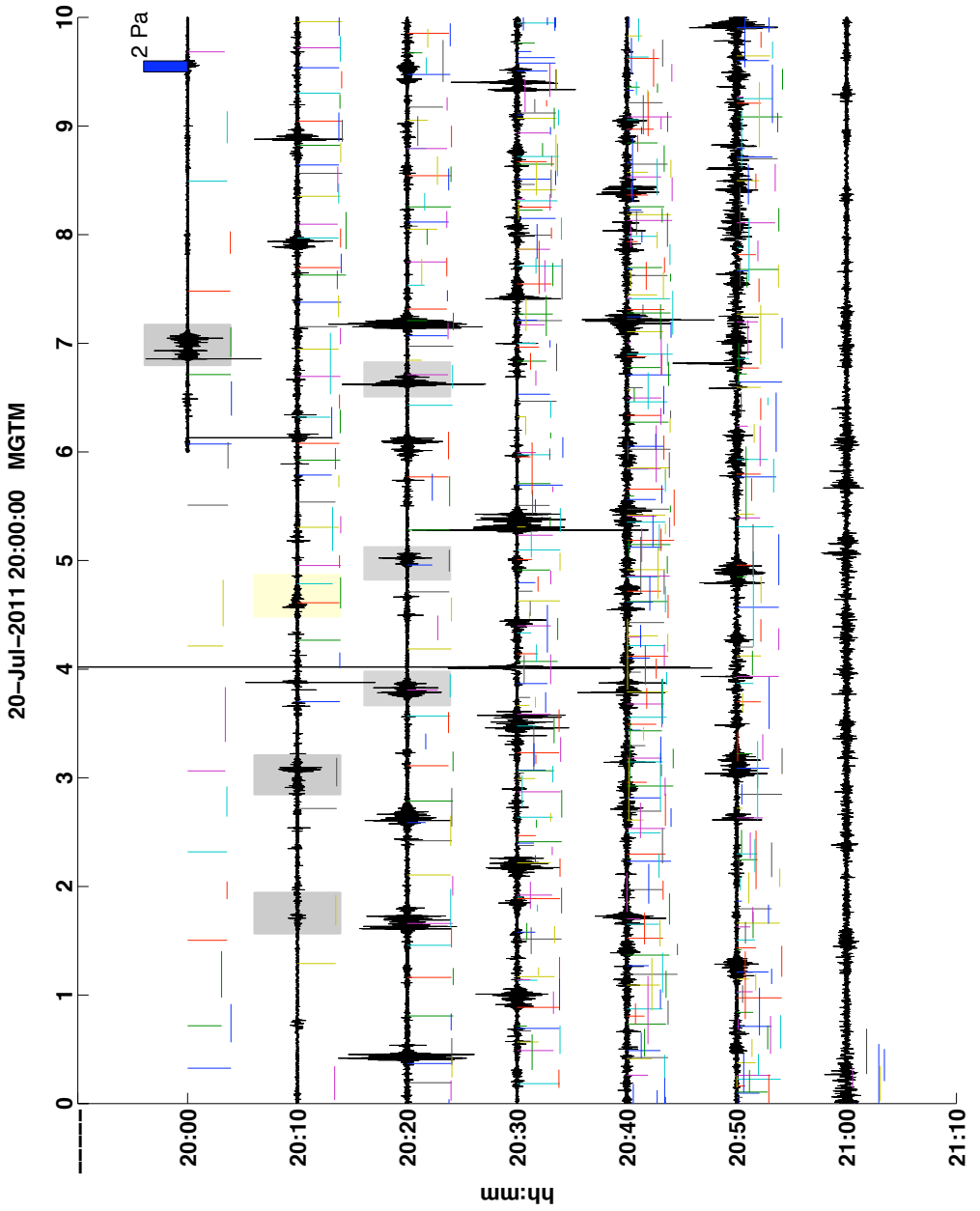

Figure A.2: The second stormy period occurs during a fairly noisy period. Overlapping thunder lasting 10 minutes begins at 21:30 GMT on 20 July 2011. There are no temporally separated thunder signals for analysis.

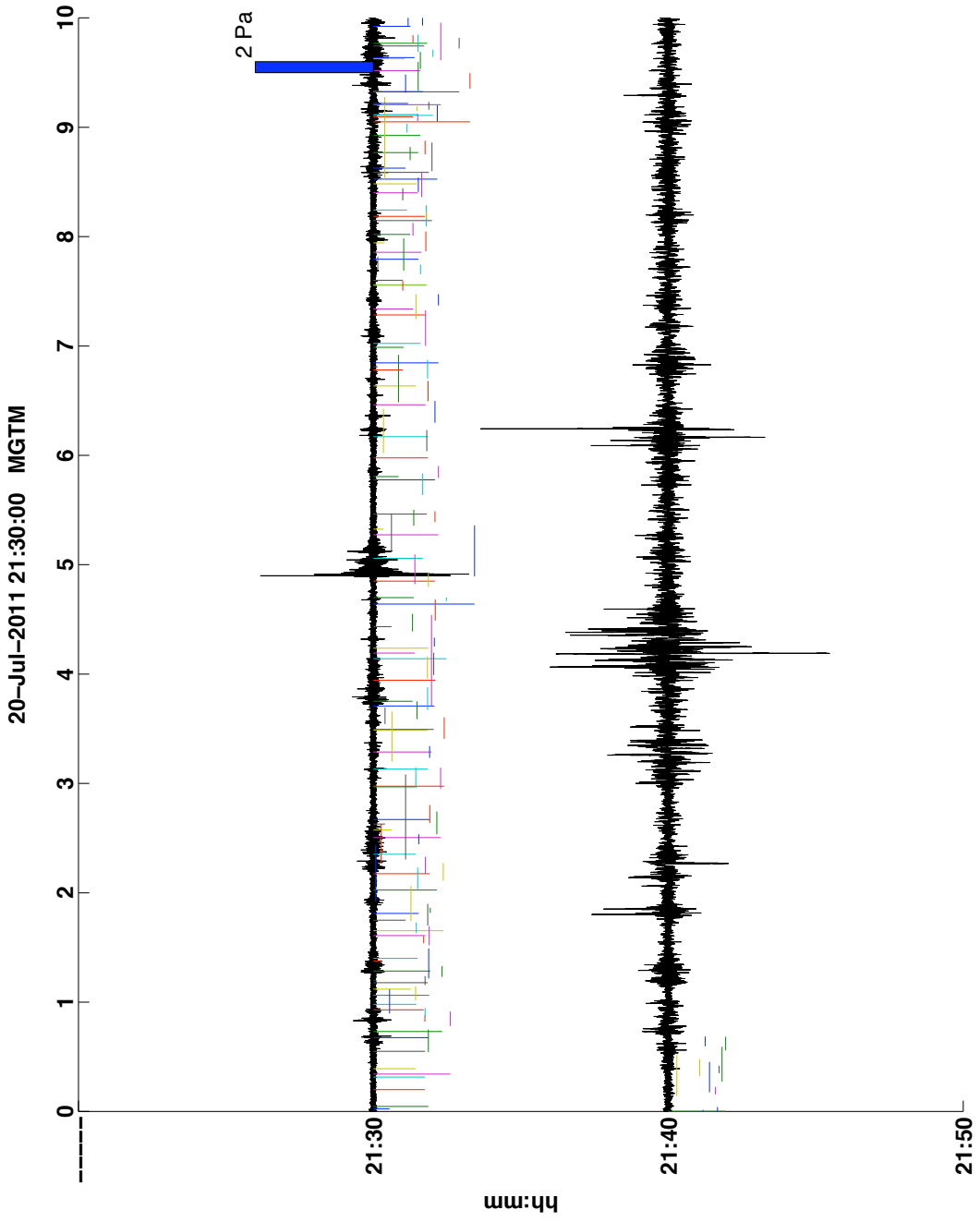

Figure A.3: The third time period is 10 minutes of isolated signal beginning at 19:10 on 22 July. There are 4 nearby LMA events. All signals have high signal-to-noise ratio and are included in the catalog.

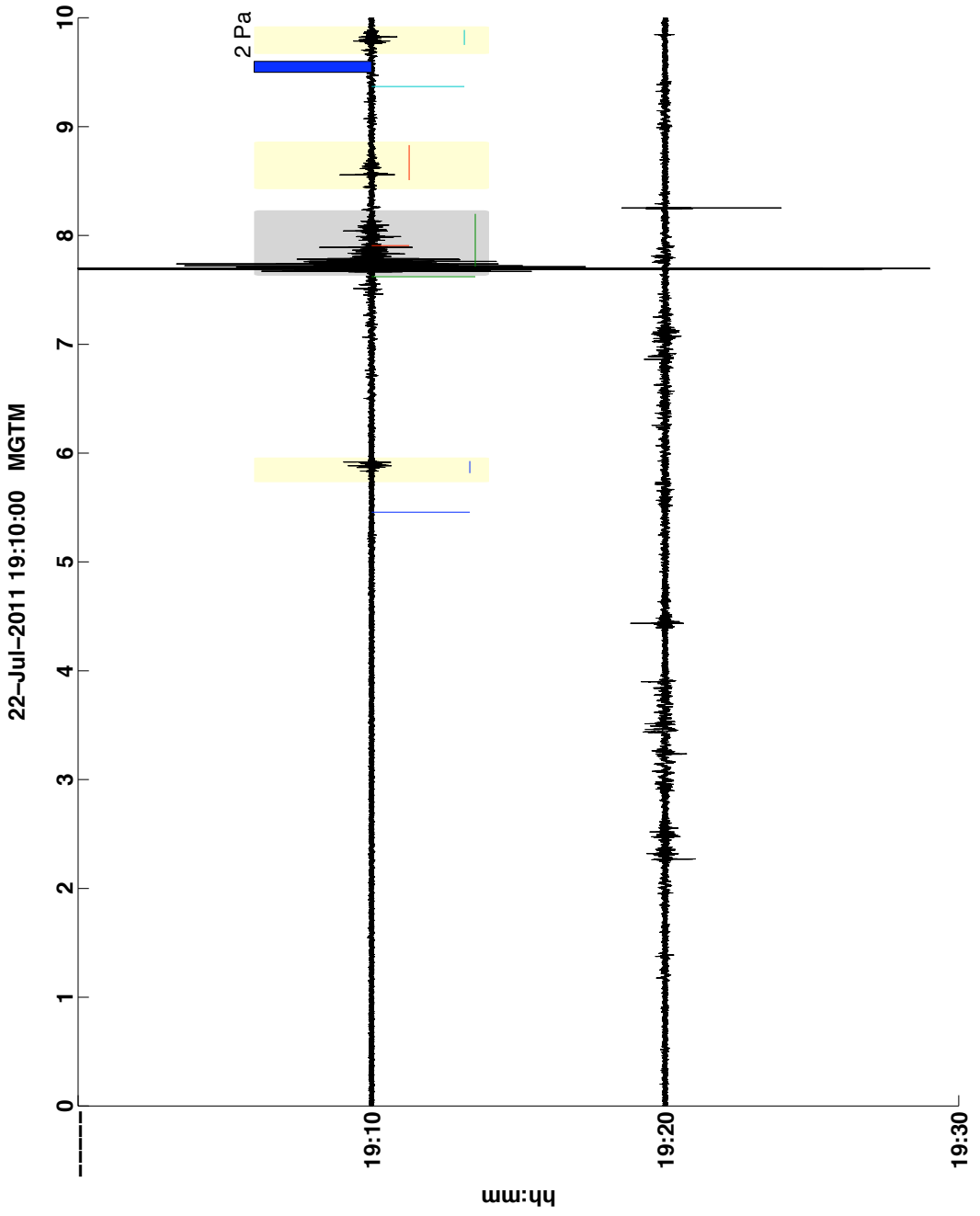

Figure A.4: Time period 4 begins approximately 2 hours after the third (at 21:00 GMT on 22 July). I searched 80 minutes of primarily overlapping thunder for signal. The last 20 minutes of acoustic signal are overwhelmed by extreme rain and/or wind noise. Prior to the onset of heavy rainfall, there are 2 signals that are included in the catalog. Overall, KVH channel 3 signal was much noisier and lower amplitude than GTM channel 3 data.

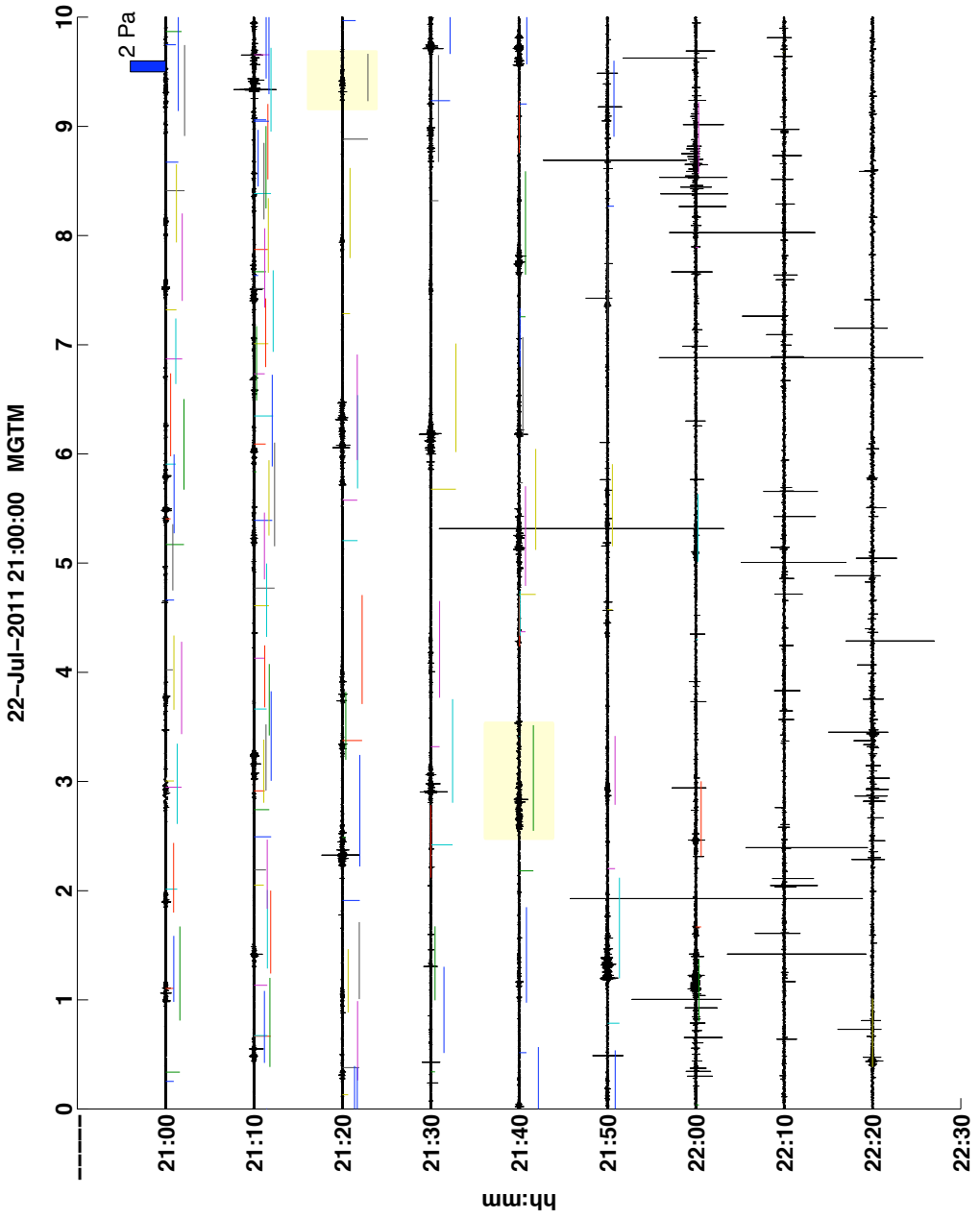

Figure A.5: This period of isolated thunder is analyzed between 17:50 and 18:30 on 24 July. The lightning and thunder are very close, often within hundreds of meters of the stations, resulting in multiple signals with maximum pressures on the order of tens of pascals (and one over 100 Pa). GTM signal is sometimes tainted by continuous noise at bands between 40 and 100 Hz. This may have been due to nearby machinery or a vehicle. I analyze 8 signals.

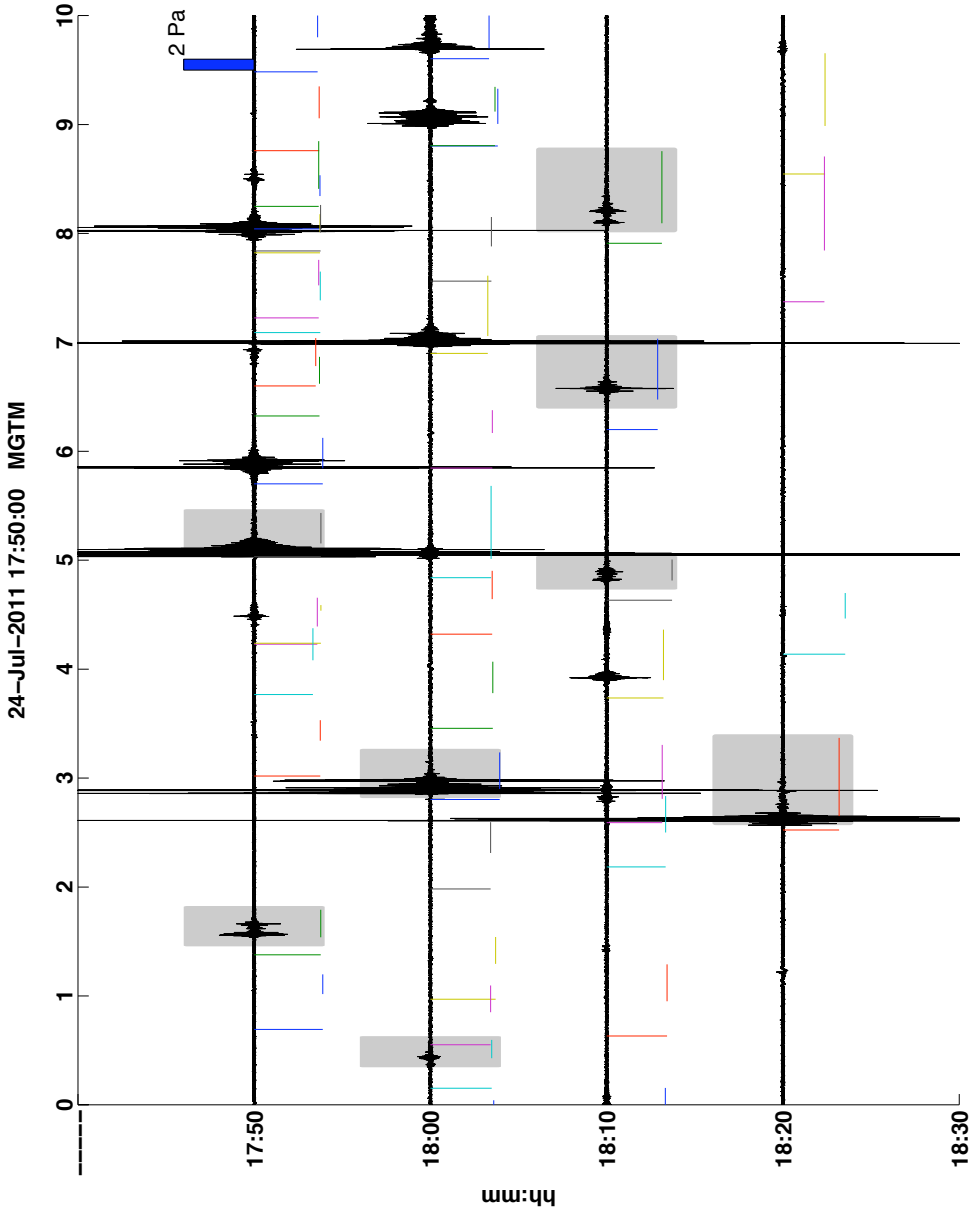

Figure A.6: The sixth storm was examined from 22:00 through 22:43 on 27 July. It includes many high-quality, isolated thunder signals. Most of the storm takes place within 2 km of the network. There are 9 signals that are high-quality at both GTM and KVH and are included in my analysis.

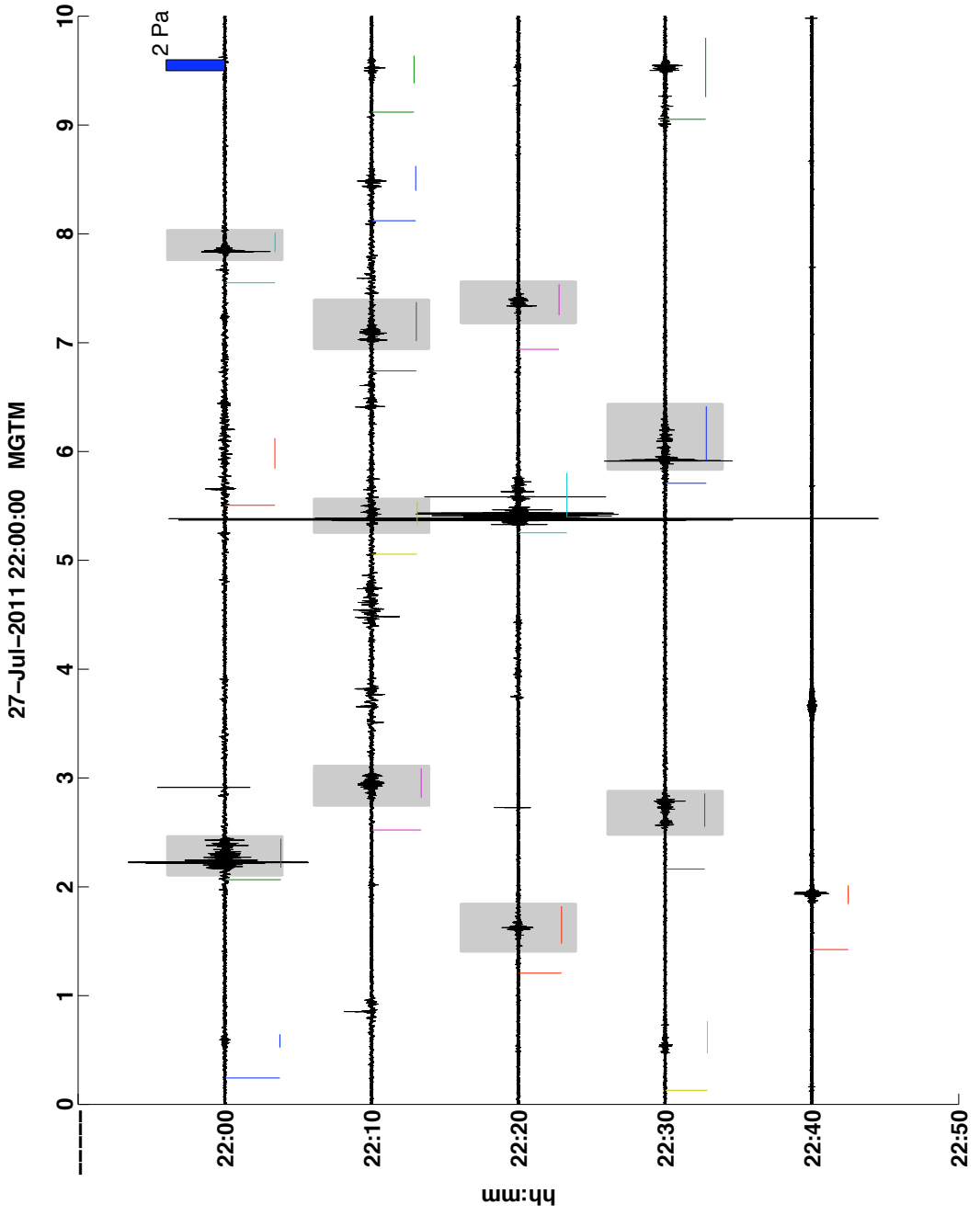

Figure A.7: The seventh time period begins about an hour after Storm 6, at around 22:50 on 27 July. The duration of detectable thunder during this storm is about 80 minutes. The storm is hybrid - beginning with isolated thunder followed by overlapping thunder that tapers off toward the end of the storm. Significant rain noise interferes even with high signal-to-noise events and only 3 are further evaluated as a result.

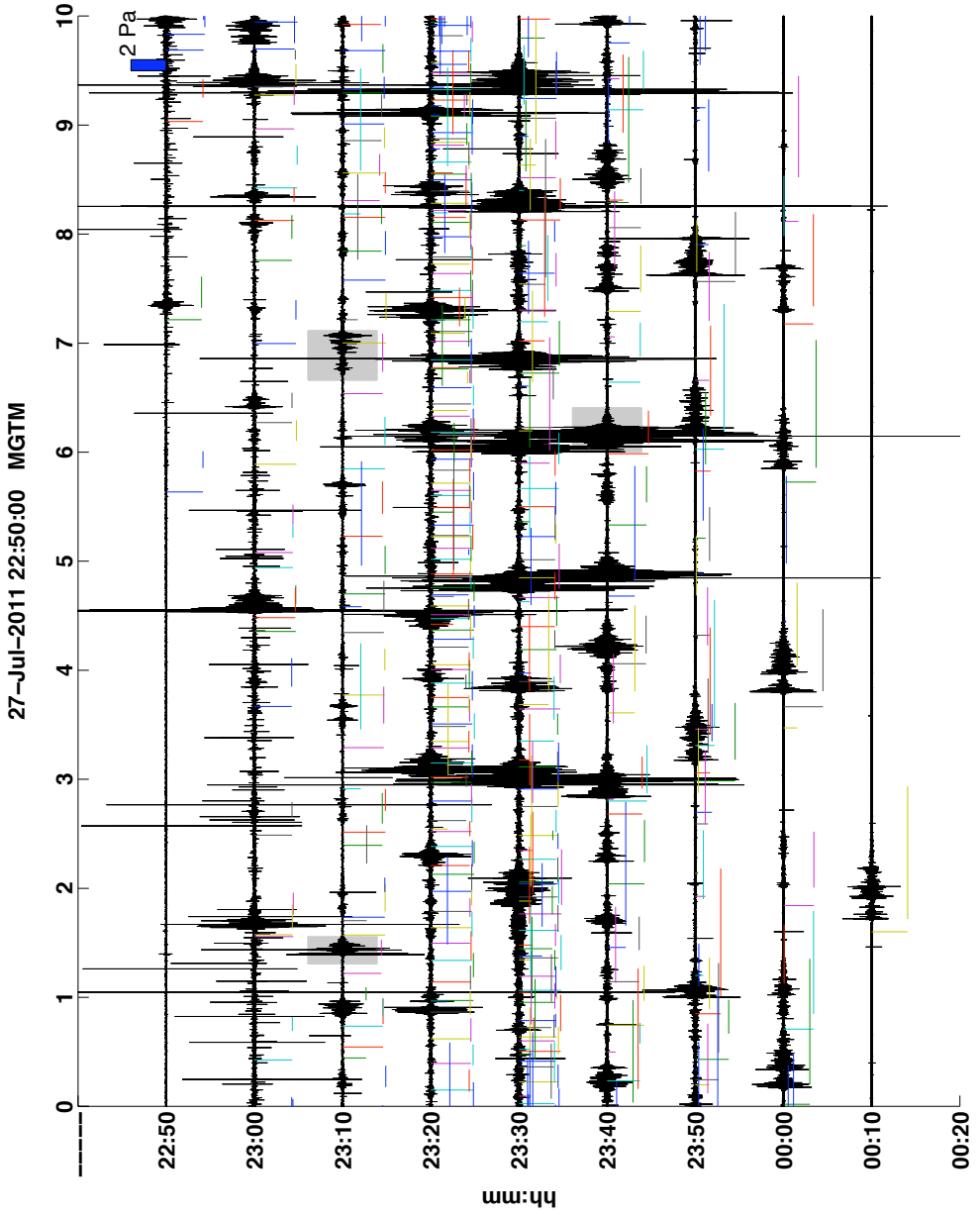

Figure A.8: This storm is evaluated for a period of about 50 minutes starting at 06:10 on 28 July. The isolated thunder is distant, about 13 km away, but some signals are recorded. After 07:00, rain noise is noticeable. The distance of the storm and low frequency background noise result in only 3 quality signals.

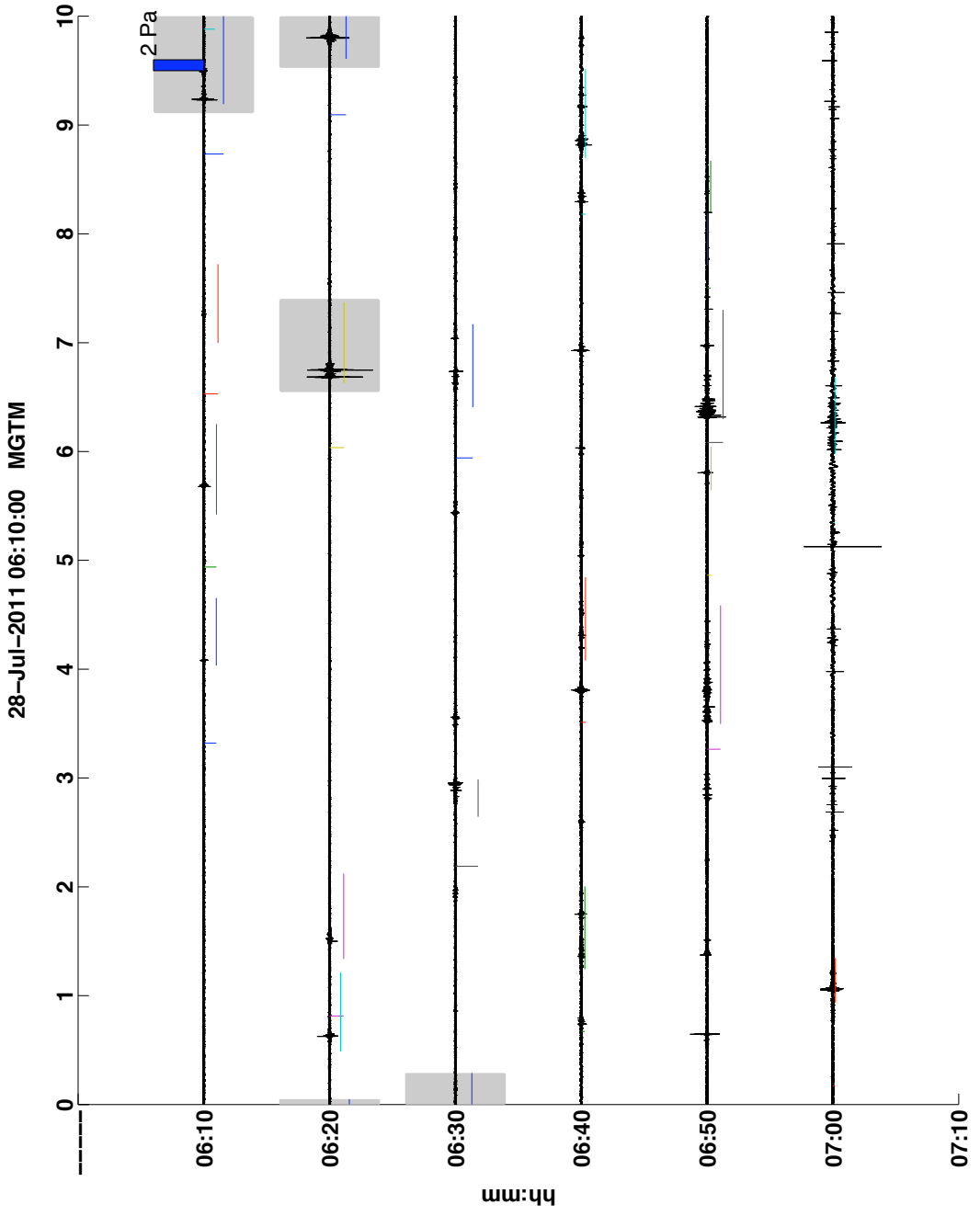

Figure A.9: Storm 9 appears hybrid, with many isolated thunder signals and up to four overlapping signals at any time. It begins at 21:33 and lasts about one hour. Rain noise is noticeable at GTM, as is occasional 60 Hz background noise. I incorporate 8 signals into my catalog.

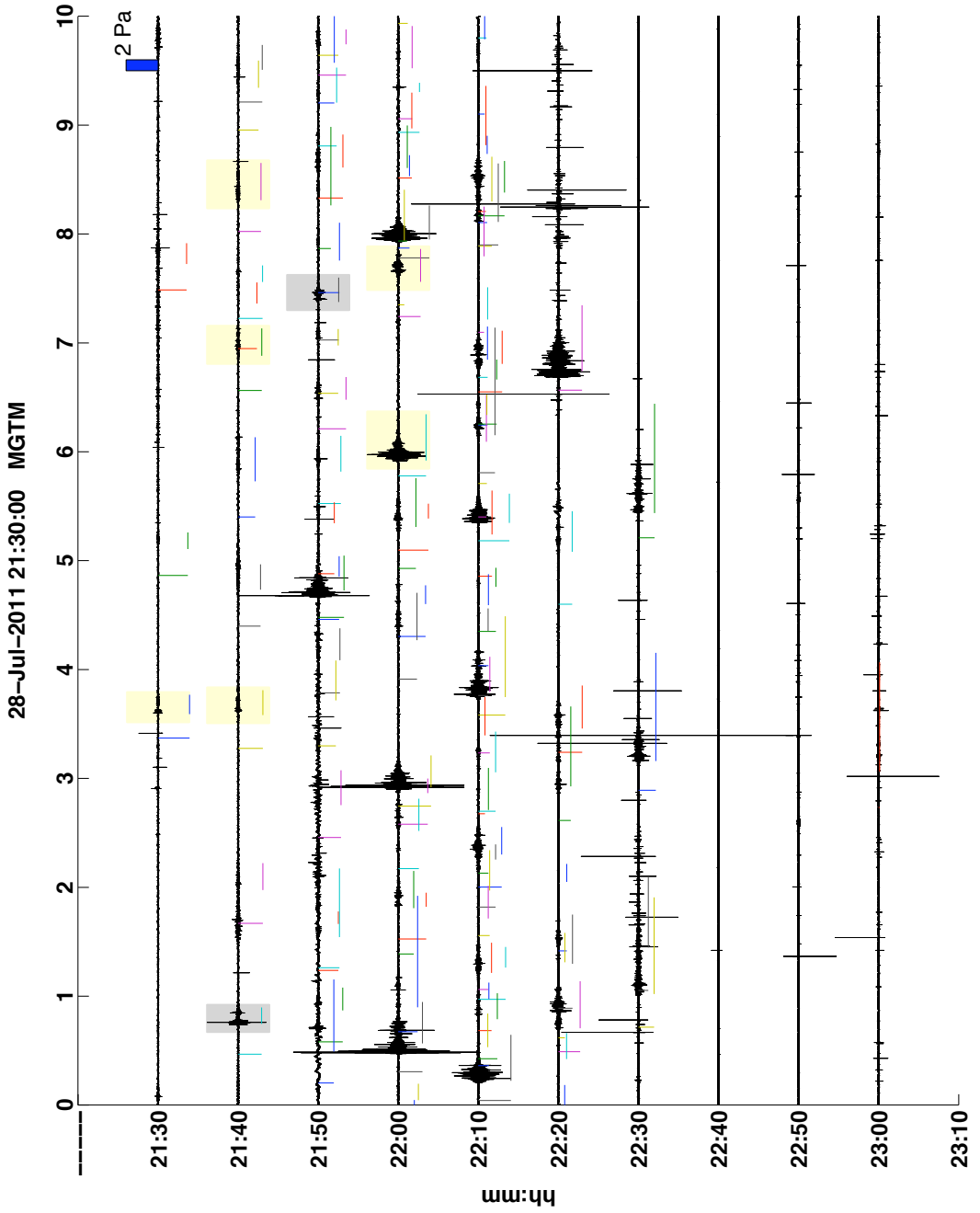

Figure A.10: The time period examined is a noisy 30-minute span of overlapping thunder followed by isolated thunder beginning at 21:50 on 30 July. My catalog includes 2 signals from this time period.

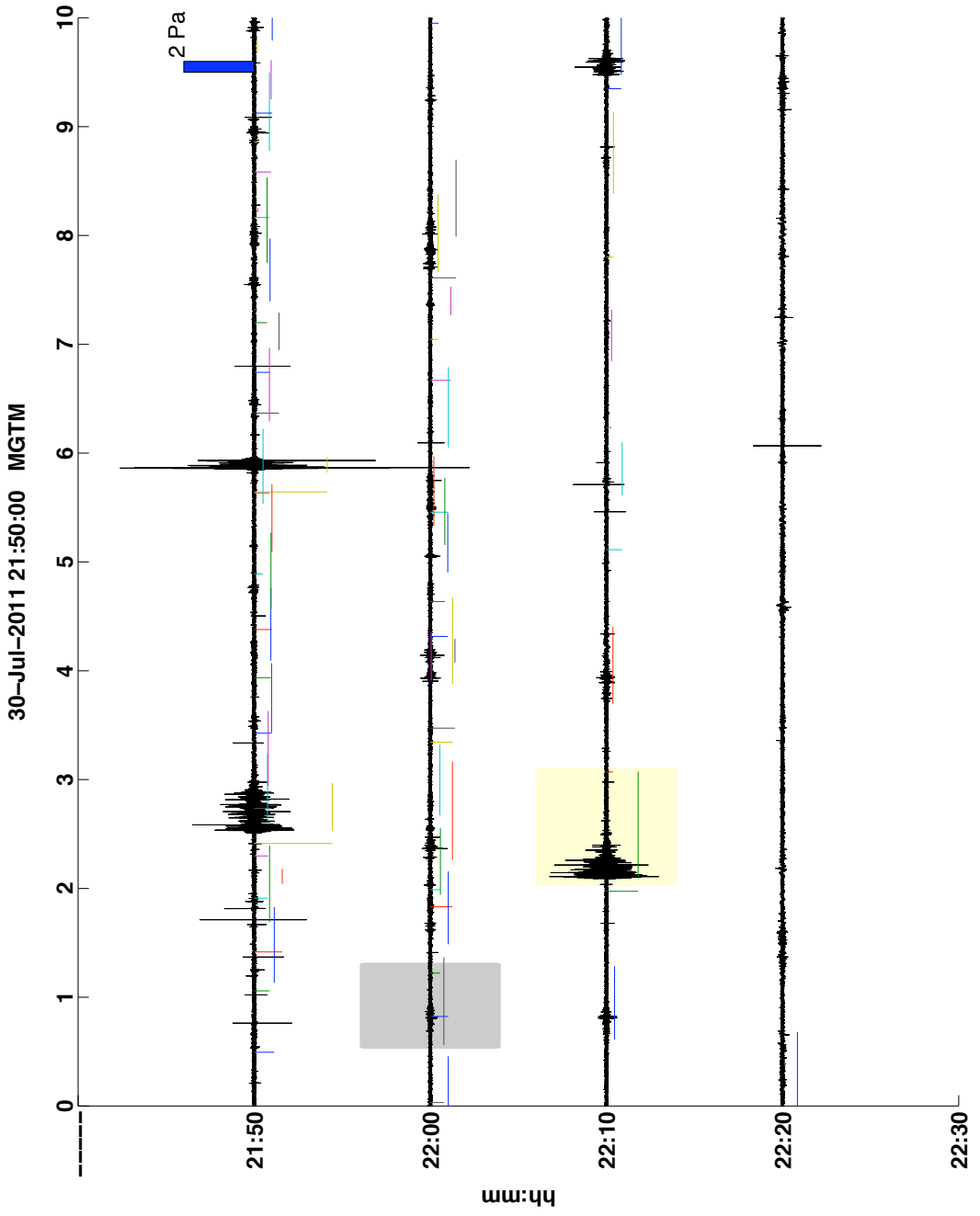

Figure A.11: Time periods 11 and 12 are the same storm, separated due to duration (and for procesing simplicity - the storm spans time in both July and August). Storm 11 includes up to twenty overlapping events events beginning at 22:30 on 31 July and lasts about 85 minutes. Rain and/or wind noise increases as the storm progresses and 3 signals are used in analysis.

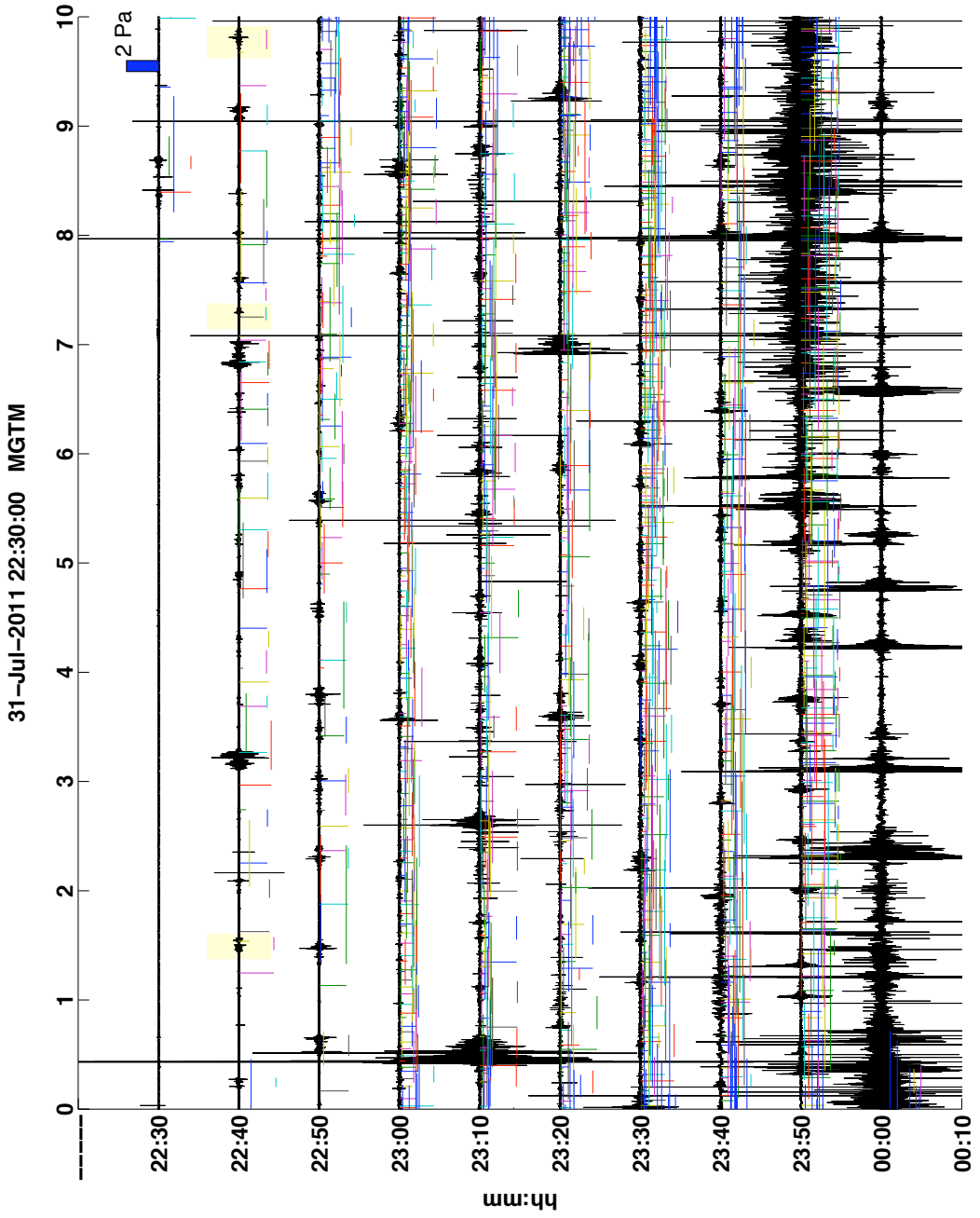

Figure A.12: Image showing a continuation of the storm on 31 July. Nearly all signals are overlapping. Due to significant background noise, no signals are included in the catalog.

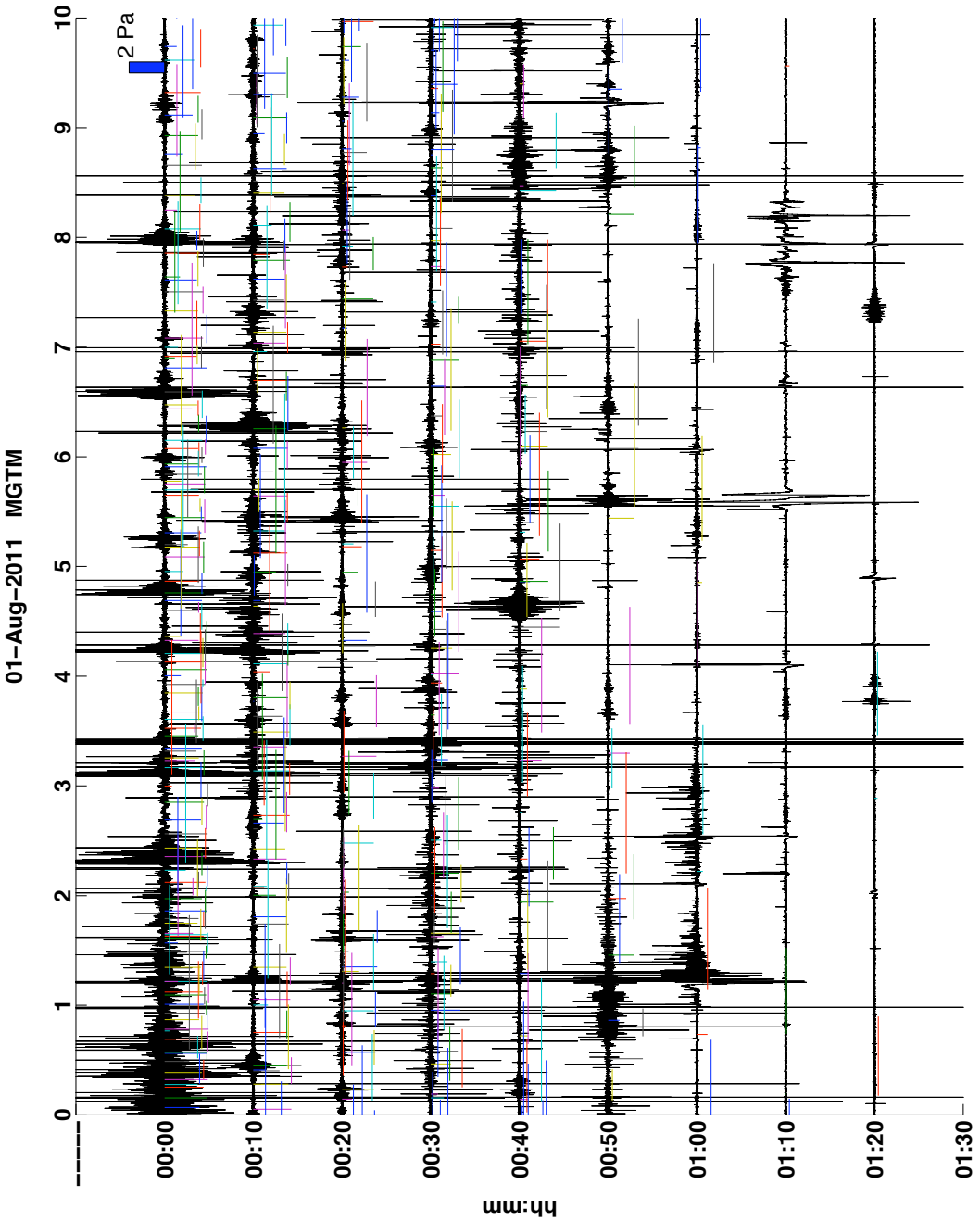

Figure A.13: The time period evaluated for storm 13 spans 01:00 through 01:45 GMT on 2 August. Thunder is characterized by overlapping signal followed by isolated events (with some overlap at the end). Much of the lightning during the second half of the storm is within a few kilometers of the network. Low-frequency background noise is prevalent and no signals are high enough quality for investigation.

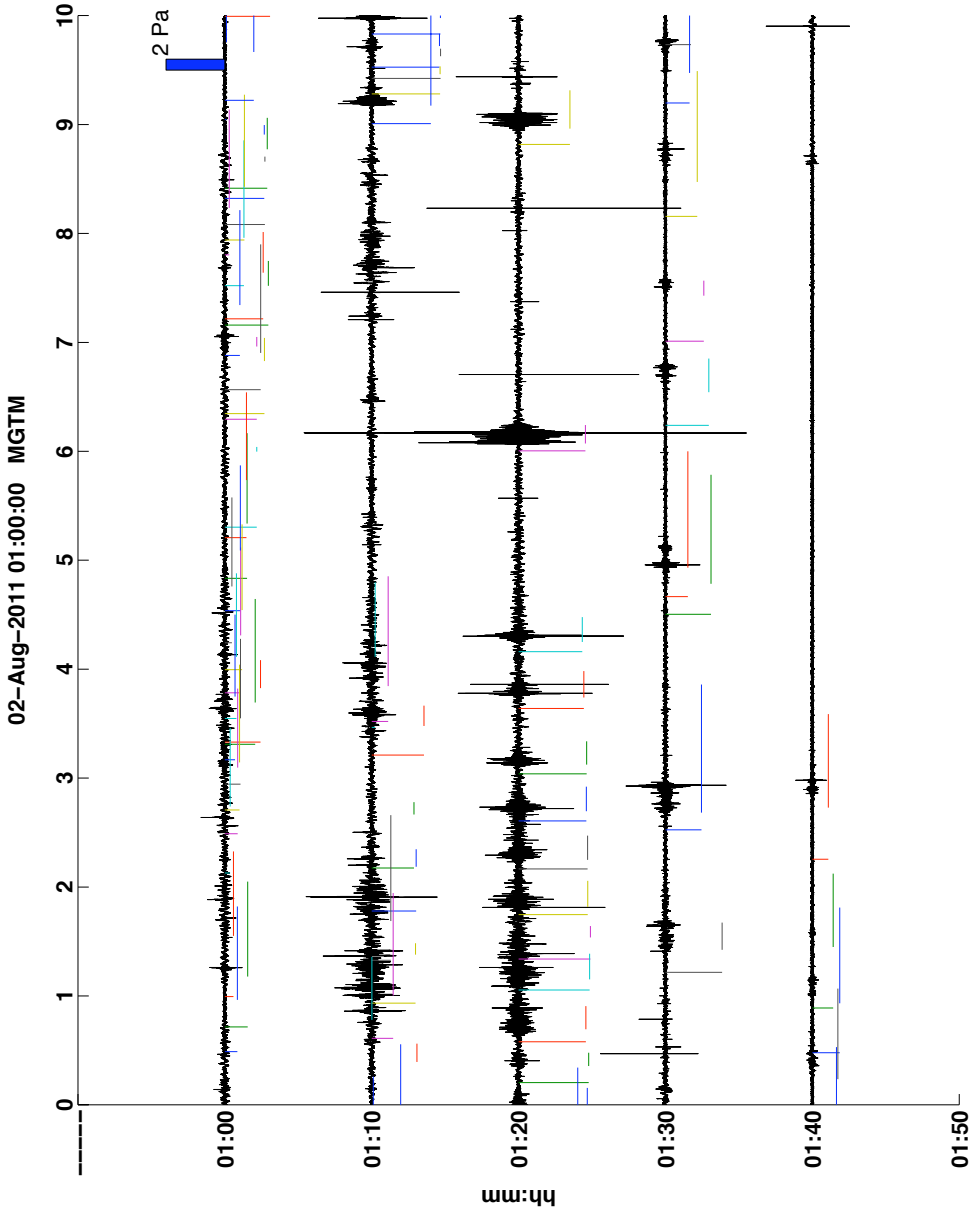

Figure A.14: The fourteenth time analyzed is long-duration, between 20:20 and 22:40 on 2 August. A period of mostly isolated signal precedes a period of quiet between 14:56 and 15:10. Isolated signals then recommence and overlap increases, though the intensity of overlap varies for the duration of the storm. Again a noisy storm, the time following the quiet period yields 2 isolated events with adequate SNR to be included in my catalog.

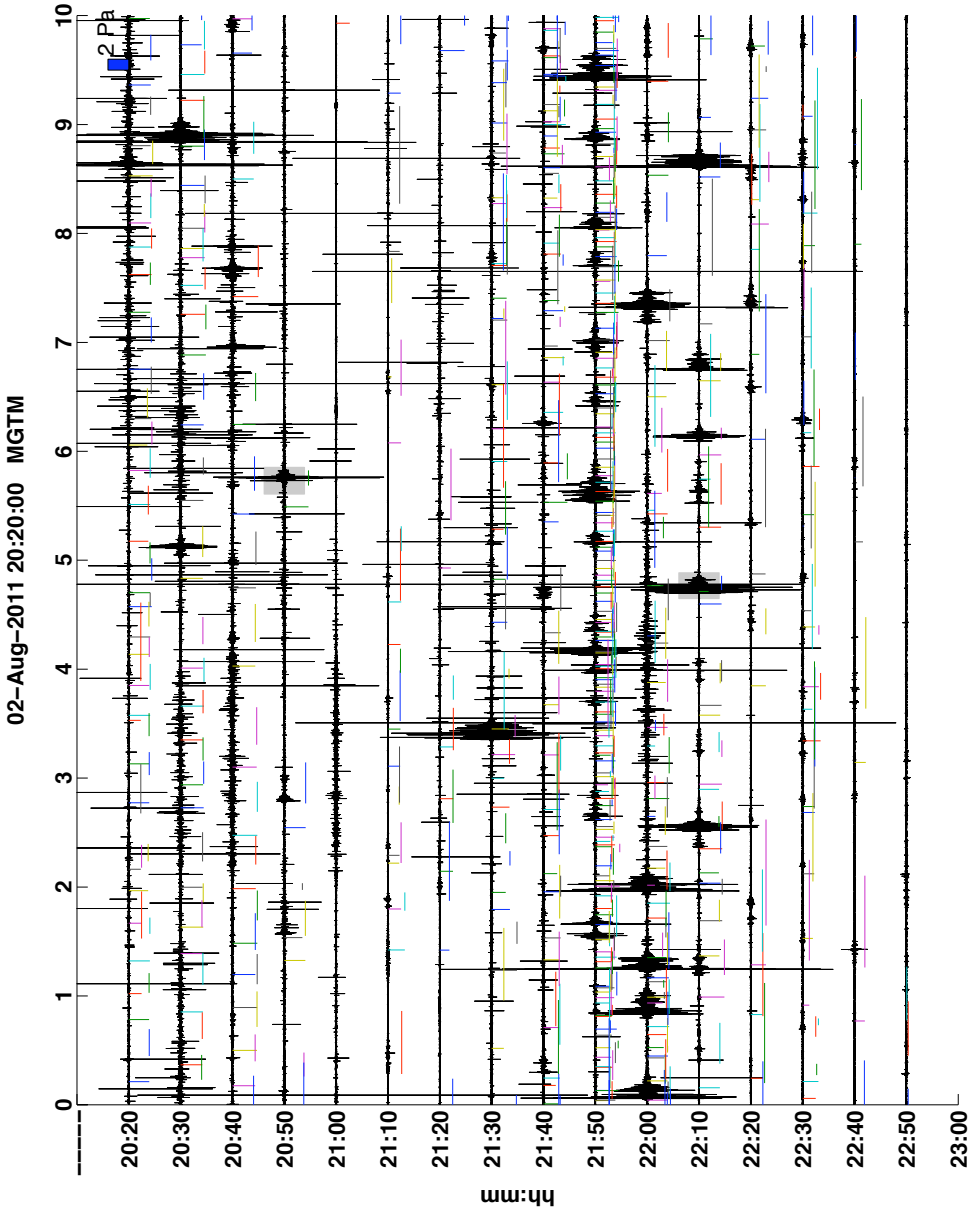

Figure A.15: The fifteenth stormy time begins at around 18:00 on 3 August, but an isolated event at 17:02 is included. While there is significant wind and rain noise for the first 30 minutes of this hybrid storm, many isolated, high-quality, nearby signals occur in the latter 20 minutes of the storm. My catalog contains 19 thunder events, including the one at 17:02. Channel 1 at GTM may have suffered damage during the storm.

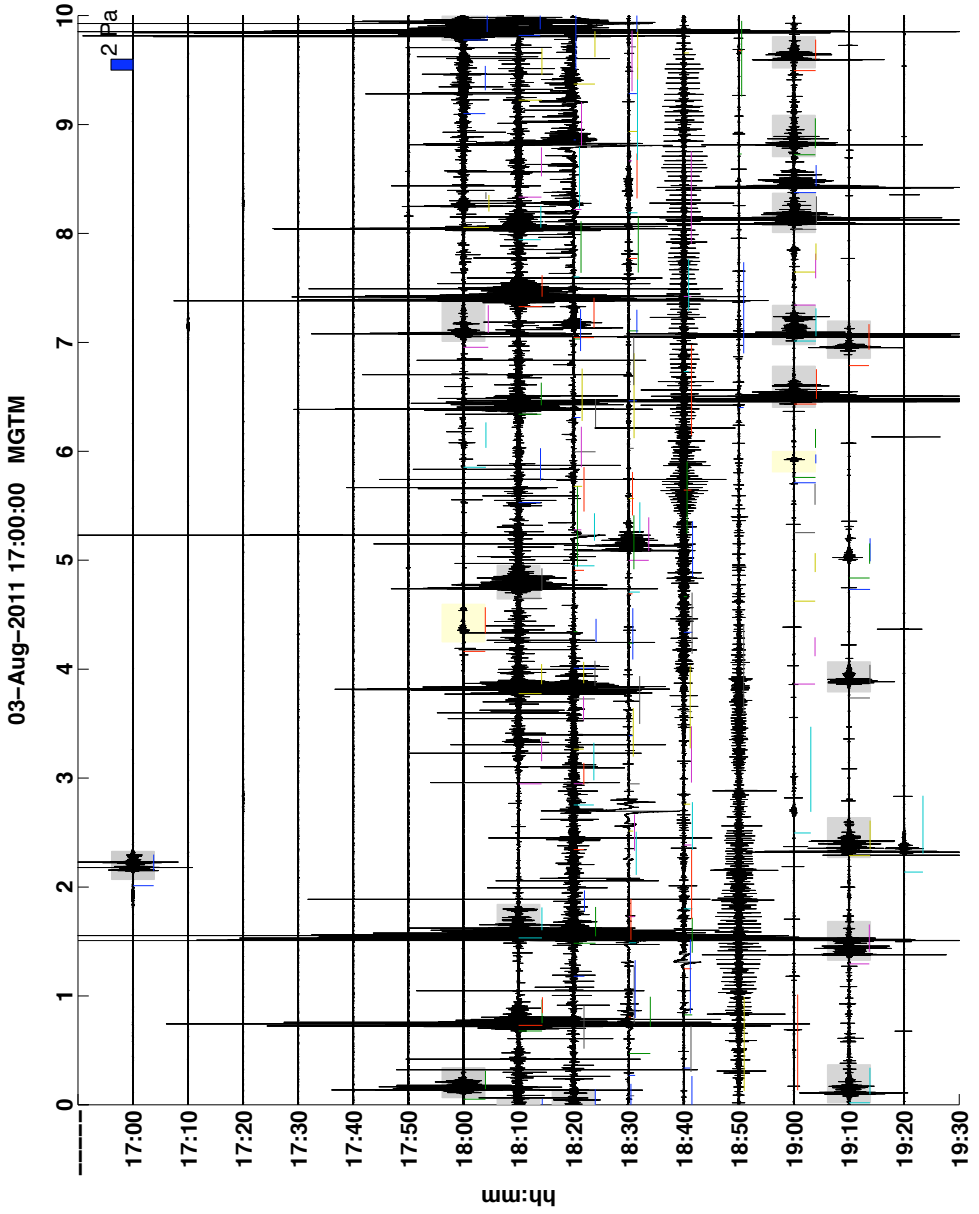

Figure A.16: Storm 16 begins at about 00:15 GMT on 4 August and is analyzed for 70 minutes. The hybrid storm includes up to 4 overlapping events in the first 35 minutes followed by a period of quiet and culminating with four high-amplitude (up to tens of Pa) isolated events. Some background noise is apparent, but 9 events are adequate for further investigation.

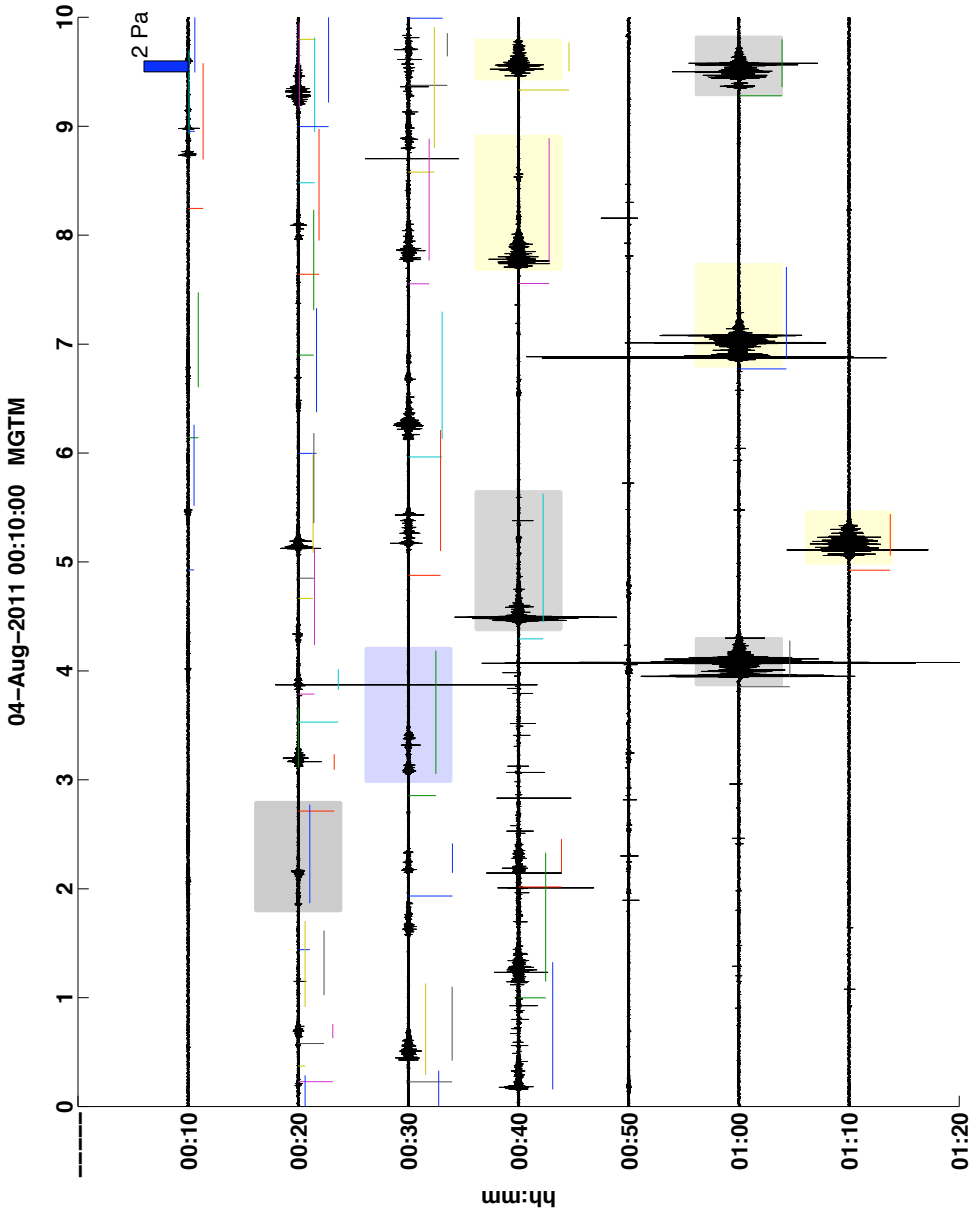

Figure A.17: This is a short, seven-minute time period of four nearby flashes on 4 August beginning at 20:50. Though flash locations relative to Langmuir are similar, the fourth flash is significantly higher in amplitude. It is the only event included in my catalog.

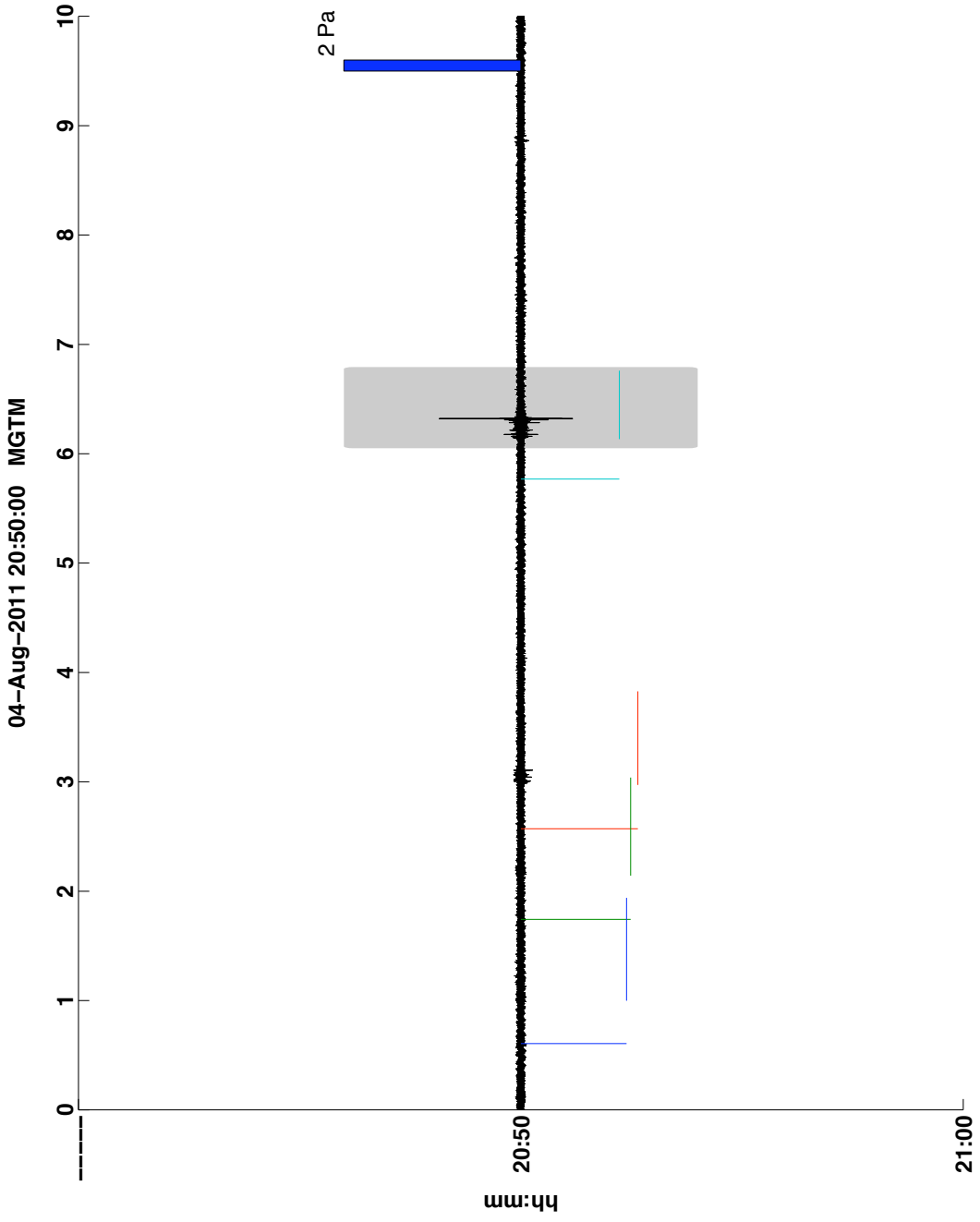

Figure A.18: This stormy period, on 4 August from 21:20 through 23:20, involves nearly continuous overlapping thunder signals (up to 15 at any given time). While background noise is relatively low for most of the storm and thunder signals have high signal, only a few isolated signals occur at the beginning of the storm. None were high enough amplitude for my catalog

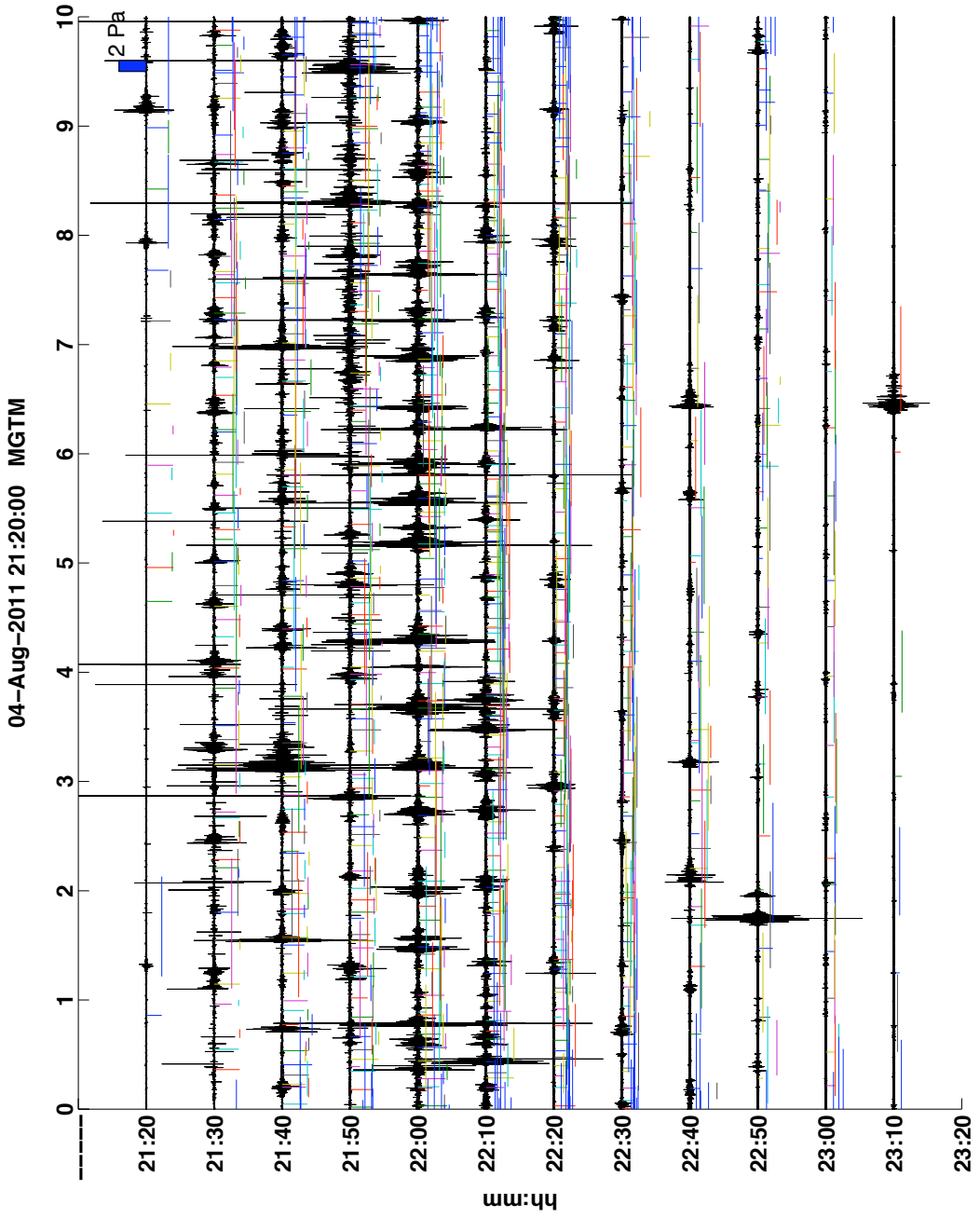

Figure A.19: Time period 19 includes five nearby, isolated events. I study about ten minutes, beginning at 20:12 on 5 August. All 5 events recorded during this time are high-amplitude and are incorporated into the catalog. There is almost no background noise. A potentially interesting note is that maximum signal amplitude decreases for each respective event.

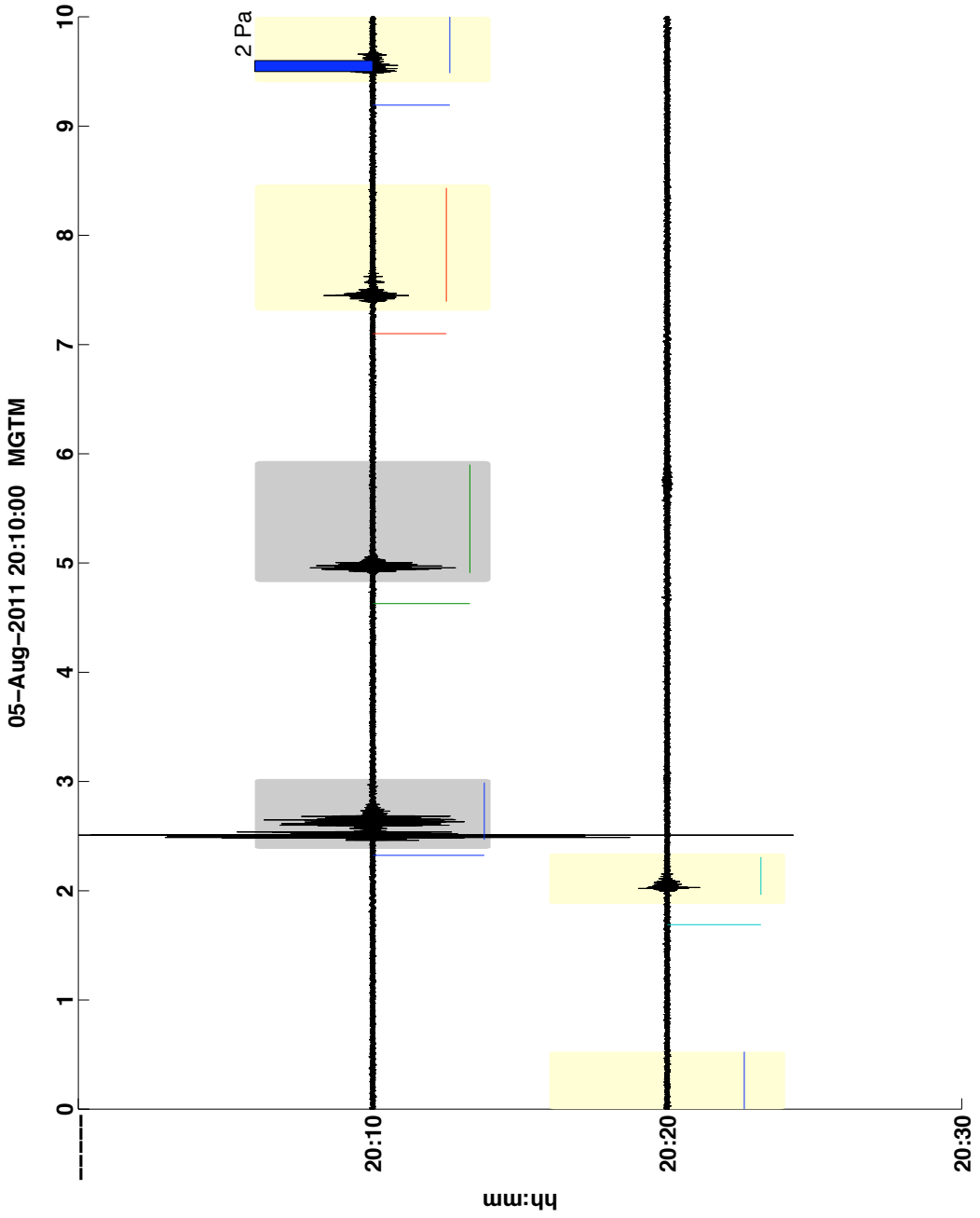

Figure A.20: This storm is evaluated over 30 minutes beginning at 00:30 on 7 August. There are relatively few events during this period and their peak amplitudes are less than 1 Pa. Background noise is minimal during this time of mostly isolated signals and 1 IC event is included in my catalog.

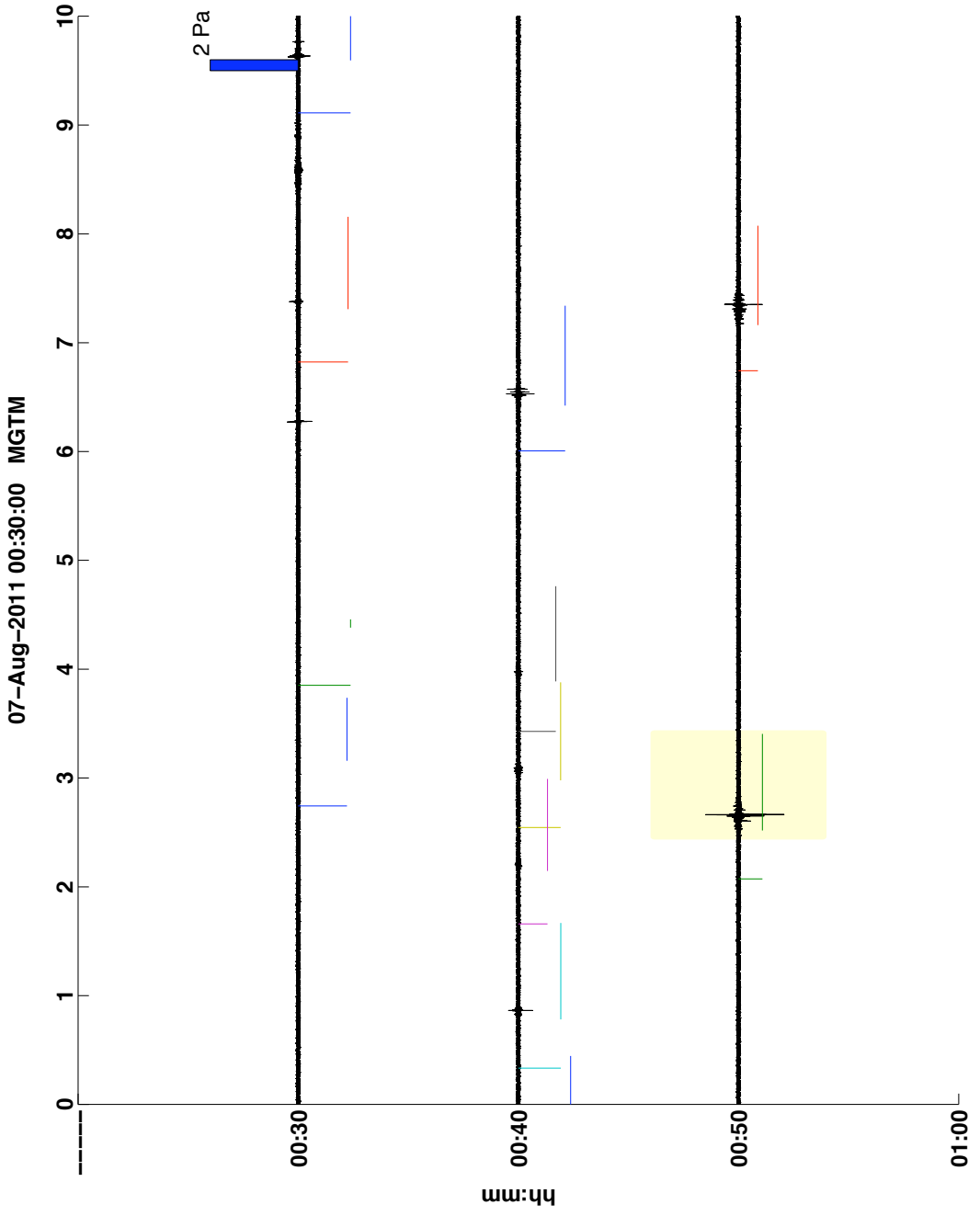

Figure A.21: This storm (beginning at 19:30 on 11 August), similar to others of long duration, begins and ends with isolated signals. However, signal overlap is surprisingly limited for much of the storm's duration. The highest number of overlapping events is 6. There is some minor background noise and occasional persistent noise in specific bands at GTM, possibly due to a nearby vehicle or machinery. Notably, there is a relatively high number of quality IC events recorded during this storm and 14 events are included in the catalog.

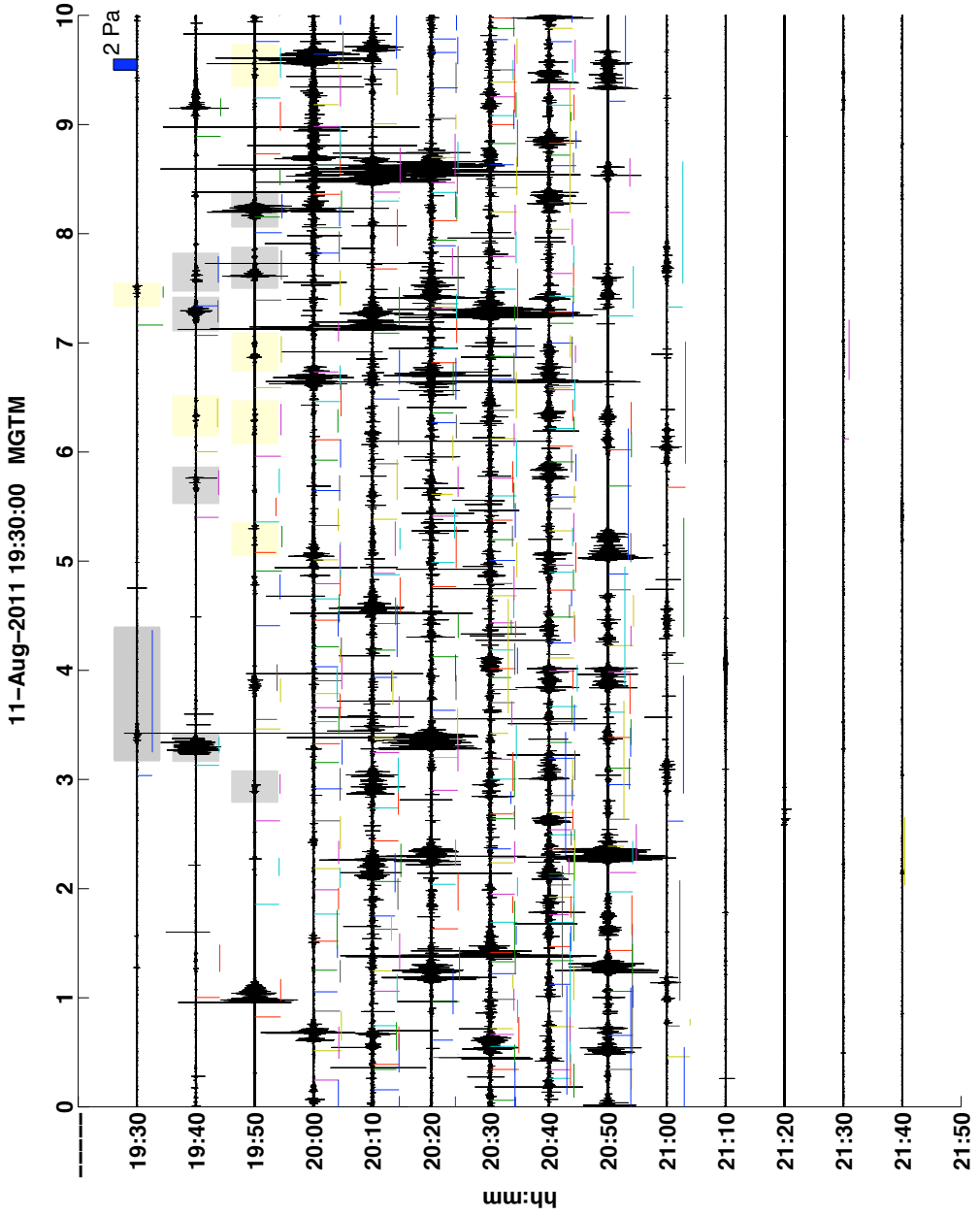

Figure A.22: Storm 22 begins at around 19:23 on 12 August and is analyzed for almost 30 minutes. The storm is close and there are frequent flashes, resulting in almost constant (but not necessarily overlapping) signal. Only 2 high-quality, isolated events are found - both are IC.

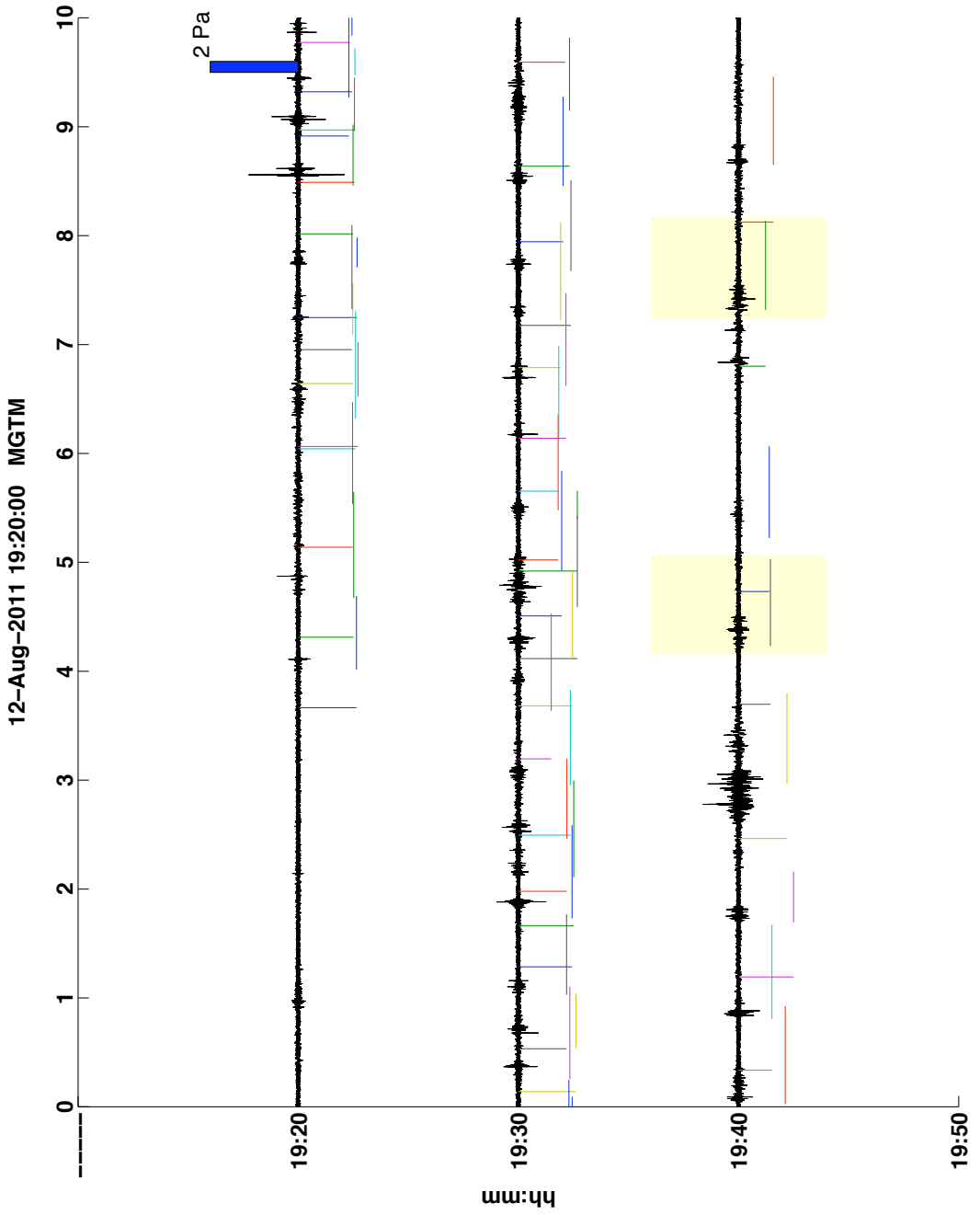

Figure A.23: The time period analyzed is 70 minutes long, beginning at 21:00 on 12 August. There are significant, isolated thunder signals generated near the network, including those from a number of nearby IC flashes. Thunder signal overlap increases then decreases between about 21:30 and 21:50. There is some unknown source of noise for a short time period at KVH. I analyze 13 thunder signals, mostly from IC events.

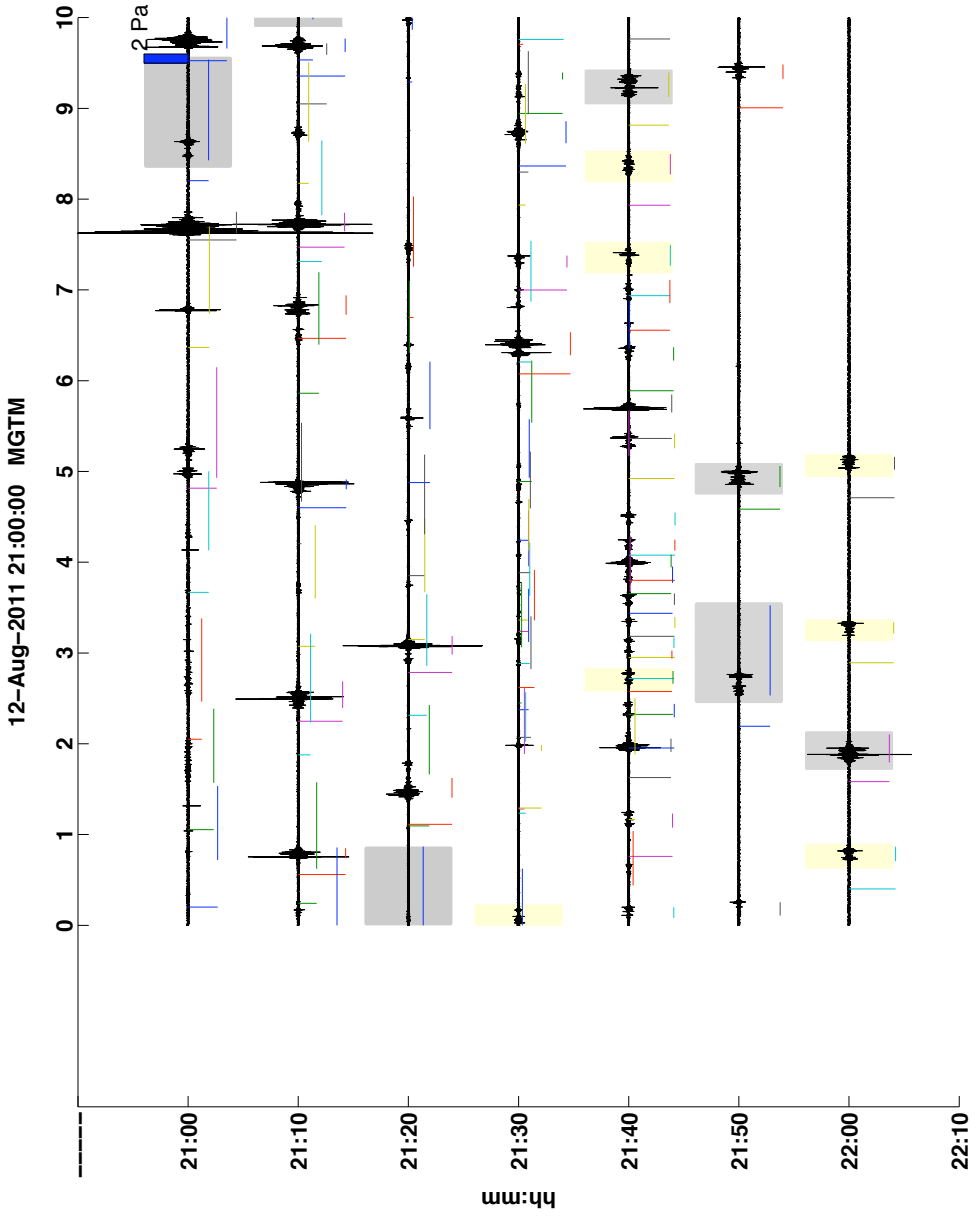

Figure A.24: Two isolated flashes occurred very close to the network between 19:22 and 19:27 on 16 August. The first is classified as an IC flash and the second is a CG with peak amplitude over 10 Pa. Both events are included in the catalog

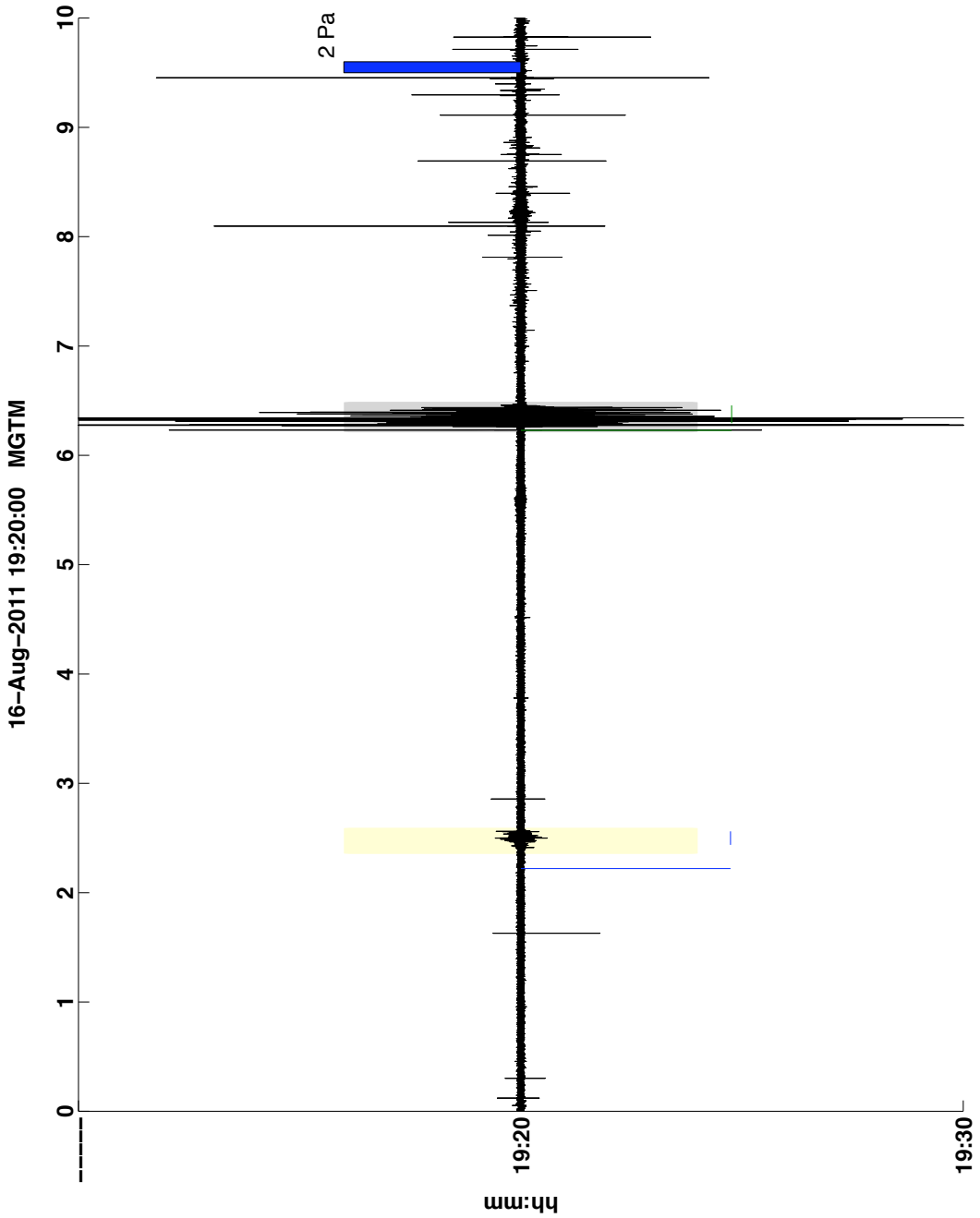

Figure A.25: An isolated CG flash occurs approximately 5 km from the network at 20:12 on 16 August. It is detected with high SNR and included in the catalog.

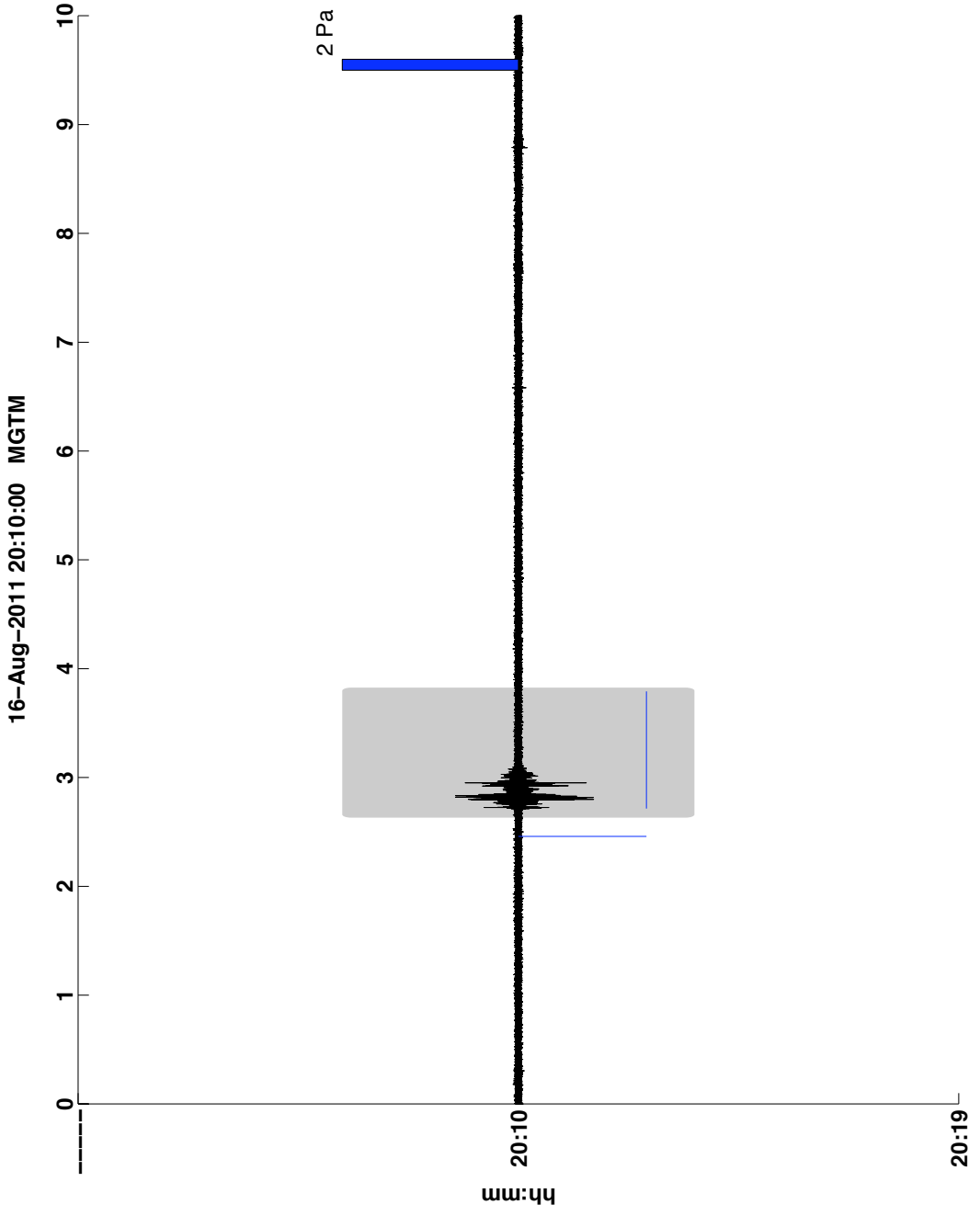

Figure A.26: A long-duration storm begins at 20:00 on 17 August and lasts for 90 minutes. I analyze 3 isolated signals that all occur near the beginning of the storm, including a CG with peak amplitude over 30 Pa at GTM. There are many flashes occurring at a wide range of distances during this storm, resulting in up to 12 overlapping signals at any time.

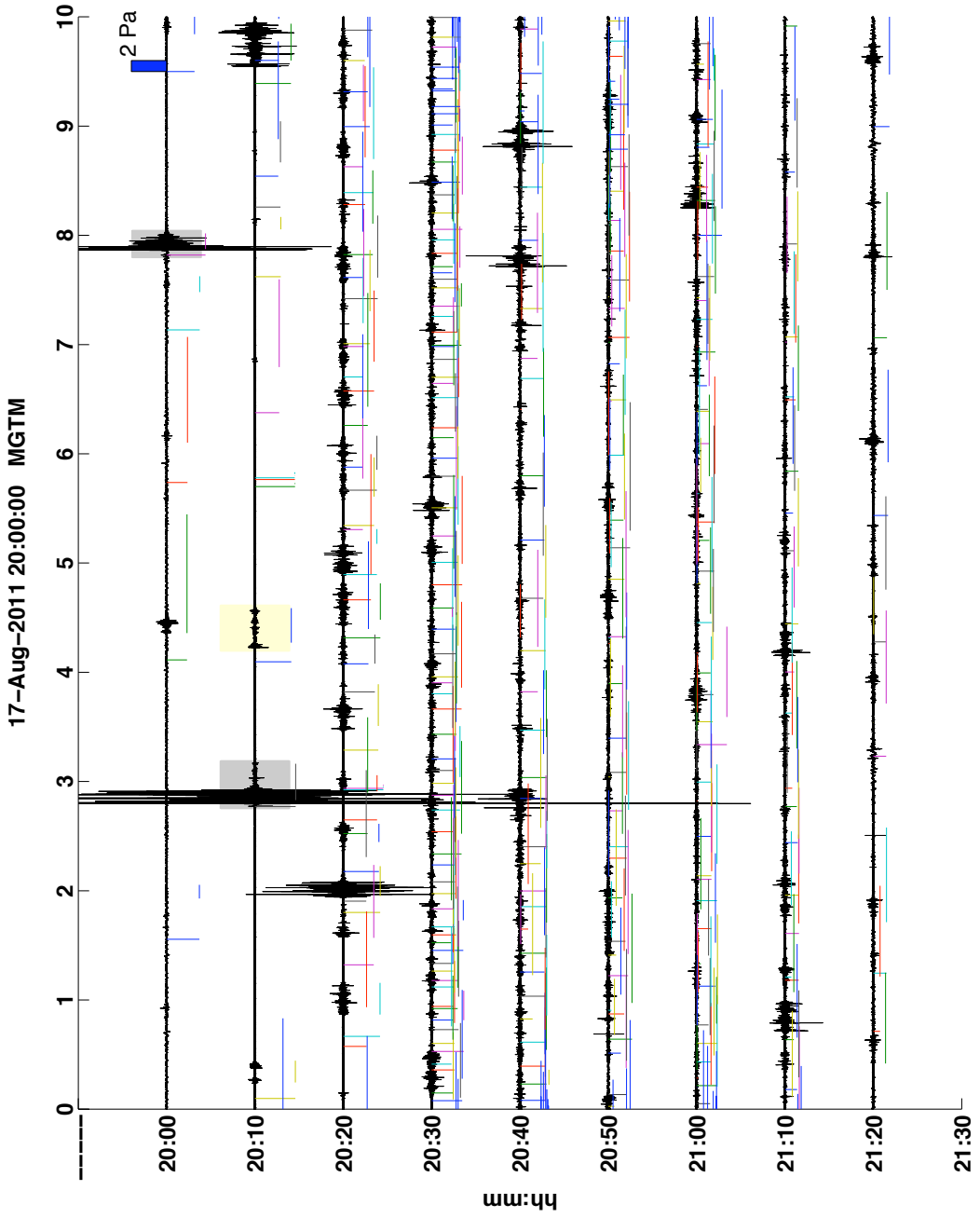

Figure A.27: Time period 27 is analyzed beginning at about 15:10 on 18 August. There are two distinct periods of mostly isolated thunder separated by about 20 minutes of quiet. There is a constant source of 60 Hz background noise at GTM for much of the storm. My catalog includes 3 thunder signals. The rapid succession of apparent LMA events beginning at about 21:55 is actually a result of a plane flying overhead. This is the only time that such interference passed my LMA filters and it does not mask a signal strong enough for analysis.

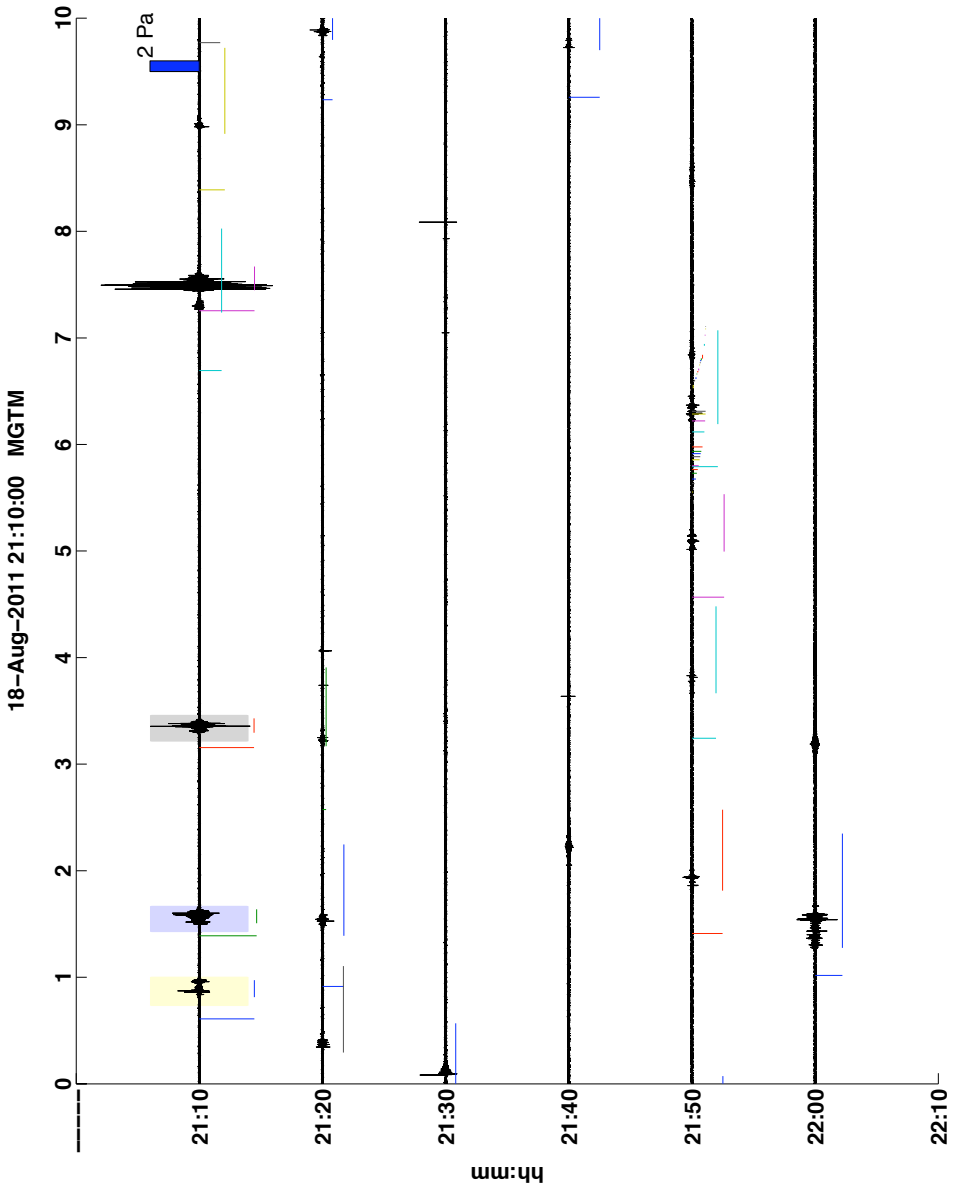

Figure A.28: This time period of mostly isolated thunder begins at around 22:43 on 19 August and is evaluated for 50 minutes. There is significant, low-frequency background noise at KVH. Only 1 very high-quality signal is recorded and analyzed.

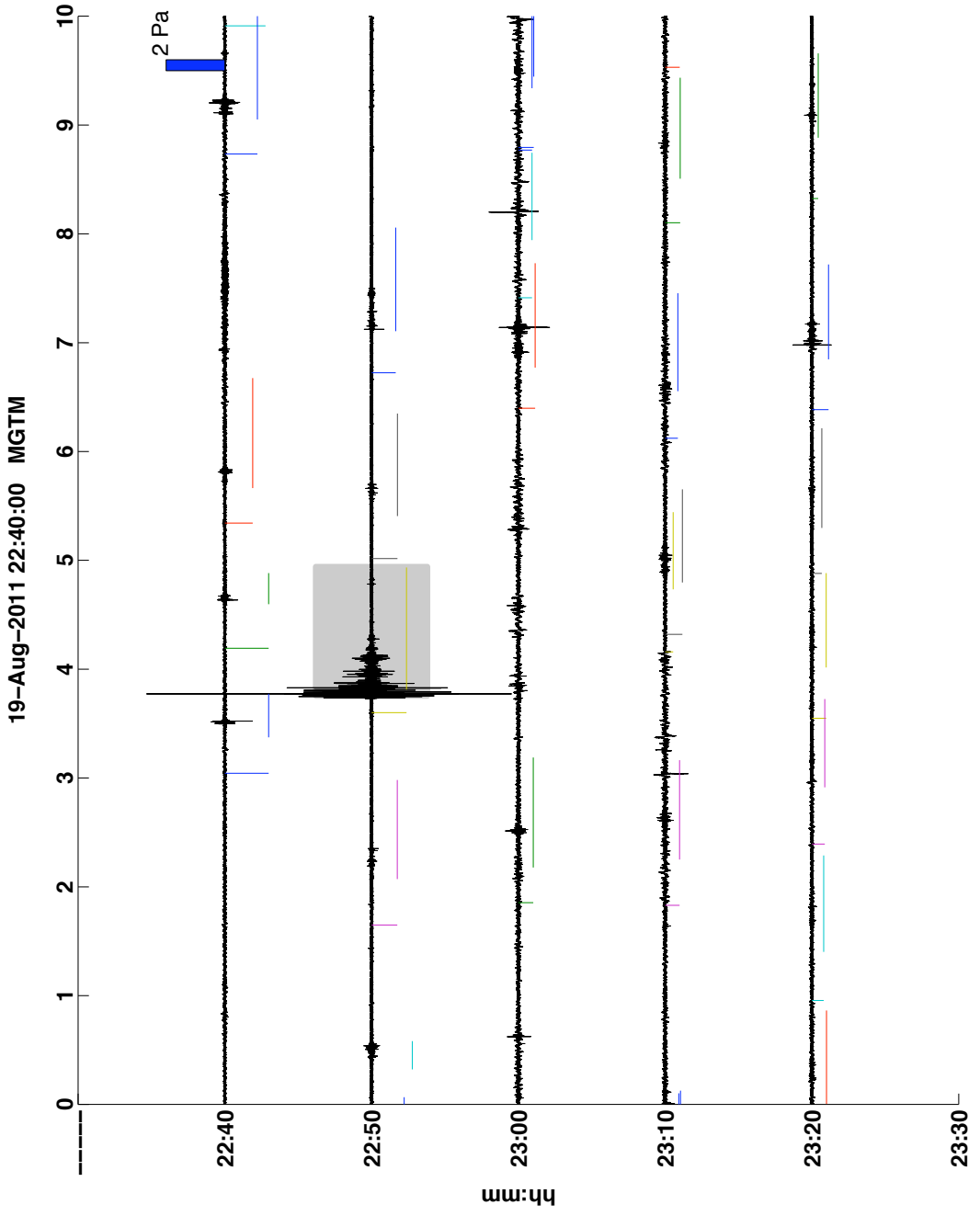

Figure A.29: The time period viewed for this storm is between 18:20 and 19:30 on 20 August. Thunder is mostly isolated, with some overlap. There is noise apparent for the first 40 minutes of the storm. The highest-quality signals are affected by bands of noise at GTM so no signals were included in the catalog.

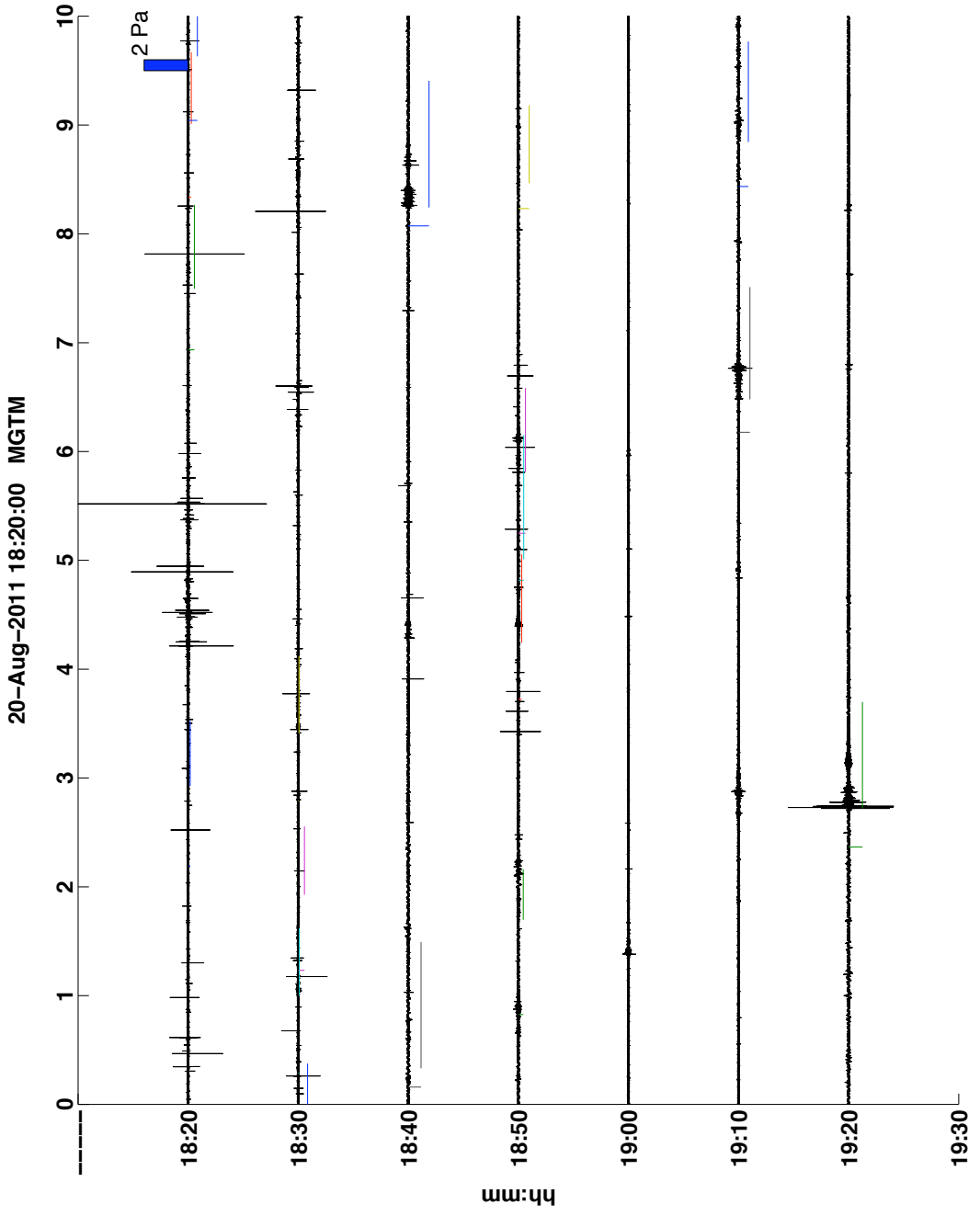

Figure A.30: Time period 30 includes 15 minutes of isolated thunder beginning at around 19:10 on 23 August, followed by just over 40 minutes of quiet, then almost 70 minutes of overlapping thunder from many distant sources. I include 11 events in the catalog - all from either the early isolated thunder period or from the end of the storm.

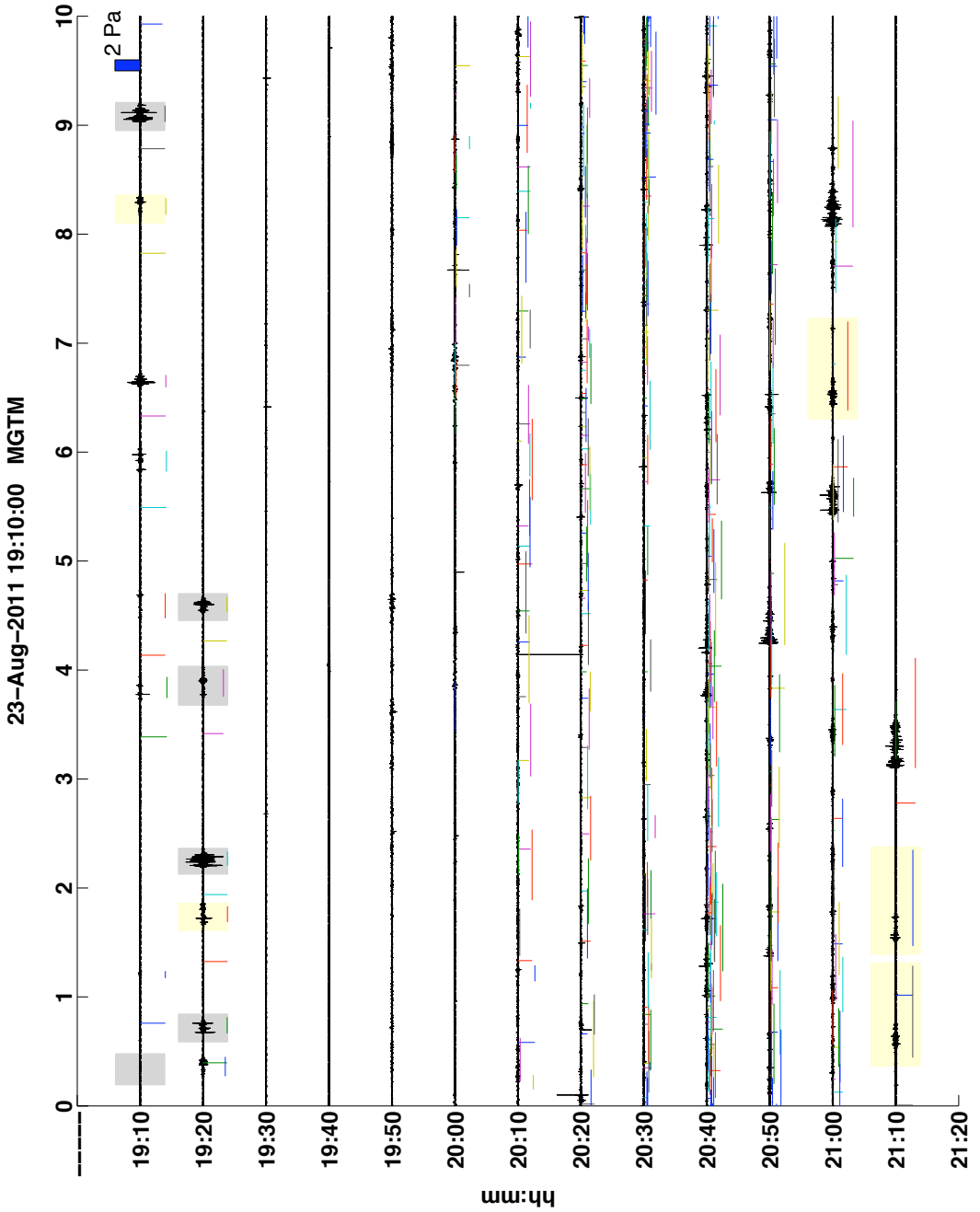

Figure A.31: The isolated thunder during this time period makes it ideal for analysis. The period spans 19 minutes starting at 23:35 on 25 August. There are 9 isolated signals propagating from nearby sources; 8 of them have adequate SNR for analysis.

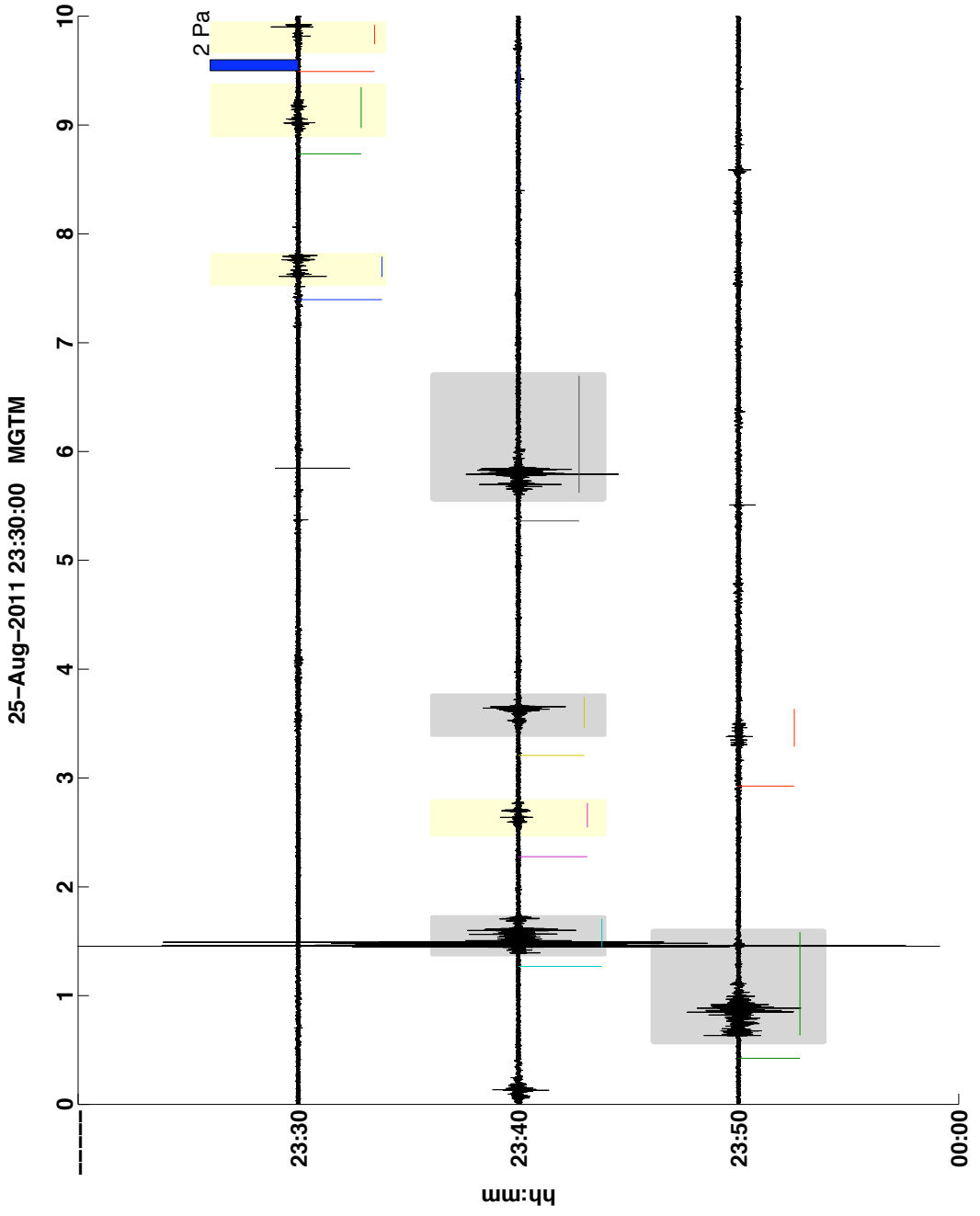

Figure A.32: Storm 32 is evaluated between 19:30 and 21:20 on 28 August. It begins with isolated thunder, followed by overlapping thunder, and ending with a few isolated events (culminating with a final, very loud event with peak amplitude on the order of tens of pascals) and 19 events are included in the catalog.

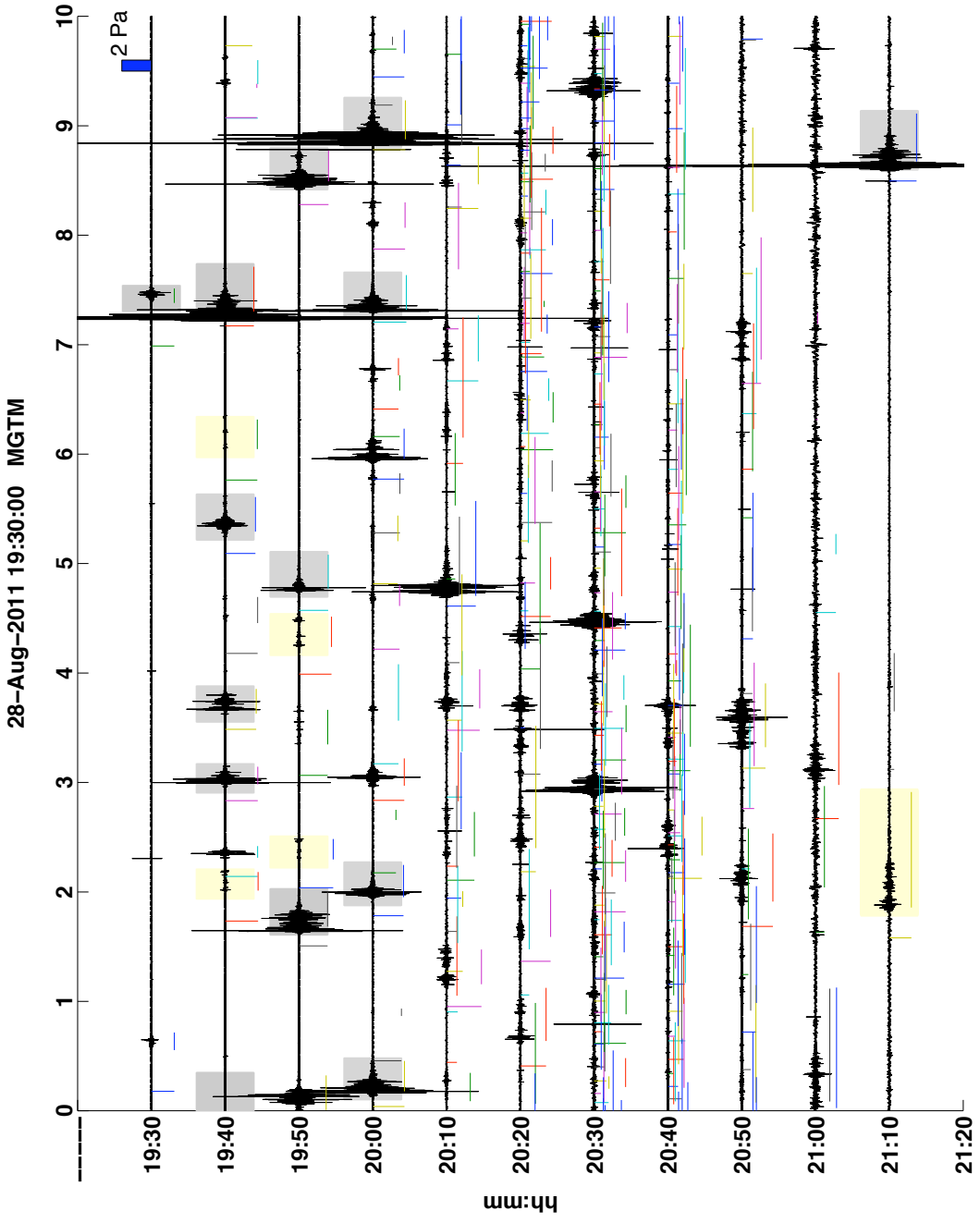

Figure A.33: Storm 33 is unique in that it is relatively long duration but includes mostly isolated thunder (with more overlap toward the end). It is evaluated for 60 minutes starting at 00:10 GMT on 3 September. There is minimal background noise and both high-quality IC and CG events are recorded, mostly in the first 40 minutes of the stormy period. None of the signals exhibit exceptional amplitudes. I investigate 23 events, nearly all from IC sources.

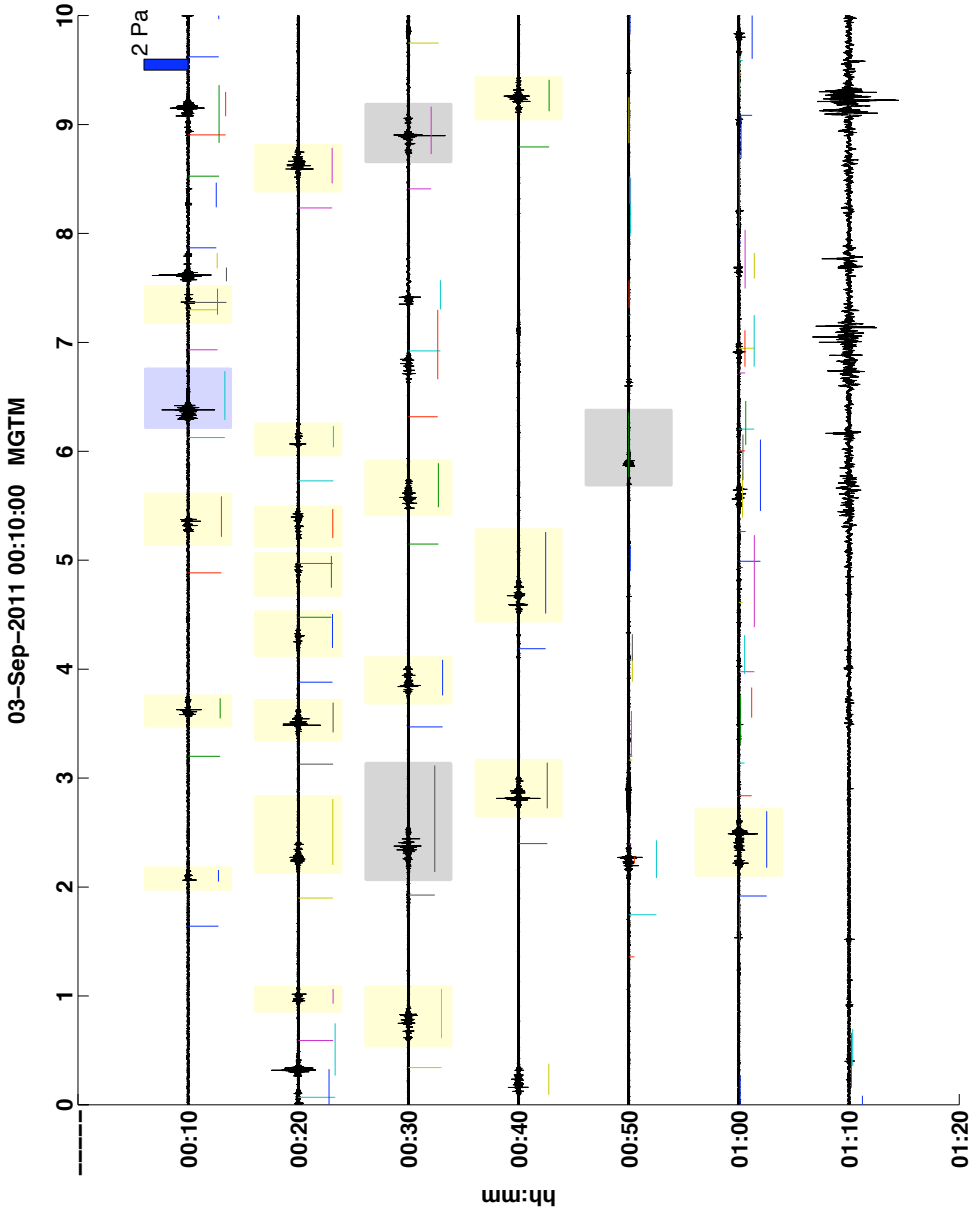

Figure A.34: The final stormy time period includes signals similar to those in the previous storm. This time period is has a higher proportion of overlapping signals. The storm begins at around 19:06 on 3 September and 60 minutes are considered. While the signals are again not high-amplitude, the background noise is minimal and 5 IC events are incorporated into the catalog.

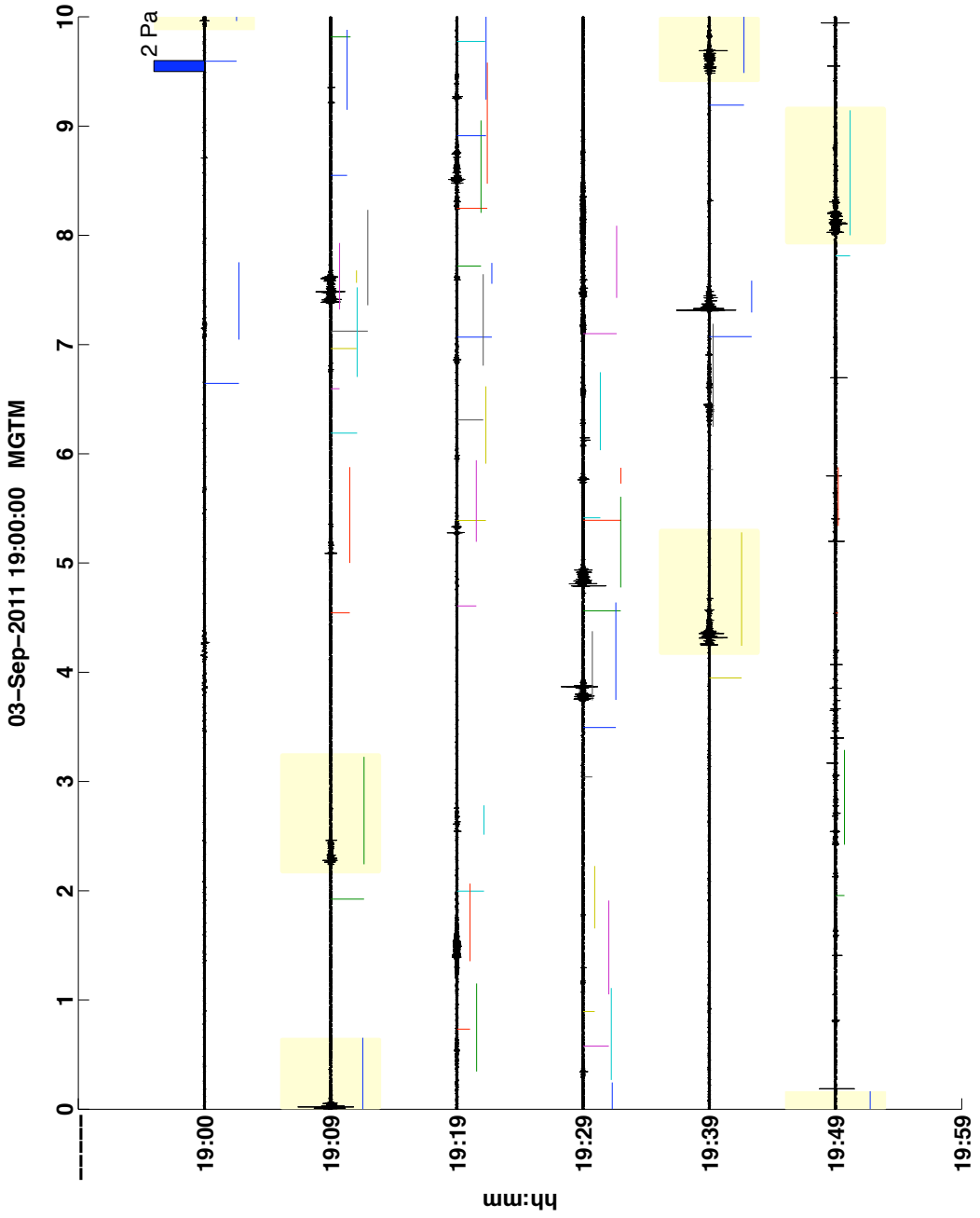

APPENDIX B

GTM AND KVH METADATA FOR CATALOG EVENTS

Table B.1: Metadata including LMA time and the picked thunder arrival and duration at GTM and KVH for the 191 cataloged events.

	LMA time (YYYY-MM-DD hh:mm:ss)	**Picked GTM time (mm:ss)**	**Picked GTM duration (s)**	**Picked KVH time (mm:ss)**	**Picked KVH duration (s)**
1	2011-07-20 20:06:42	06:50	17.6	06:50	17.7
2	2011-07-20 20:11:17	11:36	18.5	11:36	18.2
3	2011-07-20 20:12:43	12:53	17.4	12:52	17.6
4	2011-07-20 20:14:15	14:33	16.7	14:32	17.2
5	2011-07-20 20:23:34	23:42	13.7	23:40	14.3
6	2011-07-20 20:24:42	24:53	12.0	24:52	13.2
7	2011-07-20 20:26:25	26:34	10.6	26:32	11.6
8	2011-07-22 19:15:27	15:48	7.8	15:49	7.6
9	2011-07-22 19:17:37	17:39	32.1	17:40	31.4
10	2011-07-22 19:17:54	18:30	16.8	18:31	15.0
11	2011-07-22 19:19:22	19:44	9.5	19:44	10.5
12	2011-07-22 21:28:53	29:13	26.3	29:13	27.0
13	2011-07-22 21:42:10	42:30	56.0	42:31	54.0
14	2011-07-24 17:51:22	51:32	12.1	51:30	13.1
15	2011-07-24 17:55:01	55:02	8.5	55:02	11.8
16	2011-07-24 18:00:09	00:18	16.9	00:17	16.0
17	2011-07-24 18:02:48	02:50	11.4	02:49	13.0
18	2011-07-24 18:14:37	14:47	11.8	14:46	12.8
19	2011-07-24 18:16:11	16:29	16.4	16:27	16.9
20	2011-07-24 18:17:54	18:02	21.8	18:01	22.0
21	2011-07-24 18:22:31	22:33	25.1	22:32	26.8
22	2011-07-27 22:02:03	02:09	17.9	02:08	18.2
23	2011-07-27 22:07:33	07:47	8.5	07:49	10.6

Table B.1: Continued

24	2011-07-27 22:12:31	12:45	19.5	12:50	15.7
25	2011-07-27 22:15:03	15:17	15.9	15:20	13.2
26	2011-07-27 22:16:44	16:59	16.1	17:00	16.3
27	2011-07-27 22:21:12	21:30	16.3	21:30	15.2
28	2011-07-27 22:26:56	27:15	15.3	27:16	15.5
29	2011-07-27 22:32:09	32:31	20.3	32:33	19.8
30	2011-07-27 22:35:42	35:51	22.5	35:51	25.9
31	2011-07-27 23:11:13	11:22	9.5	11:24	9.0
32	2011-07-27 23:16:32	16:42	23.7	16:41	25.0
33	2011-07-27 23:45:59	46:01	21.2	46:00	21.2
34	2011-07-28 06:18:44	19:11	27.2	19:11	27.1
35	2011-07-28 06:26:02	26:37	16.0	26:38	15.1
36	2011-07-28 06:29:05	29:37	25.7	29:41	21.0
37	2011-07-28 21:33:22	33:35	11.0	33:33	12.2
38	2011-07-28 21:40:28	40:43	9.8	40:42	11.0
39	2011-07-28 21:43:16	43:32	16.2	43:31	17.2
40	2011-07-28 21:46:33	46:52	16.0	46:51	16.0
41	2011-07-28 21:48:01	48:17	16.6	48:15	22.6
42	2011-07-28 21:57:01	57:21	13.3	57:20	13.6
43	2011-07-28 22:05:46	05:53	20.4	05:53	19.8
44	2011-07-28 22:07:14	07:32	19.2	07:31	20.1
45	2011-07-30 22:09:57	10:36	26.6	10:37	36.6
46	2011-07-30 22:11:58	12:04	36.5	12:02	42.0
47	2011-07-31 22:41:14	41:26	8.5	41:24	9.1
48	2011-07-31 22:46:50	47:13	7.2	47:12	7.3
49	2011-07-31 22:49:22	49:42	11.7	49:39	12.8
50	2011-08-02 20:55:29	55:41	8.5	55:41	8.4
51	2011-08-02 22:14:35	14:41	10.0	14:43	8.1
52	2011-08-03 17:02:00	02:08	10.2	02:09	8.8
53	2011-08-03 18:00:03	00:05	13.0	00:04	12.8
54	2011-08-03 18:04:09	04:18	15.9	04:17	17.1
55	2011-08-03 18:06:57	07:01	17.7	07:02	16.7
56	2011-08-03 18:09:46	09:47	13.3	09:48	11.7
57	2011-08-03 18:11:31	11:33	15.3	11:32	15.1
58	2011-08-03 18:14:39	14:41	14.4	14:41	13.3
59	2011-08-03 18:19:49	19:50	17.8	19:49	18.2
60	2011-08-03 19:05:42	05:53	5.1	05:52	4.8
61	2011-08-03 19:06:26	06:27	12.7	06:27	15.0
62	2011-08-03 19:07:00	07:01	16.7	07:02	15.9

Table B.1: Continued

63	2011-08-03 19:08:02	08:04	16.4	08:02	17.5
64	2011-08-03 19:08:43	08:45	17.3	08:45	16.7
65	2011-08-03 19:09:29	09:33	13.0	09:33	12.8
66	2011-08-03 19:10:01	10:04	16.3	10:03	16.6
67	2011-08-03 19:11:17	11:20	18.8	11:20	18.3
68	2011-08-03 19:12:17	12:18	18.4	12:18	17.4
69	2011-08-03 19:13:44	13:48	13.4	13:49	12.6
70	2011-08-03 19:16:47	16:54	15.7	16:53	15.6
71	2011-08-04 00:21:26	21:49	29.5	21:56	23.3
72	2011-08-04 00:32:51	33:01	33.9	33:01	34.2
73	2011-08-04 00:44:17	44:24	22.7	44:25	24.4
74	2011-08-04 00:47:33	47:40	34.6	47:40	32.4
75	2011-08-04 00:49:19	49:26	19.0	49:27	16.9
76	2011-08-04 01:03:51	03:55	17.0	03:55	16.2
77	2011-08-04 01:06:46	06:49	24.7	06:49	25.1
78	2011-08-04 01:09:16	09:19	24.0	09:20	22.1
79	2011-08-04 01:14:55	15:00	23.6	14:59	24.2
80	2011-08-04 20:55:46	56:06	20.3	56:08	17.2
81	2011-08-05 20:12:19	12:27	20.0	12:27	18.8
82	2011-08-05 20:14:37	14:52	16.1	14:53	13.7
83	2011-08-05 20:17:06	17:20	20.3	17:21	22.6
84	2011-08-05 20:19:11	19:25	25.0	19:26	23.1
85	2011-08-05 20:21:41	21:57	14.1	21:59	13.4
86	2011-08-07 00:52:04	52:30	21.9	52:29	21.9
87	2011-08-11 19:33:02	33:14	30.5	33:14	23.4
88	2011-08-11 19:37:09	37:24	7.3	37:24	7.2
89	2011-08-11 19:43:07	43:13	10.4	43:14	9.9
90	2011-08-11 19:45:24	45:36	11.9	45:36	11.7
91	2011-08-11 19:46:00	46:11	18.0	46:13	17.4
92	2011-08-11 19:47:04	47:10	13.0	47:11	12.7
93	2011-08-11 19:47:20	47:31	14.1	47:31	15.0
94	2011-08-11 19:52:37	52:51	11.7	52:48	13.7
95	2011-08-11 19:54:54	55:07	12.5	55:06	13.2
96	2011-08-11 19:55:57	56:08	18.3	56:08	17.5
97	2011-08-11 19:56:35	56:46	17.4	56:46	17.3
98	2011-08-11 19:57:23	57:32	16.6	57:31	15.8
99	2011-08-11 19:58:00	58:06	14.7	58:06	14.7
100	2011-08-11 19:59:14	59:24	18.2	59:24	18.2
101	2011-08-12 19:43:41	44:12	24.6	44:11	25.8

Table B.1: Continued

102	2011-08-12 19:46:48	47:18	23.1	47:16	24.6
103	2011-08-12 21:08:12	08:23	24.7	08:22	28.5
104	2011-08-12 21:19:32	19:35	21.6	19:34	21.1
105	2011-08-12 21:39:45	40:04	8.5	40:03	9.1
106	2011-08-12 21:42:19	42:36	12.6	42:37	10.8
107	2011-08-12 21:46:56	47:15	14.3	47:15	14.6
108	2011-08-12 21:47:55	48:13	16.8	48:14	15.8
109	2011-08-12 21:48:48	49:05	18.1	49:05	18.6
110	2011-08-12 21:52:11	52:28	24.8	52:29	24.0
111	2011-08-12 21:54:35	54:49	13.7	54:50	13.3
112	2011-08-12 22:00:24	00:41	10.9	00:42	10.4
113	2011-08-12 22:01:35	01:47	18.0	01:47	17.5
114	2011-08-12 22:02:53	03:12	8.5	03:12	7.7
115	2011-08-12 22:04:42	05:01	9.5	05:00	9.7
116	2011-08-16 19:22:13	22:24	10.2	22:23	10.5
117	2011-08-16 19:26:13	26:15	11.7	26:15	11.5
118	2011-08-16 20:12:27	12:40	29.5	12:40	31.1
119	2011-08-17 20:07:49	07:50	10.3	07:49	10.8
120	2011-08-17 20:12:46	12:47	18.2	12:47	16.9
121	2011-08-17 20:14:05	14:12	23.3	14:11	24.1
122	2011-08-18 21:10:36	10:48	10.4	10:48	10.5
123	2011-08-18 21:11:23	11:29	8.7	11:28	9.0
124	2011-08-18 21:13:09	13:17	8.2	13:17	8.5
125	2011-08-19 22:53:36	53:42	36.3	53:44	34.3
126	2011-08-23 19:17:49	18:10	10.9	18:11	10.1
127	2011-08-23 19:18:47	19:01	9.7	19:02	9.4
128	2011-08-23 19:19:55	20:16	10.5	20:17	11.1
129	2011-08-23 19:20:23	20:39	9.9	20:40	8.9
130	2011-08-23 19:21:19	21:39	11.5	21:38	12.3
131	2011-08-23 19:21:56	22:10	9.9	22:12	8.9
132	2011-08-23 19:23:25	23:44	16.6	23:45	15.7
133	2011-08-23 19:24:16	24:31	9.8	24:32	9.3
134	2011-08-23 21:05:51	06:22	26.4	06:23	23.7
135	2011-08-23 21:10:00	10:26	29.8	10:26	30.6
136	2011-08-23 21:11:00	11:26	33.2	11:27	31.1
137	2011-08-25 23:37:23	37:36	12.2	37:35	12.7
138	2011-08-25 23:38:44	38:56	19.9	38:55	22.3
139	2011-08-25 23:39:29	39:44	11.4	39:44	11.4
140	2011-08-25 23:41:16	41:23	16.1	41:21	16.8

Table B.1: Continued

141	2011-08-25 23:42:16	42:32	13.8	42:31	14.2
142	2011-08-25 23:43:12	43:28	15.1	43:27	17.4
143	2011-08-25 23:45:21	45:35	24.5	45:34	26.7
144	2011-08-25 23:50:25	50:35	35.5	50:35	33.9
145	2011-08-28 19:36:59	37:22	8.3	37:23	8.3
146	2011-08-28 19:41:44	41:59	12.0	42:00	11.3
147	2011-08-28 19:42:50	42:58	8.7	43:00	8.2
148	2011-08-28 19:43:29	43:37	13.5	43:38	12.8
149	2011-08-28 19:45:05	45:14	14.3	45:15	13.5
150	2011-08-28 19:45:45	46:01	16.1	46:01	15.8
151	2011-08-28 19:47:10	47:12	18.3	47:11	18.6
152	2011-08-28 19:49:43	50:00	16.9	50:00	16.0
153	2011-08-28 19:51:30	51:36	18.2	51:37	17.0
154	2011-08-28 19:52:02	52:17	12.2	52:17	11.5
155	2011-08-28 19:53:59	54:14	17.5	54:13	17.8
156	2011-08-28 19:54:34	54:43	10.8	54:43	10.3
157	2011-08-28 19:58:16	58:24	21.7	58:25	21.4
158	2011-08-28 20:00:02	00:07	15.1	00:08	15.1
159	2011-08-28 20:01:46	01:55	11.3	01:56	11.2
160	2011-08-28 20:07:12	07:17	15.7	07:16	13.9
161	2011-08-28 20:08:46	08:49	16.8	08:48	15.7
162	2011-08-28 21:11:34	11:46	36.7	11:47	33.5
163	2011-08-28 21:18:29	18:34	25.1	18:33	28.3
164	2011-09-03 00:11:38	12:02	8.0	12:01	7.5
165	2011-09-03 00:13:12	13:32	11.3	13:31	11.5
166	2011-09-03 00:14:53	15:12	15.4	15:11	16.7
167	2011-09-03 00:16:07	16:16	19.1	16:14	20.4
168	2011-09-03 00:16:55	17:14	15.4	17:12	15.2
169	2011-09-03 00:20:35	20:54	8.8	20:52	9.8
170	2011-09-03 00:21:53	22:09	19.9	22:07	22.7
171	2011-09-03 00:23:07	23:24	15.1	23:23	16.8
172	2011-09-03 00:23:52	24:10	17.1	24:07	20.6
173	2011-09-03 00:24:28	24:44	17.5	24:43	17.4
174	2011-09-03 00:24:58	25:11	17.1	25:09	17.2
175	2011-09-03 00:25:43	26:02	11.8	26:00	12.6
176	2011-09-03 00:28:14	28:29	17.2	28:27	18.7
177	2011-09-03 00:30:20	30:34	23.9	30:32	23.9
178	2011-09-03 00:31:55	32:08	31.2	32:07	31.6
179	2011-09-03 00:33:28	33:44	20.9	33:43	20.5

Table B.1: Continued

180	2011-09-03 00:35:08	35:27	22.6	35:24	23.6
181	2011-09-03 00:38:24	38:43	25.4	38:41	25.2
182	2011-09-03 00:42:23	42:42	23.4	42:40	23.7
183	2011-09-03 00:44:11	44:27	26.0	44:26	27.7
184	2011-09-03 00:48:47	49:05	19.3	49:03	19.8
185	2011-09-03 00:55:02	55:45	23.3	55:44	24.1
186	2011-09-03 01:01:55	02:09	31.7	02:08	30.9
187	2011-09-03 19:09:35	09:55	16.6	09:52	17.5
188	2011-09-03 19:11:55	12:11	23.1	12:11	23.2
189	2011-09-03 19:43:56	44:12	29.0	44:10	30.1
190	2011-09-03 19:49:11	49:26	27.9	49:25	28.7
191	2011-09-03 19:57:48	57:57	63.1	57:56	58.9

APPENDIX C

CG AND IC EVENTS AT ALL NETWORK CHANNELS

Time series data (filtered above 4 s) and PSDs are shown at 16 channels for selected CG and IC events. PSDs are in linear scale (on the left) and with a logarithmic x-scale (on the right). Peak frequency is indicated in hertz. The LMA flash time is specified above the top left plot and station name and channel number are indicated to the left of the time series plots. Note that y-axes differ among channels. Not all sensors were used in evaluation of thunder properties - some were subject to recording issues or noise. The variation in signal characteristics across the network demonstrates the importance of multi-sensor observations of thunder. Beginning in early September, a timing error occurred at station LAN. After visual inspection, all LAN signals recorded in September were shifted forward 21 s and timing therefore cannot be assumed to be accurate.

Figure C.1: Signals and PSDs shown for all channels for a CG event on 20 July. Peak frequencies at functional sensors are below 3 Hz. Channel LAN 2 was not functioning properly for the first portion of the season.

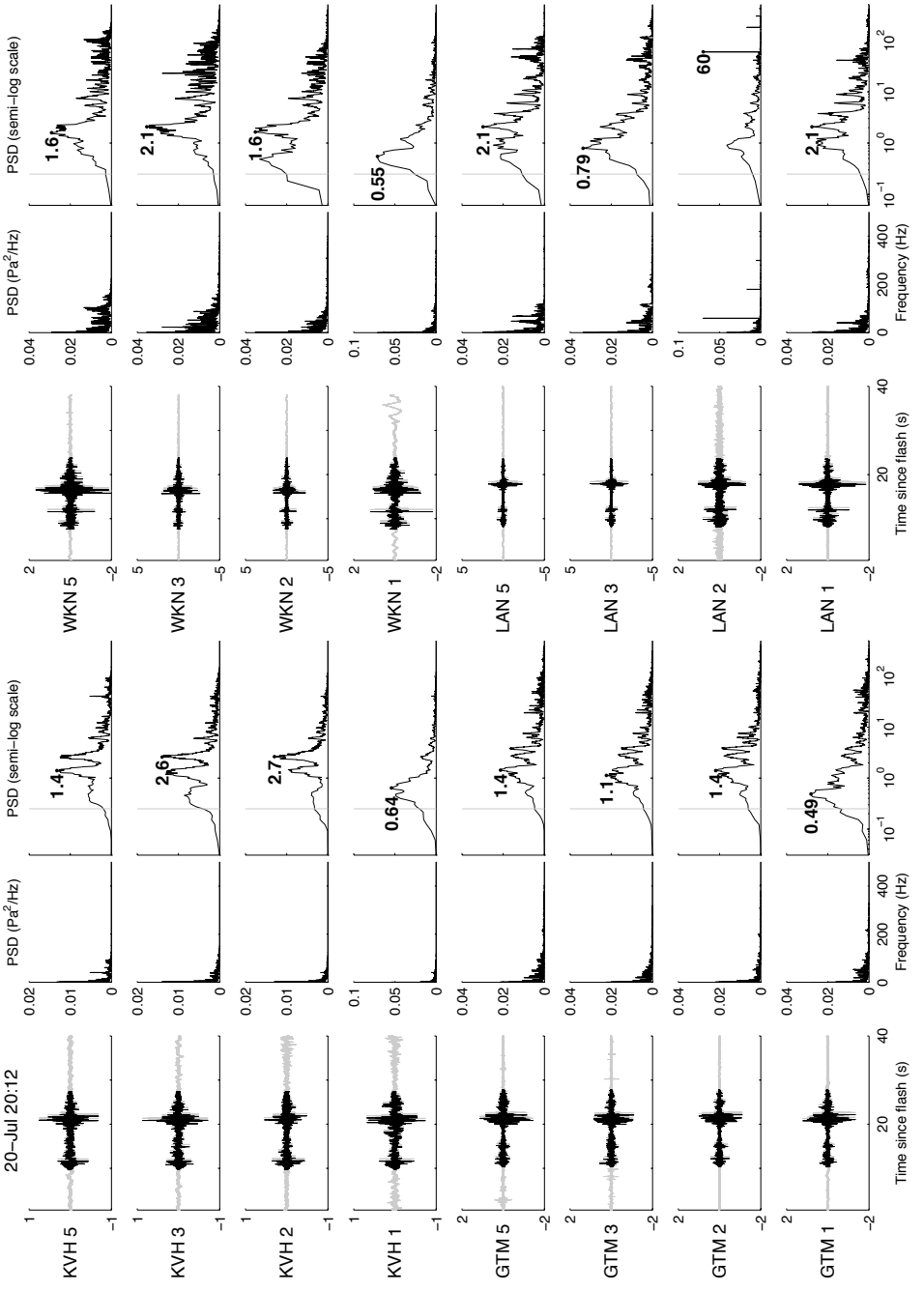

Figure C.2: A CG event occurred on 24 July with energy at low and high frequencies.

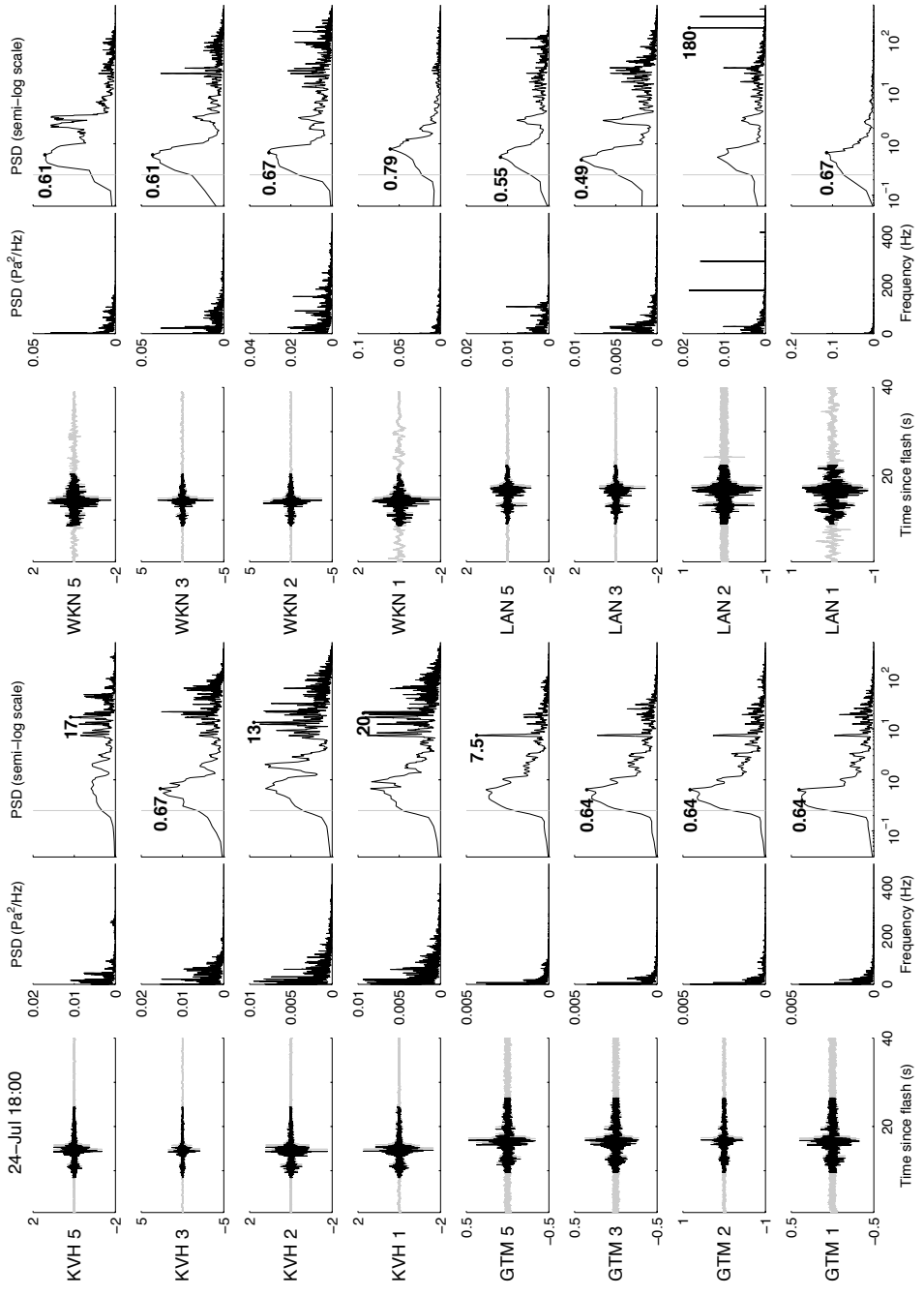

Figure C.3: Signals are shown for another CG thunder event on 24 July. Note significant differences in signal character at different arrays.

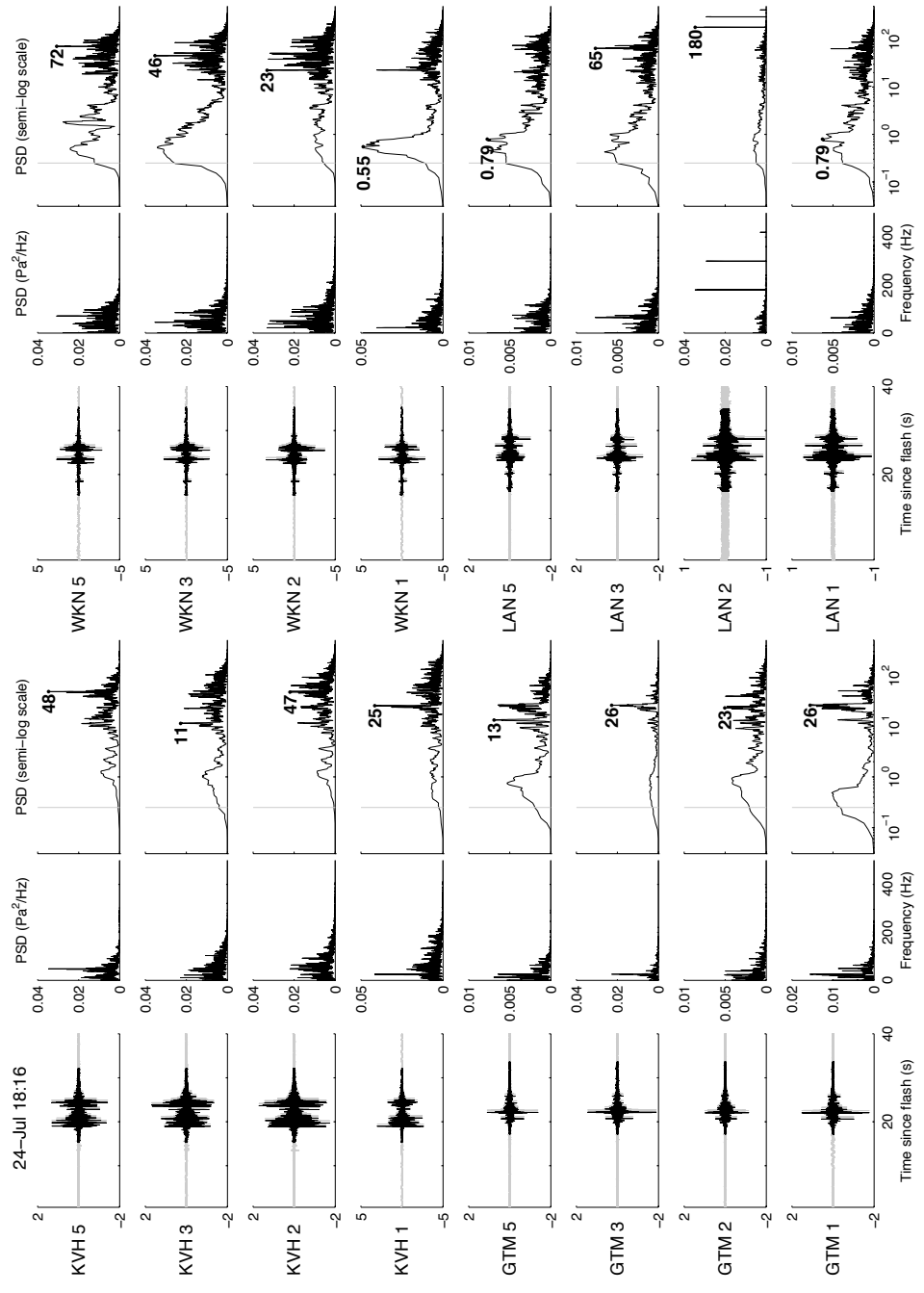

Figure C.4: Plots showing thunder and power spectra for a CG flash on 27 July. Some sensors, including LAN 2 and LAN 3, were not functioning properly.

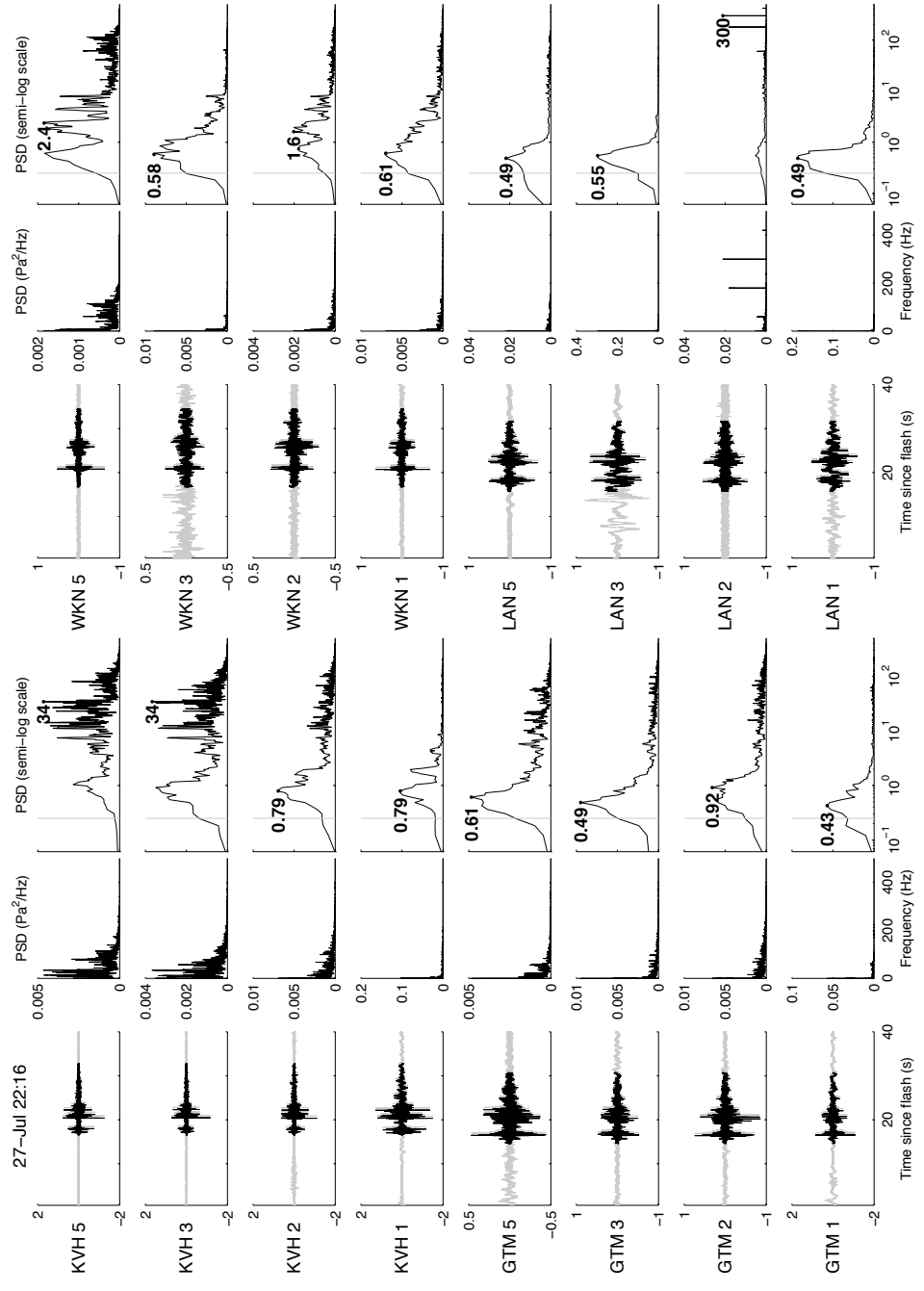

Figure C.5: A second CG event was recorded on 27 July with broadband energy at most sensors.

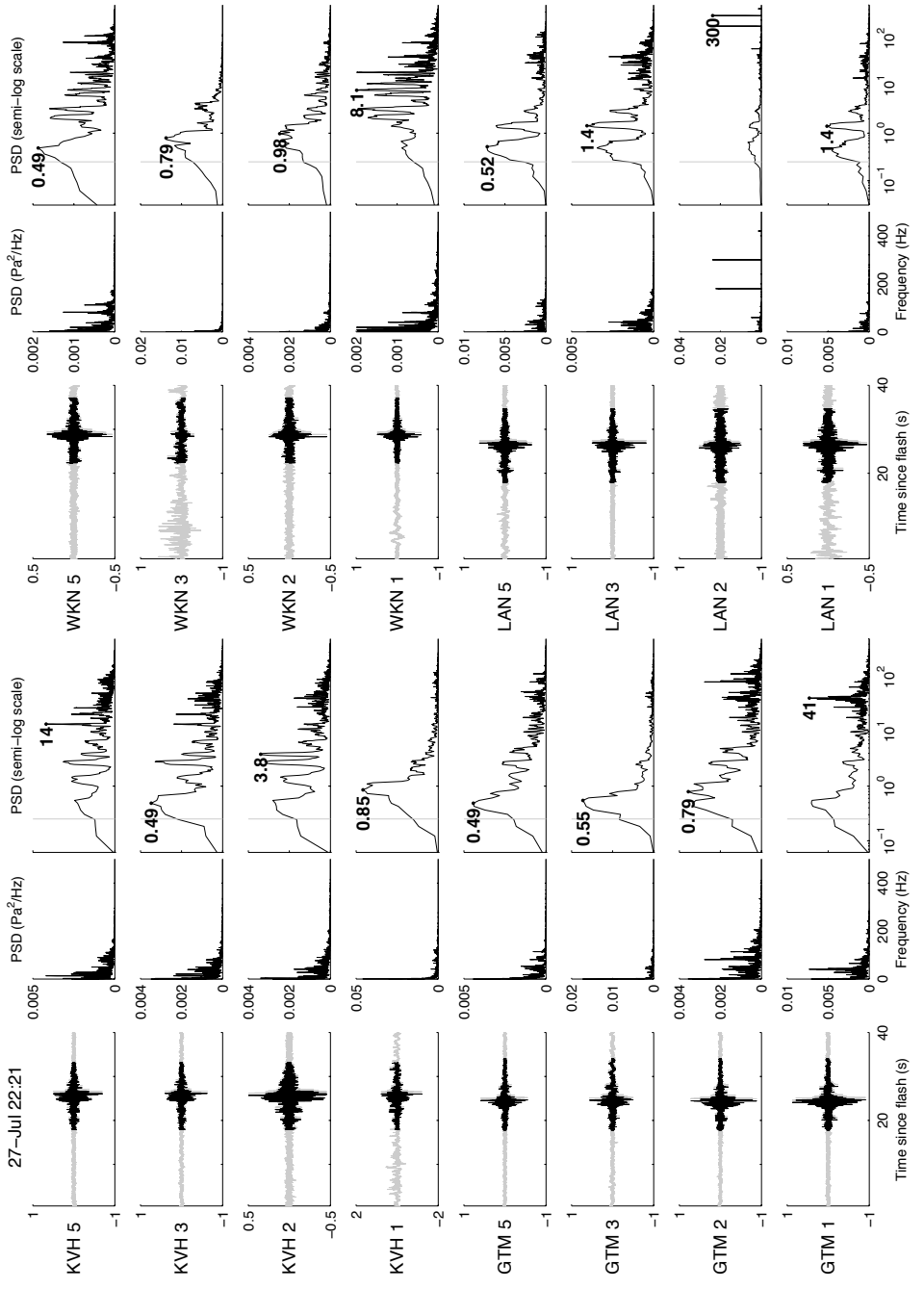

Figure C.6: Signals and PSDs are shown for a third event on 27 July. Channels occasionally experience significant noise, as do WKN 2 and WKN 3 in this case. This demonstrates the need for quality control prior to estimates of spectral content.

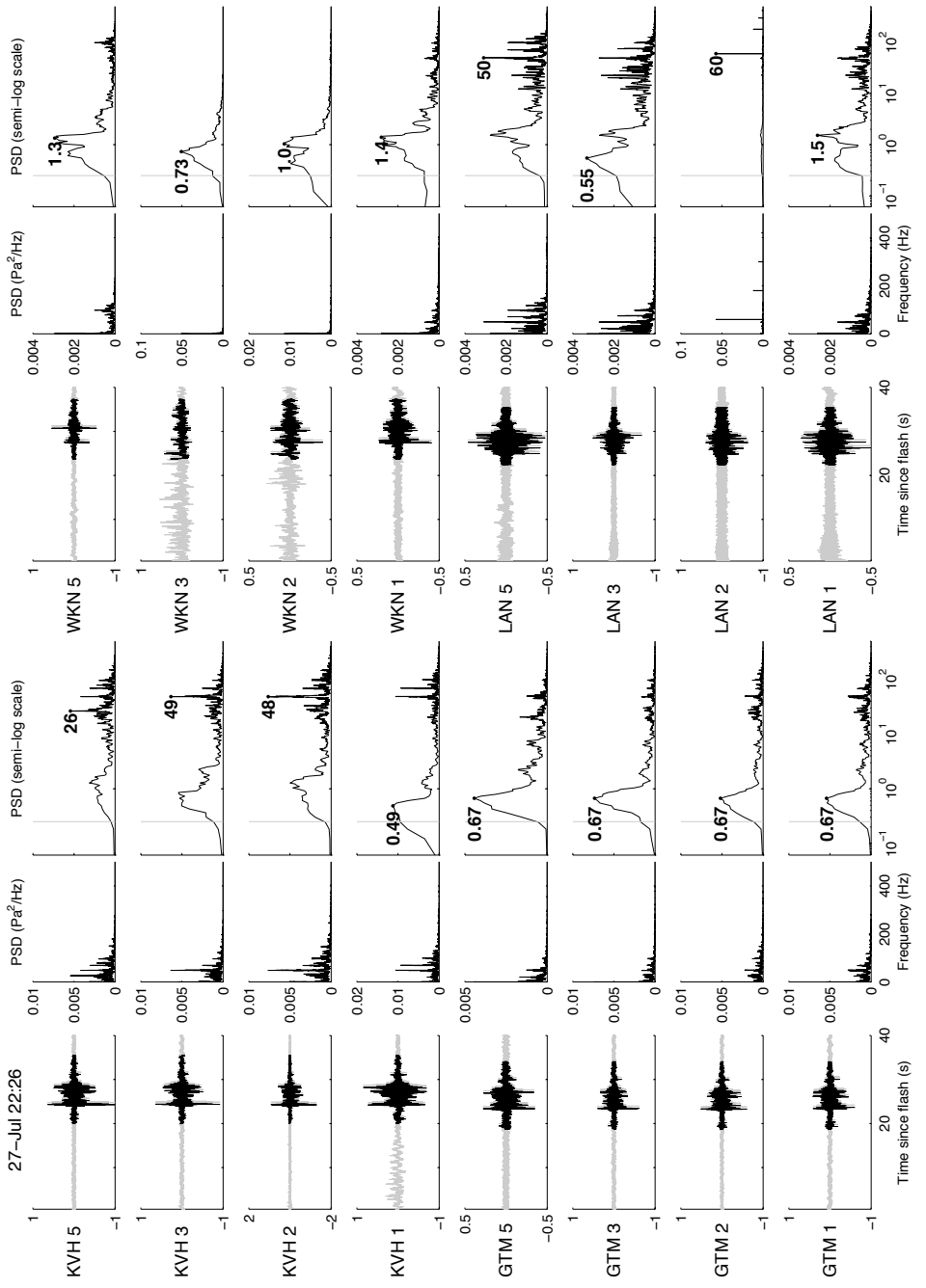

Figure C.7: Signals and PSDs are estimated for an IC event during a storm on 3 September. Stations WKN and LAN were removed for much of the month of August. Station WKN is not functioning properly. Most energy appears to be contained within lower frequencies.

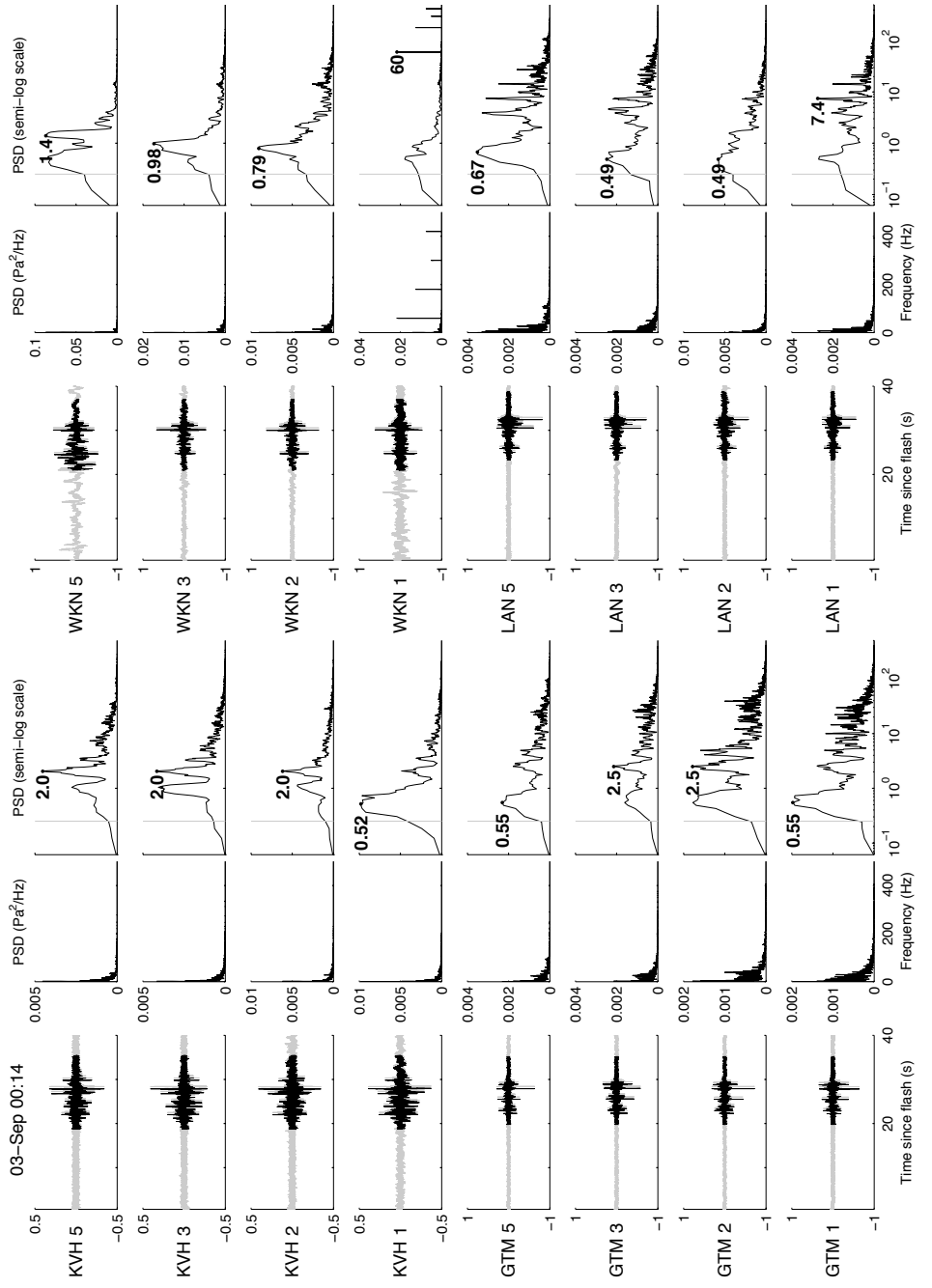

Figure C.8: Thunder signal shown from an IC event recorded on 3 September. Many high-quality IC signals were recorded during this storm.

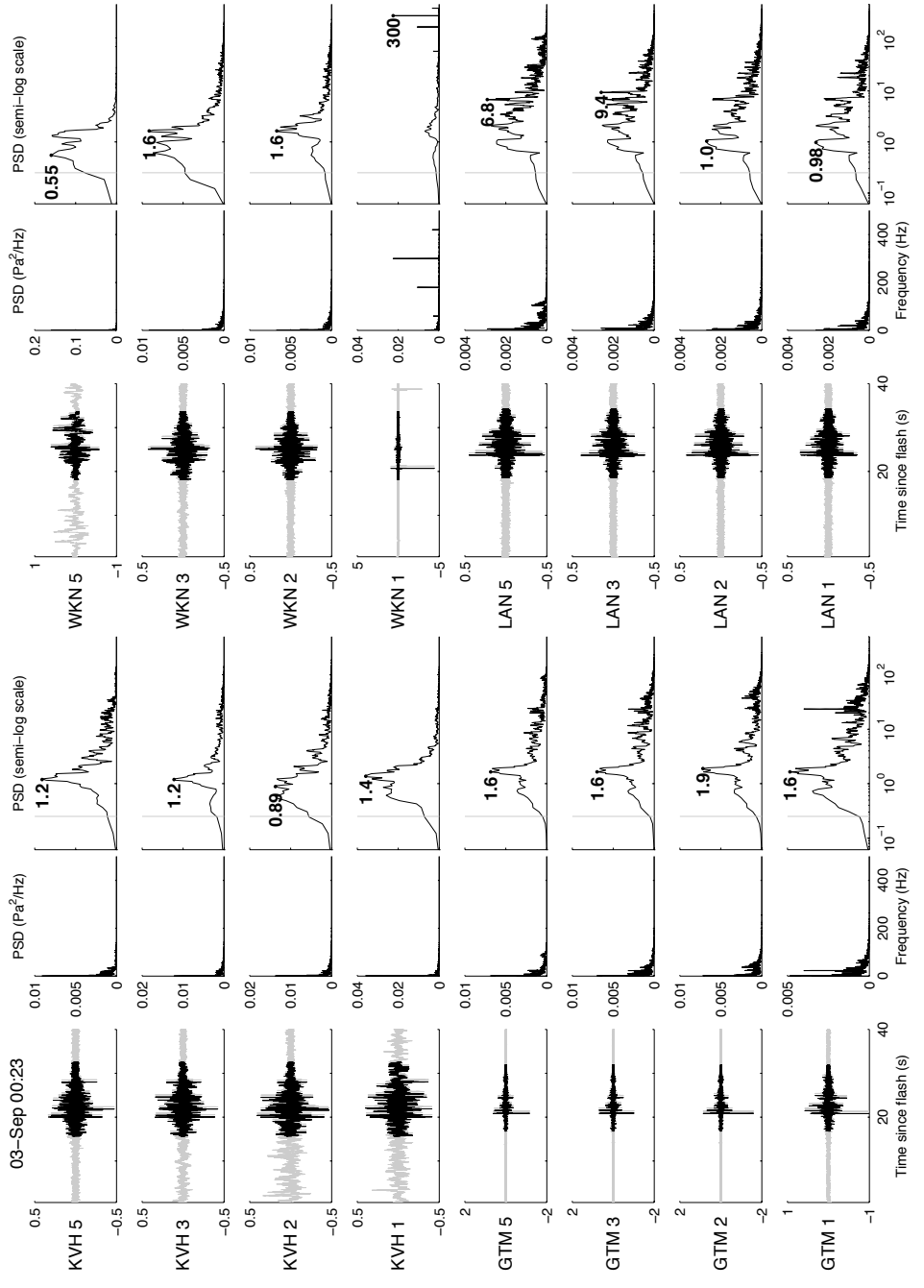

Figure C.9: Plots showing IC thunder from 3 September. Peak frequencies are usually close to 1 Hz.

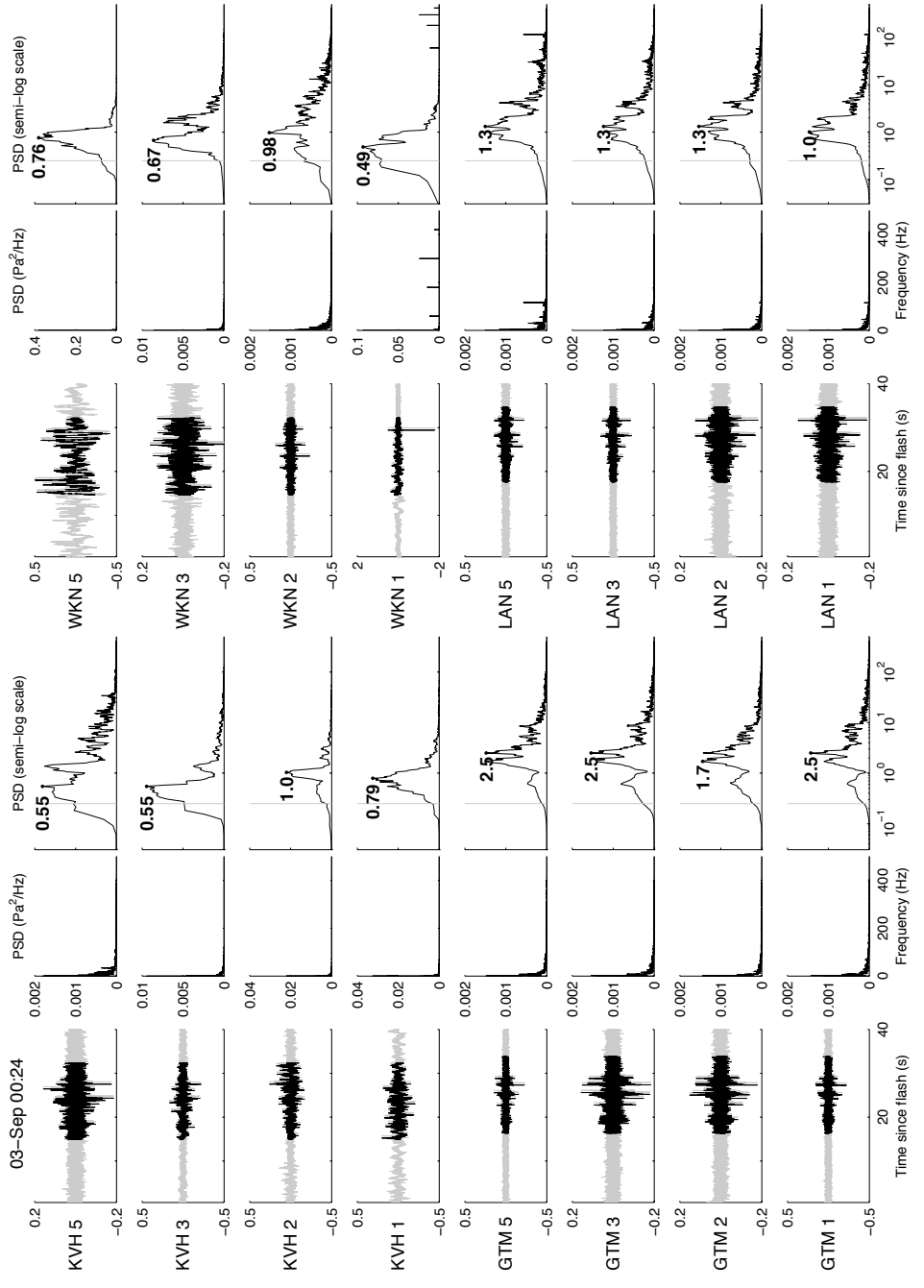

Figure C.10: Thunder signals and frequency content from another IC flash are estimated on 3 September.

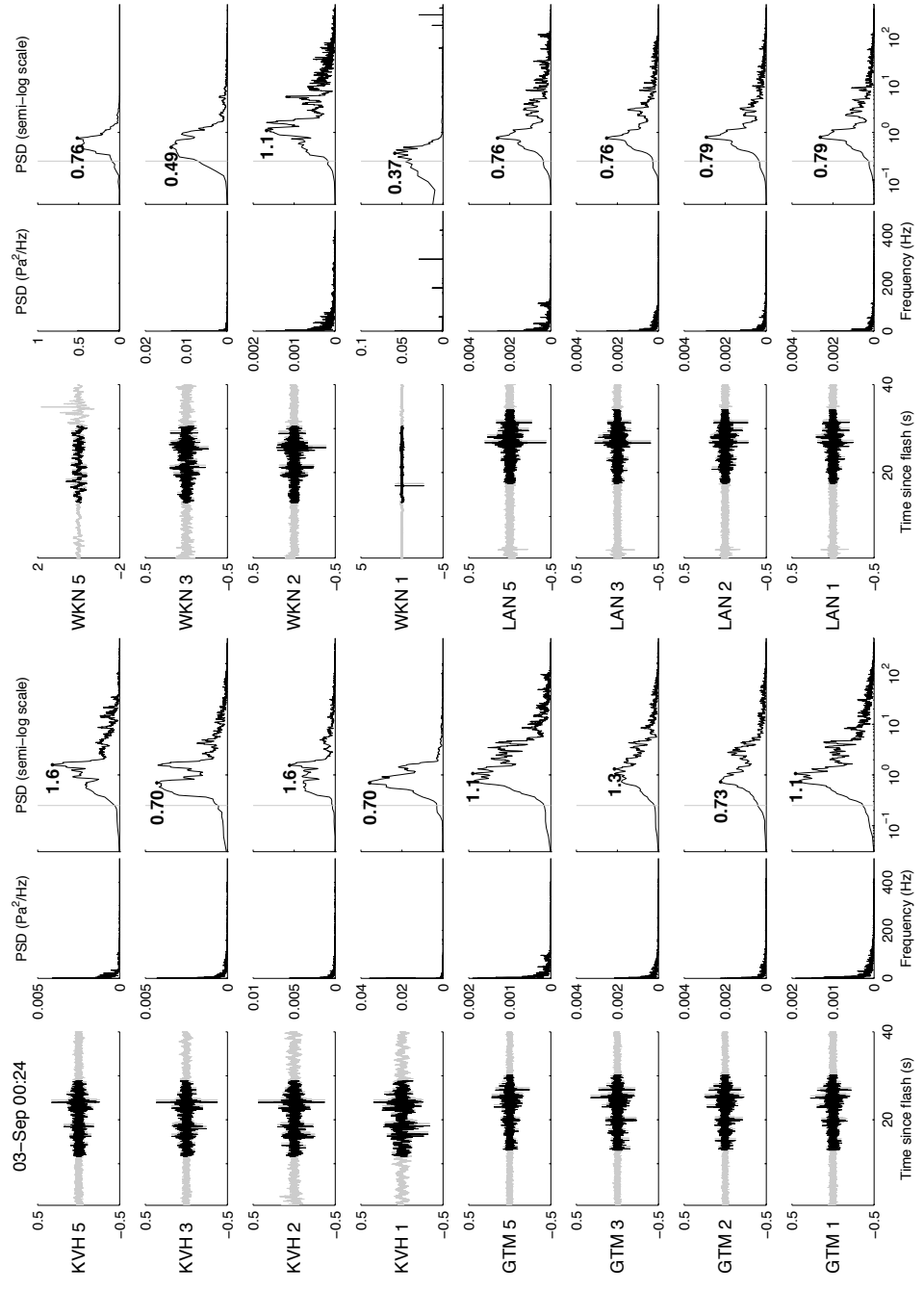

Figure C.11: A high-quality IC event that occurred on 3 September is shown. Peak frequencies are below 2.1 Hz at functioning sensors.

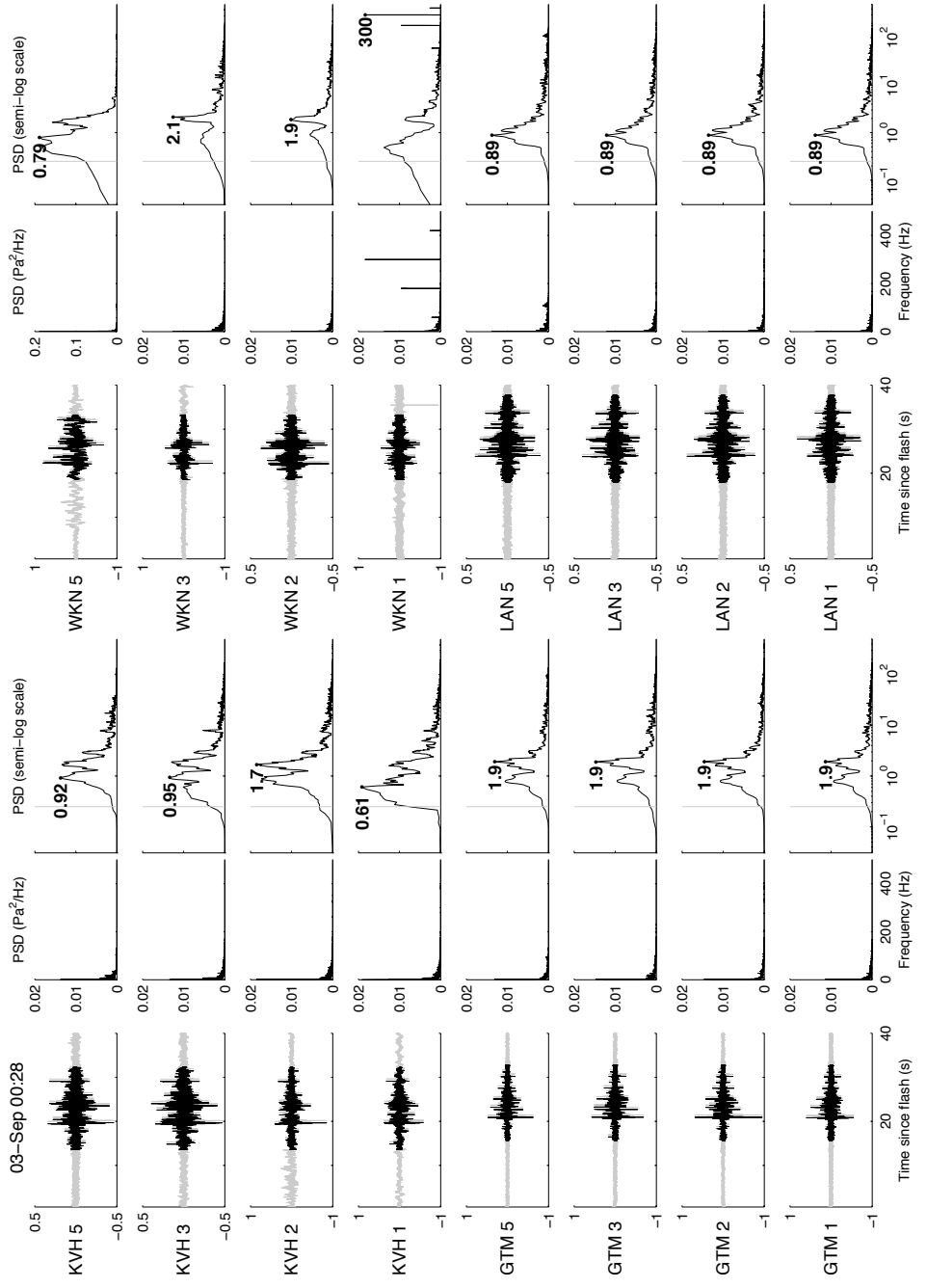

Figure C.12: IC thunder signals and PSDs during a later storm on 3 September are plotted. Characteristics vary between arrays. This event has more high frequency content than most other IC events.

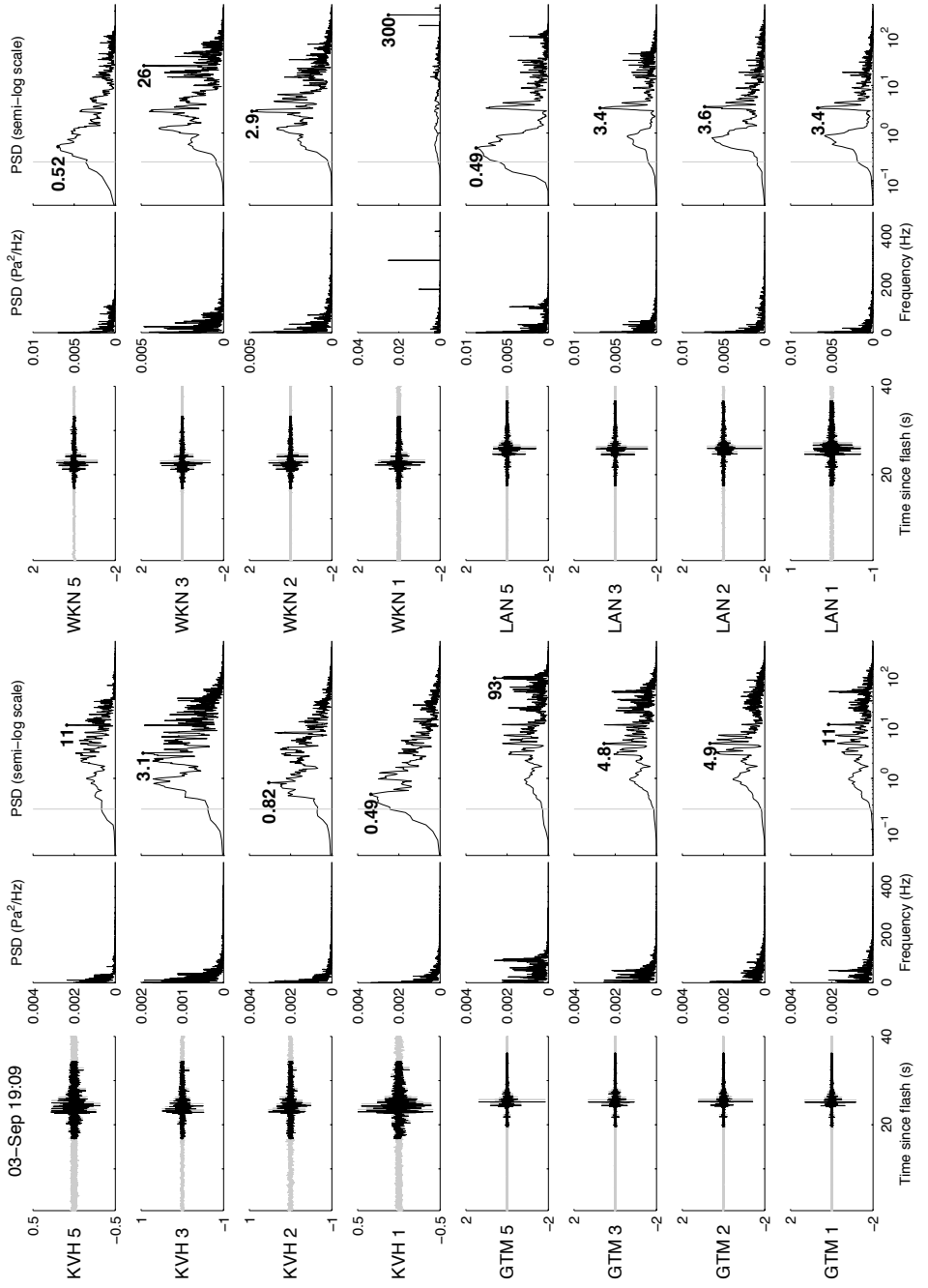

REFERENCES

Arechiga, R., J. Johnson, H. Edens, R. Thomas, and W. Rison (2011), Acoustic localization of triggered lightning, *J. Geophys. Res.*, *116*(D9), D09,103.

Assink, J., L. Evers, I. Holleman, and H. Paulssen (2008), Characterization of infrasound from lightning, *Geophys. Res. Lett.*, *35*, L15,802.

Balachandran, N. (1979), Infrasonic signals from thunder, *J. Geophys. Res.*, *84*(C4), 1735–1745.

Bass, H., and R. Losey (1975), Effect of atmospheric absorption on the acoustic power spectrum of thunder, *The Journal of the Acoustical Society of America*, *57*, 822–823.

Bohannon, J., A. Few, and A. Dessler (1977), Detection of infrasonic pulses from thunderclouds, *Geophys. Res. Lett.*, *4*(1), 49–52.

Colgate, S., and C. McKee (1969), Electrostatic sound in clouds and lightning, *J. Geophys. Res.*, *74*(23), 5379–5389.

Cummins, K., and M. Murphy (2009), An overview of lightning locating systems: History, techniques, and data uses, with an in-depth look at the us nldn, *Electromagnetic Compatibility, IEEE Transactions on*, *51*(3), 499–518.

Depasse, P. (1994), Lightning acoustic signature, *J. Geophys. Res.*, *99*(D12), 25,933–25,940.

Dessler, A. (1973), Infrasonic thunder, *J. Geophys. Res.*, *78*(12), 1889–1896.

Few, A. (1969), Power spectrum of thunder, *J. Geophys. Res.*, *74*(28), 6926–6934.

Few, A. (1985), The production of lightning-associated infrasonic acoustic sources in thunderclouds, *J. Geophys. Res.*, *90*(D4), 6175–6180.

Few, A. (1995), *Acoustic radiations from lightning*, vol. 2, pp. 1–31, CRC Press, Boca Raton, Florida.

Few, A., A. Dessler, D. Latham, and M. Brook (1967), A dominant 200-hertz peak in the acoustic spectrum of thunder, *J. Geophys. Res.*, *72*(24), 6149–6154.

Fleagle, R. (1949), The audibility of thunder, *The Journal of the Acoustical Society of America*, *21*, 411.

Holmes, C., M. Brook, P. Krehbiel, and R. McCrory (1971), On the power spectrum and mechanism of thunder, *J. Geophys. Res.*, *76*(9), 2106–2115.

Johnson, J., R. Arechiga, R. Thomas, H. Edens, J. Anderson, and R. Johnson (2011), Imaging thunder, *Geophys. Res. Lett.*, *38*(19), L19,807.

Kinsler, L., A. Frey, A. Coppens, and J. Sanders (1999), *Fundamentals of acoustics, 4th Edition*, John Wiley & Sons, Inc., New York.

Marcillo, O., J. Johnson, and D. Hart (2012), Implementation, characterization, and evaluation of an inexpensive low-power low-noise infrasound sensor based on a micro-machined differential pressure transducer and a mechanical filter, *Journal of Atmospheric and Oceanic Technology*.

Orville, R. (2008), Development of the national lightning detection network, *Bulletin of the American Meteorological Society*, *89*(2), 180–190.

Pasko, V. (2009), Mechanism of lightning-associated infrasonic pulses from thunderclouds, *J. Geophys. Res*, *114*, D08,205.

Rakov, V., and M. Uman (2003), *Lightning: physics and effects*, Cambridge Univ Pr.

Rison, W., R. Thomas, P. Krehbiel, T. Hamlin, and J. Harlin (1999), A gps-based three-dimensional lightning mapping, *Geophys. Res. Lett.*, *26*(23), 3573–3576.

Thomas, R., P. Krehbiel, W. Rison, S. Hunyady, W. Winn, T. Hamlin, and J. Harlin (2004), Accuracy of the lightning mapping array, *J. Geophys. Res.*, *109*, D14,207.

Thomson, D. (1982), Spectrum estimation and harmonic analysis, *Proceedings of the IEEE*, *70*(9), 1055–1096.

Wiens, K., S. Rutledge, and S. Tessendorf (2005), The 29 june 2000 supercell observed during steps. part ii: Lightning and charge structure, *Journal of the Atmospheric Sciences*, *62*(12), 4151–4177.

Wilson, C. (1920), Investigations on lightning discharges and on the electric field of thunderstorms, *Philos. Trans. R. Soc. London Ser. A*, *221*, 73–115.